Thermodynamic, Transport and Structural Properties of Deep Eutectic Solvent Mixtures Relevant to Capture and Conversion of CO_2 to Value Added Products

A Molecular Dynamics Study

J. Langeveld

Technische Universiteit Delft

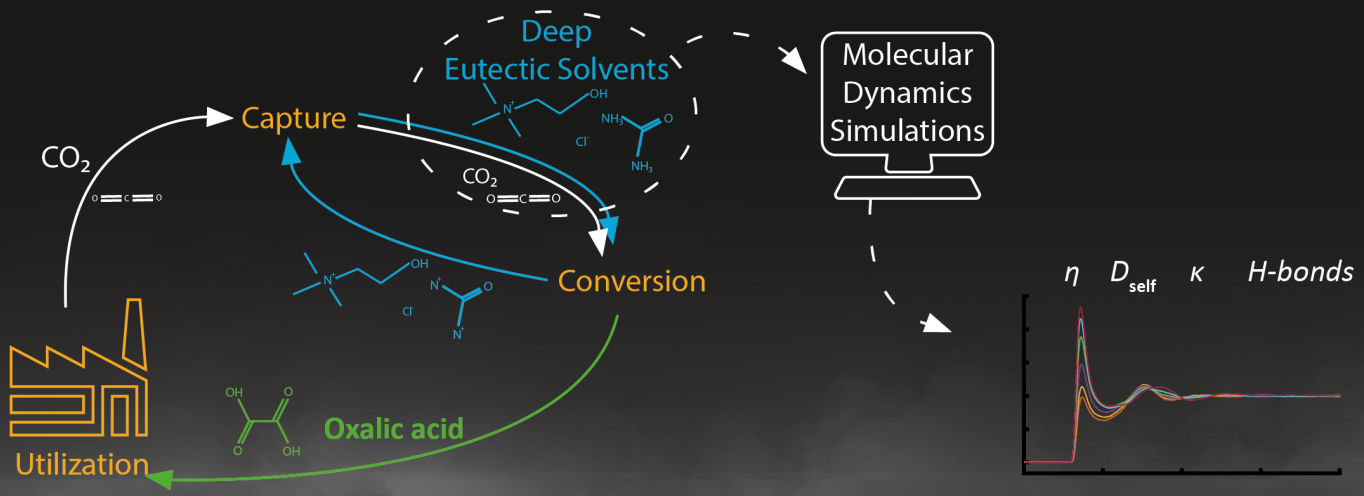

TU Delft Delft University of Technology

Thermodynamic, Transport and Structural Properties of Deep Eutectic Solvent Mixtures Relevant to Capture and Conversion of CO_2 to Value Added Products

A Molecular Dynamics Study

by

J. Langeveld

to obtain the degree of Master of Science
at the Delft University of Technology,
to be defended publicly on Monday December 13, 2021 at 01:00 AM.

Student number:	4306821	
Project duration:	February 2021 – December 2021	
Thesis committee:	Dr. ir. O. Moultos	TU Delft, supervisor
	Prof. dr. ir. T. J. H. Vlugt	TU Delft
	Dr. ir. P. Dey	TU Delft
Daily supervisor:	Dr. ir. N. Dawass	TU Delft

This thesis is confidential and cannot be made public until December 1, 2022.

TU Delft Delft University of Technology

Acknowledgements

The interest in Molecular Dynamics simulations was undoubtedly a direct consequence of the enthusiasm of Dr. Othon Moultos. During only two lectures of, in my experience, the most passionate teacher, the affection was generated, never to leave my mind again.

So a few months later, I asked Dr. Moultos for a thesis subject. Unfortunately, I had to politely decline the first proposal, as it was carbon positive, in cooperation with a major oil company. Today, I am very happy that I did so, as the next proposal led to a thesis for which I could find motivation in its ultimate goal of battling climate change.

At times, when simulations yield inexplicable outcomes after days of attempts, the extra motivation was welcome. Covid-regulations could make days turn into weeks, without many hours spent outside of the bedroom office. The expectations of the outcome of the project subsequently fluctuated. At first, everything is difficult. Then more papers start to make sense and I become naively optimistic. Eventually, reality sinks in. The best way to imagine is by looking at Figure 4.11a, covering the axis labels, and considering the vertical axis as 'Expectation of thesis outcome', normalized for final outcome, and the horizontal axis as time, normalized for total project time. Looking back, big steps in efficiency have been made. Many of the labour-intensive pre and post-processing tasks first done manually, were incrementally performed by lines of code. Illustratively, please consider Figure 4.5b, cover the axis labels, imagine the horizontal label as described above, and the vertical label as the time spend on a certain simulation.

Before the start, I thought of the graduation project as a final test, before a student gets certified to leave the university. This perception still holds, with the additional opinion of a fruitful learning experience. In a few months, I had to become a contributor to the scientific knowledge of a material class that I had never heard of before. I had to get acquainted with molecular simulations, while I had never even touched a Linux computer before. This allows me to look back proudly, but I have to emphasize that this would never have been possible without the patience and extensive guidance of my supervisors.

First of all, I would like to thank Dr. Othon Moultos for the weekly meetings. Your simulation experience helped to identify issues quickly and steer my attention in the right direction. I appreciated your quick responses to questions and the after-meeting discussions of reduced scientific nature. Next, I would like to thank Dr. Noura Dawass, who patiently helped me to get started with the simulations. Even after your PhD promotion and moving to Qatar, you took the time to provide feedback. I want to express my gratitude to the committee members, Prof. Thijs Vlugt and Dr. Poulumi Dey. Furthermore, I would like to thank all the people working at TNO, DMT Mesverwerking Fryslan, Tielo-Tech and TU Delft who are involved in the Bio-cel project: Dr. Erwin Giling, Mr. Jort Langerak, Dr. Elena Pérez-Gallent, Mr. Peter van der Broeke, Mr. Benny Bakker, Dr. Mahinder Ramdin, Mr. Thomas Zutphen, Mr. Marcel van der Schoot, Ms. Jeannine Frijns and Mr. Angel Alfonso Villanueva, for the interesting discussions during the monthly meetings. Funding for the Bio-cel project, including the contribution of this thesis, comes from the Rijksdienst Voor Ondernemend Nederland (RVO). The Nederlandse Organisatie voor Wetenschappelijk Onderzoek (NWO) funded the required simulation time on the supercomputer Snellius. I am grateful for both fundings. Lastly, I would like to thank my friends, my mother and in particular my roommates, who supported me, even though I was not always a pleasurable company during the final phase.

To conclude, a message to you, dear reader. I am honoured that you spend time reading my work, and hope you enjoy reading it. In case of any questions or remarks, do not hesitate to contact me.

Jilles Langeveld
Rotterdam, November 2021

Abstract

The current industrial application of carbon capture utilization and storage (CCUS) is limited due to technological drawbacks such as high energy demand and environmental pollution. Ionic liquids (ILs) and deep eutectic solvents (DESs) are considered promising alternative solvents for the capture of carbon dioxide (CO_2). DESs are often characterized by high viscosities, which hinders industrial application. This problem might be solved by mixing the DES with an organic solvent. This study aims to assess the DESs choline chloride-ethylene glycol (ethaline) and choline chloride-urea (reline) mixed with methanol and propylene carbonate (PC) for their suitability as a medium for the combined capture and electrochemical conversion of CO_2. Molecular dynamics (MD) simulations are performed to obtain the densities, the viscosities, the self-diffusivities, the ionic conductivities and insight into the molecular interactions of these mixtures. Independent MD simulations are performed of these mixtures with low concentrations of the solutes CO_2, oxalic acid and formic acid. Complementary studies within the Bio-cel project are conducted to characterize the solubility and electrochemical reaction of CO_2 and the techno-economics.

The viscosities of the mixtures monotonically decrease for an increase of mole fraction of organic solvent, which is benign for the application of CCUS. The self-diffusivities of all constituents increase monotonically for an increase of mole fraction of organic solvent. The ionic conductivity is calculated based on the ion self-diffusivities. Ionic conductivity optima are found at a mole fraction of DES of approximately 0.6 for ethaline-PC and approximately 0.2 for ethaline-methanol and reline-methanol. For higher mole fractions of organic solvent, the ionic conductivity decreases due to a depletion of ions. Radial distribution functions (RDFs) are used to analyze the intermolecular interactions. RDF peaks between chloride-choline and chloride-ethylene glycol show an increase for an increasing mole fraction of organic solvent, which was unexpected. The numbers of hydrogen bonds decrease for addition of methanol to pure deep eutectic solvent. For addition of propylene carbonate, this decrease is less pronounced. The depletion of hydrogen bonds at low mole fractions of deep eutectic solvent is in correspondence with the decrease in viscosity and increase in self-diffusivities. The results indicate that, for the studied properties, deep eutectic solvents mixed with organic solvents are more favourable than pure deep eutectic solvents for the absorption and electrochemical conversion of CO_2.

List of Figures

List of Tables

Nomenclature

Abbreviations

CO_2RR Carbon dioxide reduction reaction

A pre-factor / Dynamic variable for MSD

AA All Atoms

ACPYPE AnteChamber PYthon Parser interfacE

AMBER Assisted Model Building with Energy Refinement

BmimCl/$AlCl_3$ 1-butyl-3-methylimidazolium chloroaluminate

CCUS Carbon capture utilization and storage

Ch^+ Choline

Cl^- Chloride

DES Deep eutectic solvent

EMD Equilibrium molecular dynamics

FA Formic acid

FE Faradaic efficiency

FF Force fields

GAFF General Amber Force Field

HBA Hydrogen bond acceptors (choline chloride)

HBD Hydrogen Bond Donor (urea & ethylene glycol)

IEA International Energy Agency

IL Ionic liquid

LAMMPS Large-scale Atomic/Molecular Massively Parallel Simulator

LJ Lennard-Jones

MAD Mean average deviation

MD Molecular Dynamics

MEA monoethanolamine

MSD Mean-squared-displacement

NEMD Non-equilibrium molecular dynamics

NPT Isothermal, isobaric

NVT Canonical (Isochoric, isothermal)

NWO Nederlandse Organisatie voor Wetenschappelijk Onderzoek

OA Oxalic acid

OCTP On-the-fly computation of transport properties

OPLS Optimized Potentials for Liquid Simulations

PC Propylene carbonate

PPPM Particle-particle particle-mesh

RDF Radial Distribution Function

RVO Rijksdienst Voor Ondernemend Nederland

TraPPE Transferable Potentials for Phase Equilibria Force Field

UA United Atoms

VFT Vogel-Fulcher-Tamman model

VMD Visual Molecular Dynamics

Chemical Names

1-butyl-3-methylimidazolium chloroaluminate $C_8H_{15}ClN_2$ $AlCl_3$

Carbon dioxide CO_2

chloride Cl

Choline $C_5H_{14}NO$

Ethaline Choline chloride-ethylene glycol

Formic acid CH_2O_2

Methanol CH_3OH

Oxalic Acid $C_2H_2O_4$

Reline Choline chloride-urea

urea CH_4N_2O

Other Symbols

ϵ Dispersion energy

γ Surface tension / Desired transport coefficient

κ Ionic conductivity

$\mathbf{r}$ Position vector

ρ Density / Number density

σ Zero-crossing distance

ε_0 Permittivity of free space

ξ Dimensionless constant, 2.837298

ξ_{ion} Ion association

N_{HB} Number of hydrogen bonds

$\langle\rangle$ Ensemble average

η	Dynamic viscosity
B	Fitting parameter
E	Activation energy for viscous flow
$g(r)$	Radial distribution function
M	Molar mass
N	Number of molecules
q	Atom charge / Ion charge
r	Distance / Radius average sized void
T	Temperature
U	Potential Energy
V	Volume
x	Mole fraction

Physical Constants

k_{B}	Boltzmann constant
e	Euler's number / Elementary charge
R	Molar gas constant

Subscripts

α	Index
β	Index
inf	Corrected for finite-size effects
k	Index
i	Index
j	Index
ave	Average
c	Cutoff

Contents

1 Introduction

Despite all the efforts to increase the share of renewable energy, the yearly global CO_2 emissions are still rising. Over the past 800,000 years, the atmospheric CO_2 concentration has not exceeded 300ppm, until the start of the industrial revolution [1]. Currently, the atmospheric CO_2 concentration has reached 415 ppm [2]. Due to the pace at which the earth is subsequently warming, many species will not be able to adapt and will become extinct. Other examples of potential resulting problems are sea level rise, local droughts, increased occurrence of hurricanes and ocean acidification. In 2015, the Paris Climate Agreement was signed by 186 countries responsible for over 90% of CO_2 emissions. In this agreement, all countries promised to take the necessary action to limit global warming to a maximum of 2 °C compared to pre-industrial levels. Subsequently, many agreements have followed, which translate the goals into targets and deadlines. The European Green Deal, proposed in 2020, raises the target to reduce greenhouse gas emissions by 55% compared to 1990. Moreover, the European Union aims to be climate-neutral by 2050 [3].

Carbon capture utilisation and storage (CCUS) is expected to play an important role to reach these targets. Even if all required energy for heating and electricity is renewable, there will be a need for CCUS. The International Energy Agency (IEA) [4] states that CCUS can tackle emissions in sectors where other technology options are limited, such as in the production of cement, iron and steel or chemicals, and to produce synthetic fuels for long-distance transport. Furthermore, CCUS can remove CO_2 from the atmosphere by combining it with bio energy or direct air capture to balance emissions that are unavoidable or technically difficult to abate [4]. Nevertheless, the industrial application of CCUS is still limited. Today, there are 21 CCUS plants deployed to capture a total of 41 Mt CO_2 each year [4]. According to the IEA Sustainable Development Scenario, net global CO_2 emissions from the energy sector must fall to zero by 2070. The IEA states that 10.4 Gt of CO_2 should be captured from the energy sector by then. To reach this 250 fold increment of CCUS, the cost to capture CO_2 has to decrease. Therefore, technological advancement should facilitate lower operational and capital costs [4].

CO_2 can be used directly, or converted into higher value products. Oxalic acid (OA) has an exceptional market value. In 2019, OA had a market price of approximately 500 $/tonne [5], and a global market value of 715 M$ [6]. In industry, approximately equal quantities of oxalic acid are used for metal treatment, in the chemical industry [7], and for textile treatment, as a bleaching agent. Moreover, oxalic acid could be used to form ethylene glycol [8], which has a yearly production of 34.8 M tonne at a price of roughly 1500 $/tonne [9], mainly for the plastics industry. Formic acid (FA) is mainly used in industry as a food preservative for livestock feed and for the production of leather. Its market price is approximately 400 $/tonne.

In order to extract CO_2 from a gas stream, absorption and adsorption can be used. The industrial state-of-the-art is based on chemical absorption using amines as solvents [4]. There are several disadvantages to this method such as a high energy demand and the release of toxic gasses. Previous studies have shown promising potential for the use of ionic liquids (ILs) and deep eutectic solvents (DESs) as sorbents, due to their high solubility of CO_2, low solubility of other common gasses and low vapour pressure [10]. Furthermore, they are praised for their high tunability. Their properties could be tuned by selection of its constituents, mixing with other components, or changing the process conditions. The solubility of some DESs are highly sensitive to changes in pressure, which can be exploited

in a cyclic process to desorp the CO_2 [11–13]. Most conducted studies are focused on assessing solvents solely for the absorption-desorption process. A hurdle for application in industry, is the high viscosity that characterises most DESs.

The goal of this research is to find an answer to the question: are DESs, mixed with organic solvents, suitable as a medium for absorption and electrochemical reduction of CO_2? In order to asses the DESs-organic solvent mixtures for this application, this study aims to find its viscosity, self-diffusivity, ionic conductivity and structural behaviour as a function of the DES concentration. If these DESs will one day be applied in industry, for CCUS or other purposes, one has to know these properties to design and control the required equipment. This study will focus on DESs, since previous research shows several advantages compared to ILs, such as low toxicity, good biodegradability, and economical production [14]. As DESs have only been discovered recently, they have been studied less intensively than ILs. For more information about ILs in general, the reader is referred to several review studies [15–17].

Since the family of DESs comprises 10^6 - 10^8 possible binary combinations, and (computational) time is limited, only a small selection can be studied in this research. A selection was made to match complementary studies, which investigate the solubility of CO_2, OA and formic acid (FA, also known as methanoic acid), and the performance of the electrochemical conversion. In this study, two choline-chloride (Ch^+Cl^-) based DESs are investigated: Ch^+Cl^--urea and Ch^+Cl^--ethylene glycol (EG), known as reline and ethaline, respectively. These DESs have been studied before, however, a gap in research can be identified for transport properties of the mixtures reline-methanol, ethaline-methanol and ethaline-propylene carbonate (PC). These mixtures will be investigated, as well as the interaction of these mixtures with CO_2, OA and FA. OA is of interest for economic reasons, while FA is often found to be produced in experiments of complementary studies.

To be able to assess the mixtures for their suitability as CO_2 absorbent and conversion medium, the ideal solvent is characterized. For the absorption step, a high solubility of CO_2, low vapour pressure, high thermal stability, and high selectivity to CO_2 are desired. Furthermore, it should be nonreactive with CO_2, and remain liquid over a wide range of temperatures and pressures. DESs are often viscous, limiting mass transfer and increasing pumping costs. Therefore, its viscosity should be minimized. For the reaction step, a catalytic behaviour for conversion to oxalic acid is desired. For the final separation, a low solubility of oxalic acid would be beneficial, allowing for crystallization and precipitation of oxalic acid. A complementary study at our research group conducted by Dr. Dawass aims to find solubility properties of CO_2, FA and OA in the same mixtures, using Monte Carlo simulations. A complementary study by Dr. Gallez and her students, conducted at TNO, aims to characterize the electrochemical reaction of CO_2 facilitated in the same mixtures. The techno-economics of a hypothetical production plant are studied by Dr. Ramdin together with students from Delft University of Technology and by students linked to the company DMT. At the time of writing, these complementary studies have not been published yet.

Traditionally, transport properties are obtained via experiments. However, such measurements are often costly and difficult or dangerous to perform [18]. Molecular dynamics simulation is a powerful alternative for obtaining transport coefficients and gaining a better understanding of the underlying physicochemical mechanisms [19].

Following this introduction, in Chapter 2, the available literature on DESs, CO_2 capture and electrochemical conversion of CO_2 to oxalic acid are discussed. In Chapter 3, the methods of using Molecular Dynamics to calculate the density, viscosity, self-diffusivity, radial distribution function and number of hydrogen bonds are specified. Next, the obtained results are presented and discussed in Chapter 4. the main conclusions are shared in Chapter 5. Lastly, recommendations for further research are given in Chapter 6.

2

Literature Review

This section will provide a literature review on DESs and their relevant properties for CO_2 absorption and conversion. An overview of methods for carbon capture is given. Studies conducted on the electrochemical conversion of CO_2 to oxalic acid will be discussed. The main findings are higlighted in Section 2.6.

2.1. Types of Deep Eutectic Solvents

DESs are systems formed from a eutectic mixture of Lewis or Brønsted acids and bases which can contain a variety of anionic and/or cationic species [10]. DESs were first discovered by Abbot et al. [20] in 2003, when they noted an exceptionally deep melting point depression at the eutectic composition of certain hydrogen bond donors (HBDs) and acceptors (HBAs).

Since they share many physical characteristics with ILs, DESs are acknowledged as a relatively new class of ILs. Although these terms have been used interchangeably in the literature, these are actually two different types of solvents. Both ILs and DESs are generally characterized by high thermal stabilities, low volatilities, low vapour pressures and tunable polarities. DESs distinct themselves from ILs by their low toxicities and biodegradabilities and are considered preferable since DESs are usually easier and less expensive to prepare [14].

All DESs discovered thus far can be divided into five types. *Type I* combines a quaternary ammonium salt with a metal chloride. *Type II* consists of a quaternary ammonium salt and a metal chloride hydrate. *Type III* is made up of a quaternary ammonium salt and an HBD. *Type IV* consists of a metal chloride hydrate and an HBD. The relatively new *type V* is composed of only nonionic, molecular HBAs and HBDs [21, 22]. Thus far, the majority of research focuses on *type III* DESs [14]. This study examines the DESs reline and ethaline, which are both *type III* DESs.

2.2. Tunability of Deep Eutectic Solvents

DESs are praised for their tunability, meaning their properties can be adjusted by changing the composition and conditions. Hansen et al. [14] list the most common HBDs (18) and HBAs (26). This list only contains *type III* DESs and is far from comprehensive, nevertheless, it consists of 468 potential DES combinations. Considering all HBAs and HBDs, an estimated total of 10^6 - 10^8 possible binary combinations can be made [14]. Studies have been conducted on ternary DESs, allowing for even more potential combinations. The transport properties of DESs have proven to be sensitive to mixing with water, especially to decrease the viscosity [19]. Furthermore, their behaviour is highly dependent on the mixing ratio HBD:HBA. Thus far, most research focused on DESs at their eutectic ratio. Investigating DESs at other ratios is considered one of the key steps towards industrial application [14]. Lastly, the process conditions can be altered. The CO_2 solubility, amongst others, is dependent on temperature and pressure, at different sensitivities per DES. Considering the great number of combinations of HBAs, HBDs, ternary mixture components and process conditions, optimizing for a given application would require experiments or simulations through millions of configurations. As stated by Hansen et al. [14]: 'tunability cannot be considered to be a practical feature of DESs if creating solutions with particular

properties is all guesswork.' Therefore, DESs research aims to develop a fundamental understanding to build models to 'tune' for specific applications.

2.3. Properties of Deep Eutectic Solvents

This section provides a brief overview of information in literature about the viscosity, ionic conductivity and CO_2 solubility of DESs.

2.3.1. Viscosity

DESs tend to have high viscosities, with values reported ranging from 10^1 to 10^4 mPa · s at ambient conditions [14]. The two most commonly applied models to describe the viscosity of DESs are the Arrhenius and Vogel-Fulcher-Tammann (VFT) models. The Arrhenius model is stated as:

$$\eta_{\text{Arrhenius}} = Ae^{E/\text{RT}} \tag{2.1}$$

where η, E, A and R denote the viscosity, the activation energy for viscous flow, a pre-factor, and the molar gas constant, respectively. This equation is valid only for liquids at high temperatures or for viscosities measured over a small temperature range. The VFT model is often used for wide ranges of temperatures [23]. The VFT equation is stated as:

$$\eta_{\text{VFT}} = A' e^{B/(T-T_0)} \tag{2.2}$$

where A' denotes the pre-exponential factor, the theoretical viscosity at infinite temperature, B denotes the fitting parameter that accounts for the activation energy of viscous flow, and T_0 the ideal glass transition temperature. Some natural DESs have been reported to behave non-Newtonian and thereby require more complex models than Arrhenius or VFT [24]. An example of a VFT fit is provided in Figure 2.1 [25].

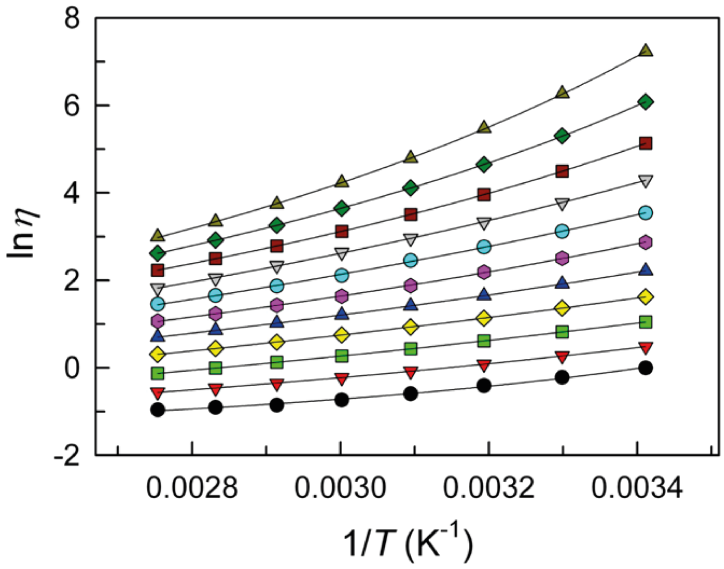

Figure 2.1: ln(η) as a function of 1/T, as an example of the Vogel-Fulcher-Tamman (VFT) model applied to mixtures of reline-water at different mole fractions, from a study by Yadav and Pandey [25]. The mole fraction of reline decreases from 1 (grey upward triangle) to 0 (black circle). The VFT fit is represented by the lines.

2.3.2. Ionic Conductivity

DESs exhibit lower ionic conductivity than high-temperature molten salts. Abbot et al. [26] state this difference can be explained by Hole theory, which relates the ionic conductivity to the size of ions and viscosity. Hole theory explains that during melting, ILs or DESs form empty spaces caused by thermally generated fluctuations in local density. The radius of the average-sized void (r) is related to the surface tension of the liquid γ by:

$$4\pi\left(r^2\right) = \frac{3.5k_{\text{B}}T}{\gamma} \tag{2.3}$$

where k_B is the Boltzmann constant and T the absolute temperature. When the ions are small compared to the holes, they can move easily. Subsequently, the viscosity is low and ionic conductivity high. A widely used relation between the self-diffusivity of the ions and the ionic conductivity, the Nernst-Einstein equation, is discussed in Section 3.3.4.

2.3.3. CO_2 Solubility

Most DESs studied thus far exhibit lower CO_2 solubility compared to conventional ILs. However, recently the solubility was measured for hydrophobic DESs for the first time, showing values comparable with conventional ILs [27]. In another study, measured solubility is compared with predicted values using a PC-SAFT based model, showing reasonable correlation [28].

2.4. Capture of CO_2

There are various separation technologies available for CO_2 capture. A selection of these technologies can be applied as post-combustion capture: adsorption, physical absorption, chemical absorption, cryogenics separation and membranes [29]. The only technology used in the industry thus far is chemical absorption using amines, for example, monoethanolamine (MEA) [30]. Figure 2.2 shows a flow diagram of the process [31]. Flue gas is cooled before it is sweetened. It is brought into contact with lean MEA, yielding a rich solvent loaded with approximately 0.4 molCO_2/mol MEA [29]. The gas is washed with water and released into the atmosphere. By absorbing CO_2, the solution heats up, to 313 - 323 K. The solution is heated in a heat exchanger before it enters the stripper. It is heated to 373 - 393 K, at pressures around 1.5 to 2 atm [31]. The resulting costs and energy requirements of this heating is the major barrier to commercializing this technology on a larger scale [29, 30]. If an existing power plant would be equipped with this technology, the energy output would be lowered by 25-40% [32].

Other drawbacks of chemical absorption using MEA include the corrosiveness, degradation of the solvent by oxygen and the volatility of MEA, which causes environmental pollution [33]. To avoid this energy penalty for CO_2 capture, physical absorption is proposed [33]. By using solvents that are chemically stable and exhibit low vapour pressures, the aforementioned drawbacks can be minimized. Ultimately, the desorption step of CO_2 might be avoided completely, by combining the capture and conversion steps.

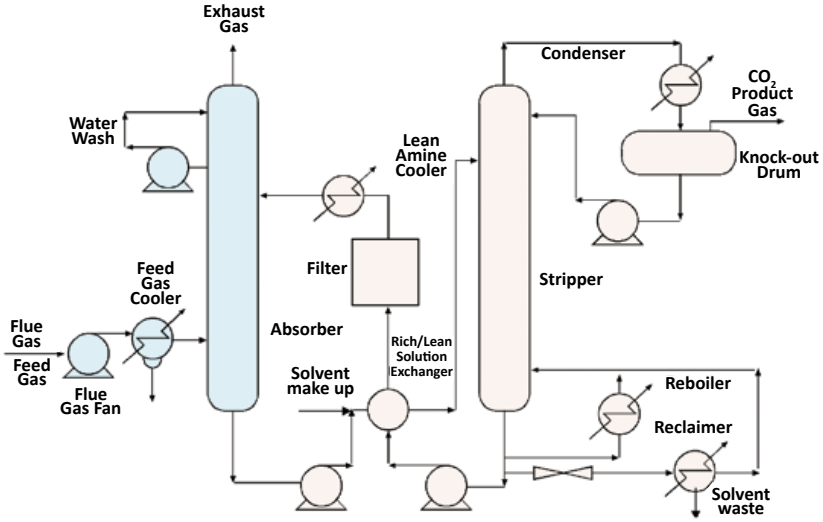

Figure 2.2: Process flow diagram for CO_2 capture from flue gas by chemical absorption. From IPCC [31].

2.5. Electrochemical Reduction of CO_2

The electrochemical reduction reaction of CO_2 (CO_2RR) has several advantages compared to biological, thermochemical and photochemical conversion: fine control of reaction rates and selectivities through the applied voltage, wide scalability due to modular electrolyzer designs and excellent coupling

to intermittent renewable energy sources due to the fast response time of electrochemical systems [34]. OA and FA are just two out of various possible products, depending on the process conditions, solvent, catalyst and electrode material. Studies have been conducted for decades on electrochemical reduction of CO_2. However, few studies have focused on ILs and DESs with conversion to FA and/or OA. The application of CO_2 electrolyzers in the industry remains largely unaddressed so that fossil carbon sources are used instead [35].

An electrolysis cell always has at least three components: two electrodes in contact with an electrolyte. The electrolyte is either a liquid or a solid material that can conduct ions but is impermeable to electrons. The ionic conductivity of the electrolyte depends strongly on temperature. Typical reaction products are carbon monoxide (CO), FA (CH_2O_2), methanol (CH_3OH), methane (CH_4), ethylene (C_2H_4), ethanol (C_2H_5OH), n-propanol (C_3H_8O) and OA ($C_2H_2O_4$). Electrode materials can have a significant effect on the products formed. Most studies compare a selection of copper, gold, silver, platinum, lead, indium, mercury, tin, thallium, zinc and glassy carbon electrodes [36, 37]. A distinction is made between aqueous and non-aqueous solutions. An electrolyte that contains water favours alternative CO_2RR pathways over the formation of oxalic acid. This dependency on water content is demonstrated in a study by Tomita et al. [36], varying water concentration in a CO_2RR, using a Pt electrode in an electrolyte of aqueous tetraethylammonium perchlorate/AN with a current density of 5 mA/cm^2 (Figure 2.3). Moreover, it is explained by Eneau-Innocent et al. [38] that an electrolyte that contains active protons, results in the reaction between a radical anion intermediate $CO_2^{\bullet -}$ and a proton to form FA. Therefore, a non-aqueous aprotic electrolyte is required to produce OA. Both DESs that are discussed in this study contain choline, which is protic. Table 2.1 2.1 provides an overview of the dominant reaction products resulting from different cathode materials in aqueous and non-aqueous electrolytes [37].

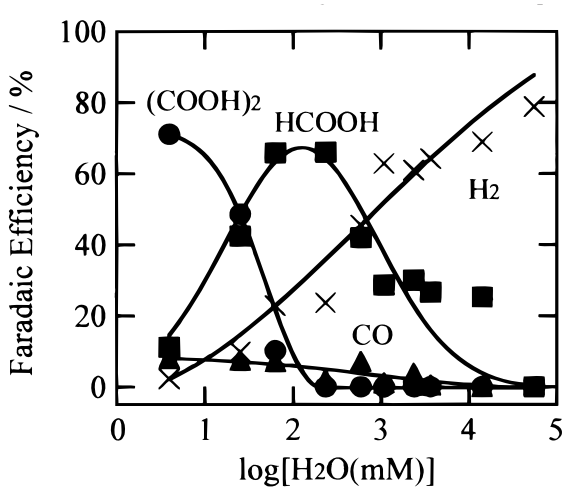

Figure 2.3: Faradaic efficiency of electrochemical reduction of CO_2 towards oxalic acid ($(COOH)_2$), formic acid (HCOOH), carbon monoxide (CO) and dihydrogen (H_2) with varying H_2O content with an aqueous tetraethylammonium perchlorate/acetonitrile electrolyte and platinum electrode. From a study by Tomita et al. [36].

Table 2.1: The dominant products that result from different reaction pathways as described by Ikeda et al. [37]. The column headers refer to the cathode material, the row headers refer to the electrolyte.

	Ag	Au	Hg	In	Pb	Sn	Ti	Zn
Aqueous	Carbon monoxide	Carbon monoxide	Formic acid	Formic acid	Formic acid	-	-	Carbon monoxide
Non-aqueous	-	Carbon monoxide	Oxalic acid	-	Oxalic acid	Carbon monoxide	Oxalic acid	Carbon monoxide

In the next subsection, the CO_2RR towards oxalic acid using different solvents is highlighted, for comparison. Next, studies conducted thus far using DESs as reaction medium will be discussed, and the under-explored research topics are identified. It should be noted that this study will not asses DESs for their selectivity and yield of oxalic acid, since the method of MD simulations is not suited. To assess the DES-organic solvent mixtures for their selectivity and yield facilitating CO_2RR towards OA and FA, complementary experimental studies are performed.

2.5.1. Alternative Solvents for Electrochemical Reduction of CO_2 to Oxalic Acid

Ikeda et al. [37] reported selective (>75mol%) production of oxalic acid in a non-aqueous electrolyte of tetraethylammonium perchlorate and PC, using cathodes of lead, thallium and mercury, with faradaic efficiencies between 60% and 78%. Kumar et al. [39] report the formation of OA with a selectivity of 90% and faradaic efficiency of 51% using a copper-based metal-organic framework. Recently, a master thesis conducted by Boor [40] reports a large trade-off between current density and faradaic efficiency for CO_2RR towards OA. The best results were obtained with lead as the cathode in a catholyte of PC + tetraethylammonium chloride, saturated with CO_2 and platinum as the anode, in an anolyte of 0.5M H_2SO_4, separated by a Nafion 117 cation-exchange membrane. Optimizing for current density in a batch-wise process resulted in a current density of $-17\,mA/cm^2$ and a faradaic efficiency of 45%.

ILs have attained increased attention for their catalytic behaviour as electrolytes for the CO_2RRs. The addition of ILs to electrolytes significantly decreases the onset potential for the CO_2RR and helps to suppress the undesired hydrogen evolution reaction [41]. However, most studies address aqueous solutions, which are outside the scope of this study since it hinders the formation of OA. The interested reader is referred to review studies by Lim et al. [42], and Chen et al. [43]. One study conducted by Yang et al. [44] shows a major dependency on the electrolyte for the products formed, experimenting with different ILs in an acetonitrile solution. The best results for production of OA was achieved using an aprotic aromatic ester-functionalized IL, 4-(methoxycarbonyl) phenol tetraethylammonium ([TEA][4-MF-PhO]). A current density of $9.03\,mA/cm^2$ with a faradaic efficiency of 86% at -2.6 V (vs. Ag/Ag+) were measured, and the OA formation rate was as high as $168.4\,\mu mol/cm^2h$, which is the highest reported value found to date. However, for industrial applications, the ILs are often too expensive, and higher current densities are desired. DESs are often less expensive [45].

2.5.2. Electrochemical Reduction of CO_2 Using Deep Eutectic Solvents

Like ILs, DESs are characterized by a low onset potential for the CO_2RR [41]. The majority of studies investigating DESs used for CO_2RRs focus on aqueous solutions. Vasilyev et al. claim to be the first to explore non-aqueous DESs as a medium for the CO_2RRs, in a paper published in 2019 [45]. They studied the performance using a silver cathode and a reline electrolyte, both neat and as an additive in solvents. For the neat system, the faradaic efficiency (FE) towards CO and the current density were found to be 15.8% and below $0.1\,mA/cm^2$, respectively. Hydrogen was formed as a by-product at a FE of 17.0 %. These (poor) results were attributed to the high viscosity, which hinders mass transfer causing depletion of CO_2 at the electrode surface. To reduce the viscosity, water was added (15 vol%), yielding a current density of $0.6\,mA/cm^2$ and FEs of 59% and 26%, for CO and H_2, respectively. These results indicate that viscosity is the main hurdle for using neat reline for the CO_2RR. Neat ethaline was investigated, which reached a current density of $0.4\,mA/cm^2$ and FEs of 78% and 9.9% for CO and H_2, respectively. The better performance correlates to the lower viscosity of ethaline, which is $37\,mPa*s$ for ethaline and $750\,mPa*s$ for reline at 298 K and 1 atm. Vasilyev et al. found the best results with an electrolyte of 1 M Ch^+ Cl^-+2 M EG in PC, providing a current density of $8\,mA/cm^2$ and FEs of 101.8% (CO) and 1.6% (H_2).

2.6. Synopsis

The goal of this literature study was to find the relevant current knowledge about DESs and electrochemical conversion of CO_2. The five types of DESs as described by Hansen et al. [14] were identified. The models that are used in literature to calculate properties of DESs have been discussed, coming to the overall conclusion that due to the complex particle interactions, it is difficult to predict DES properties. The conventional amine based method of CO_2 capture was discussed. For electrochemical conversion of CO_2, the impact of both the electrolyte and the electrodes have been discussed. From non-DES-specific studies [36, 37], it was found that the formation of OA is only preferred over other reaction products for specific cathode materials and aprotic electrolytes. Other information from literature, concerning studies that model the relevant solvents and solutes of this study using Molecular Dynamics are reviewed in Chapter 3. The little available literature data on transport properties of the relevant mixtures are discussed in Chapter 4, to compare to values found in this study.

3

Methods

In this study, Molecular Dynamics (MD) simulations will be used to compute the equilibrium and transport properties of several DESs. MD simulations are similar to real, physical, experiments, in the sense that we prepare a sample of a material, we couple the sample to measurement instruments and we monitor the sample for a certain duration. To account for noise, average values over time are calculated [46].

The principle of MD simulations relies on numerically integrating Newton's equations of motion for all interacting particles in a system. The forces between particles are calculated using inter-atomic potentials. The implementation and parameterization of these potentials are not trivial, especially for complex liquids such as DESs. The method is discussed in Section 3.1. For each time step, the new particle velocities and positions are calculated. By doing so, a well-configured system will reach equilibrium. Proceeding, the system will evolve for more time steps, during which data is sampled. The configurations of the simulations are described in Section 3.2. Lastly, the calculations which use the sampled data to determine transport properties are discussed in Section 3.3.

3.1. Force Fields

To calculate the interatomic interactions, many different force fields (FFs) have been developed. A trade-off between accuracy and computation time is made, depending on the modelled system. Two commonly used families of FFs are Assisted Model Building with Energy Refinement (AMBER) [47] and optimized potentials for liquid simulations (OPLS) [48]. AMBER was originally designed for biomolecules and later extended for other molecules by Wang et al. [49] to the General Amber Force Field (GAFF). OPLS was developed with liquids in mind, with an important distinction between united atom models (OPLS-UA), where hydrogen atoms next to carbon atoms are grouped with the carbon atom, and all-atom models (OPLS-AA), where all hydrogen atoms are modelled explicitly. Both models are based on the general form of the summation of the potential energy of equation 3.1:

$$U_{\text{potential}} = U_{\text{bond stretching}} + U_{\text{bond bending}} + U_{\text{bond torsion}} + U_{\text{non-bonded}} \tag{3.1}$$

where the major differences between the two FFs are found in the non-bonded contribution and the parameterization of all interactions. Both AMBER and OPLS represent the potential energy contributions by bond stretching and angles using Hooke's Law. Three potentials for the dihedrals are used in this study, identified in the software as charmm, opls and multi/harmonic. For the equations of the potentials, the reader is referred to appendix B and the documentation of LAMMPS (Large-scale Atomic/Molecular Massively Parallel Simulator) [50]. The used parameters can be found in Appendix B.

The non-bonded interactions are described as the sum of the Lennard-Jones (LJ) potential and the electrostatic potential, as in equation 3.2:

$$U_{\text{non-bonded}} = U_{\text{LJ}} + U_{\text{Coulomb}} \tag{3.2}$$

where

$$U_{\mathrm{LJ}} = 4\epsilon\left[\left(\frac{\sigma}{r}\right)^{12} - \left(\frac{\sigma}{r}\right)^{6}\right] \qquad r < r_{\mathrm{c}} \tag{3.3}$$

and

$$U_{\mathrm{Coulomb}} = \frac{q_i q_j}{4\pi\varepsilon_0 r} \qquad r < r_{\mathrm{c}} \tag{3.4}$$

in which U_{LJ} denotes the Lennard-Jones potential, U_{Coulomb} denotes the electrostatic potential, ϵ is the dispersion energy, σ is the zero-crossing distance, r is the distance between the two atoms, r_{c} is the cutoff distance, q_i and q_j are the charges of the atoms, ε_0 is the permittivity of free space [46, 47, 51]. The LJ potential is made up out of the attractive London dispersion forces and the Pauli repulsion forces. Figure 3.1 shows a schematic representation of the interatomic interactions described above. In the following subsections, the FFs of choice are discussed.

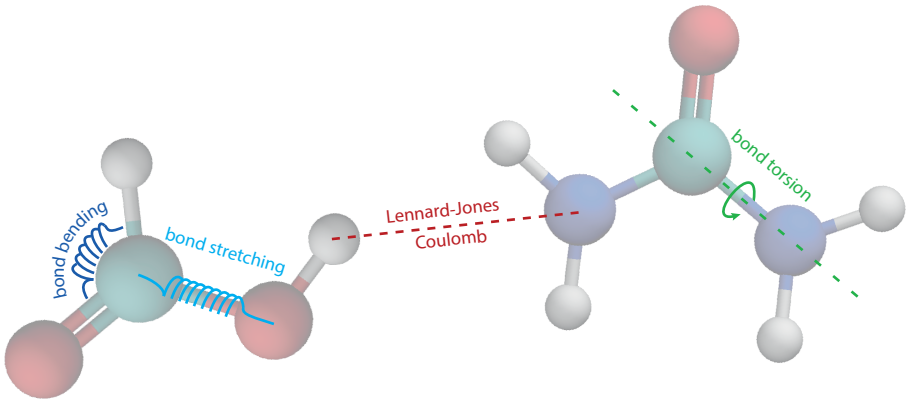

Figure 3.1: Schematic representation of the interatomic interactions, as modelled using equation 3.1. The represented molecules are formic acid (left) and urea (right).

3.1.1. Deep Eutectic Solvents

GAFF was used to model ethaline and reline. Several studies using GAFF to model DESs have been conducted [11, 19, 52, 53]. Perkins et al. [53] and Celebi et al. [19] demonstrated reasonable results using GAFF to model these DESs to determine their transport properties, both pure and in aqueous solutions. The parameters used in this study are equal to those of the studies of Celebi et al. [19] and Perkins et al. [53], who determined the electrostatic potential using the HF/6.31G* level of theory. All the FF parameters used in this study are tabulated in appendix B.

Reduced charges are used, to account for charge transfer and polarization effects. IL studies showed that down-scaling of ion charges is essential in order to make reliable predictions on the dynamics. The reason is that reduction of electrostatic interactions allowed for faster ion dynamics with better correspondence to experimental data [54]. Borodin [55] identified that many-body polarisable FFs are needed to allow for the charge fluctuation in ions, in order to achieve reliable MD simulations. In polarizable FFs, the charges fluctuate depending on their position to relative to their neighbours. However, this results in computationally costly simulations and requires the development of new polarisable FFs for each newly studied IL. Therefore, in this study the effects of polarisation and charge transfer are not taken into account explicitly but only implicitly through ion charge scaling. Perkins et al. found best agreement with experimental density and transport data using scaled ion charges of $\pm$ 0.9 e and $\pm$ 0.8 e for ethaline and reline, respectively [53]. Therefore, these are the values used in this study.

3.1.2. Organic Solvents and Solutes

Carbon dioxide is modelled using the transferable potentials for phase equilibria-flex (TraPPE-flex) FF. The parameters are taken from a study by Aimoli et al. [56]. Methanol is modelled using TraPPE-UA, in which the carbon atom and its bonded hydrogen atoms are modelled as one united atom, as proposed

by Chen et al. [57]. OA is modelled using the OPLS FF, with parameters taken as proposed in the study by Doherty et al. [58]. FA is modelled as proposed by Salas et al. [59], who determined the values to reproduce the dielectric constant, surface tension and density of pure PC at different temperatures. It was slightly modified by our group, by setting finite σ and ϵ value to the hydrogen atom H_F2. PC is modelled using GAFF, with the help of antechamber python parser interface (ACPYPE) [60], a python wrap of antechamber [61]. Charges are used as determined at the 6.31G* level of theory by Silva et al. [62]. PC exists as 2 enantiomers. Simulations have been performed to compare the viscosity, self-diffusivity and the density of racemic and enantiopure PC. The comparison is shown in Appendix F. The differences are considered negligible. For all reported results related to PC, simulations were performed with enantiopure (S)-PC.

3.2. Molecular Dynamics Simulations

MD simulations of the DESs ethaline and reline, mixed with the organic solvents methanol and PC, were performed over the entire range of mole fractions, at 298.15 K and atmospheric pressure. Reline - PC mixtures were excluded, as these do not mix well. Furthermore, distinct simulations were performed of the aforementioned mixtures including 5 additional molecules of carbon dioxide, formic acid or oxalic acid, at the same thermodynamic conditions. For clarity, the reported mole fractions neglect the fraction of solutes. This is considered legitimate, as the concentrations of these solutes are low. By cross-checking simulations with and without solutes, no correlation between the addition of the solutes and the values of the transport properties was found. Thereby, this assumption is valid. The number of molecules of each simulation can be found in table 3.1, including the size of the initial cubic simulation box. The box lengths before calibration were set based on estimations using the expected density (interpolated) from literature, added by 3 or 4 Å to avoid atom-overlap. Initial configurations were made using the software tool packmol [63].

In this study, one mole of DES is defined as the sum of the constituents divided by the number of constituents. Ch^+ and Cl^- are considered distinct molecules in this definition. Since both reline and ethaline are modelled at their eutectic ratio of HBA:HBD = 1:2, this results in the used definition of molar mass of DES M_{DES}:

$$M_{\mathrm{DES}} = \frac{1}{4}M_{\mathrm{Ch^+}} + \frac{1}{4}M_{\mathrm{Cl^-}} + \frac{1}{2}M_{\mathrm{HBD}} \tag{3.5}$$

where $M_{\mathrm{Ch^+}}$ is the molar mass of choline, $M_{\mathrm{Cl^-}}$ is the molar mass of chloride, and M_{HBD} is the molar mass of the hydrogen bond donor. Please note that different definitions are used in literature, therefore conversion calculations were made for the comparison with literature data. Since $M_{\mathrm{Ch^+}}$ = 104.170 g/mol, $M_{\mathrm{Cl^-}}$ = 35.453 g/mol, M_{urea} = 60.055 g/mol and M_{EG} = 62.070 g/mol, the molar masses of the DESs are M_{Reline} = 64.933 g/mol and M_{Ethaline} = 65.941 g/mol.

LAMMPS (version December 2018) [50] was used for the MD simulations. Periodic boundary conditions were employed in all directions. To calculate the long-range electrostatic potentials, the particle-particle particle-mesh (PPPM) method, with a relative error of 10^{-6}, was used. Cut off radii were set to 12 Å for Lennard-Jones and short-range electrostatic interactions. The Lorentz-Berthelot mixing rules were employed for interactions between different atom types. The Verlet algorithm was used to integrate Newton's equations of motion, with a time step of 1 fs.

The required data sampling was done in the canonical (NVT) ensemble. However, to get there, a series of steps were performed. First, the energy of the system is minimized by the conjugate-gradient method, to a tolerance of 10^{-4} in a maximum of 1000 steps. Next, the system evolves for 5 to 17 ns (depending on the modelled composition), in the isothermal-isobaric (NPT) ensemble. A Nosé-Hoover thermostat and barostat are employed. The volume over the last 100 ps is averaged, and set as the box size for the successive simulation steps. The calculated density is a direct result of this volume. Following, the system is equilibrated in the canonical (NVT) ensemble for 1 to 2 ns (again depending on the modelled composition). A Nosé-Hoover thermostat is employed. At this point, five equivalent simulations with different random seed numbers are made. The energy is minimized, by gradually increasing the time step from 0.0001 to 1 fs, in 13 increments, each for 10,000 time steps, followed by 500 to 2000 ps. Lastly, the required data for the transport property calculations are gathered during a production run in the canonical ensemble during 10 ns for mixtures and pure solvents, and 100 ns for pure DESs. The transport properties and RDFs were computed with the help of the OCTP (on-the-fly computation of transport properties) plugin for LAMMPS [18]. This plugin makes use of the Einstein

relations, together with the order-n algorithm [46], as modified by Dubbeldam [64]. By cross-checking the results of simulations with and without solutes, for non-solute related transport properties and RDFs, it was found that all values are reasonably close, and no notable discrepancies were found. Therefore, reported values of non-solute related properties were based on averages of all of these simulations. Uncertainties for all calculated transport properties were calculated as the standard deviation of the aforementioned equivalent simulations.

Table 3.1: The number of molecules of each simulation setup and the initial cubic simulation box length, before calibration. PC and DES are abbreviations for propylene carbonate and deep eutectic solvent, respectively. 4 molecules of DES are equal to 1 molecule of choline, 1 molecule of chloride and 2 molecules of the hydrogen bond donor. Simulations including carbon dioxide, formic acid or oxalic acid are equal to those listed, except for an addition of 5 carbon dioxide, formic acid or oxalic acid molecules, respectively.

		Number of Molecules					
x_{DES}	DES	Solvent	Reline	Ethaline	Methanol	PC	Initial box length [Å]
1	Ethaline	-		800			47
1	Reline	-	800				46
0	-	Methanol			800		41
0	-	PC				400	42
0.1	Ethaline	Methanol		400	3600		69
0.2	Ethaline	Methanol		400	1600		57
0.4	Ethaline	Methanol		400	600		49
0.6	Ethaline	Methanol		500	333		49
0.8	Ethaline	Methanol		600	150		49
0.1	Ethaline	PC		100		900	55
0.2	Ethaline	PC		200		800	54
0.4	Ethaline	PC		300		450	50
0.6	Ethaline	PC		500		333	50
0.8	Ethaline	PC		600		150	47
0.1	Reline	Methanol	400		3600		68
0.2	Reline	Methanol	400		1600		55
0.4	Reline	Methanol	400		600		46
0.6	Reline	Methanol	500		333		45
0.8	Reline	Methanol	600		150		44

3.3. Computation of Transport Properties

To calculate transport properties from the motion of molecules over time, the Einstein method is used in an equilibrium molecular dynamics (EMD) simulation environment. Alternatively, non-equilibrium molecular dynamics simulations (NEMD) could be used. Hereby, the system is subjected to external flows or driving forces, after which the transport properties are determined by investigating the system's response. NEMD simulations generally require fewer simulation steps to acquire statistically sufficiently good transport properties, due to a much larger signal to noise ratio [65]. However, in EMD, multiple transport properties can be calculated simultaneously. Furthermore, the resulting properties from NEMD highly depend on the applied driving force [65]. Therefore, EMD is the method of choice in this study.

The Einstein method is described as:

$$\gamma = \frac{\langle (A\,(t) - A\,(0))^2 \rangle}{2t} \tag{3.6}$$

where γ is the desired transport coefficient, A is its corresponding dynamic variable, t is time, and the angle brackets $\langle\rangle$ denote the ensemble average [46]. At large t, the relation between t and the mean-squared displacement (MSD) of A, $\langle (A(t) - A(0))^2$, is linear. This slope provides the desired transport coefficient [18]. To judge the linearity condition, the MSD is plotted as a function of t on a log-log scale, where the linearity condition is satisfied for a slope of 1. In this study, a slope was considered valid between 0.9 and 1.1. The slope-1 criterion also allows the user to determine if the simulation has

evolved over sufficient time. An example of a log-log plot of an MSD for diffusivity of the Cl^- anion in a 20 mol% mixture of reline with methanol is provided in Figure 3.2. To be robust for small discontinuities of the MSD at increasing sampling order, the average value of the slope at three consecutive data points is used to calculate the slope instead of linear regression. In preliminary calculations, the difference for these two methods in the calculated slope in continuous regions was considered negligible. In the following subsection, a efficient way of sampling is introduced. Next, the computation of the transport properties viscosity, self-diffusivity and ionic conductivity are specified.

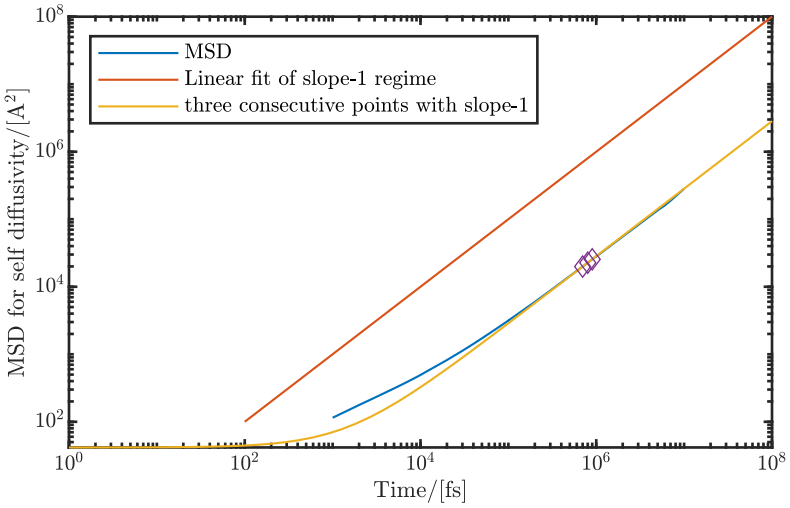

Figure 3.2: The mean-squared-displacement (MSD) related to the self-diffusivity of chloride in ethaline-methanol with x_{DES} = 0.2. The three consecutive data points with a slope closest to unity were found to be at most 0.027 off unity. The self-diffusivity was calculated to be 6.97×10^{-10} m^2/s, at 298 K and 1 atm.

3.3.1. Order-*n* algorithm

Conventionally, the ensemble averages of equation 3.6 are sampled at a fixed frequency [46]. Many systems incorporate a broad range of dynamic timescales. To sample at a high frequency is inefficient in terms of computational resources and data storage. The order-n algorithm has been introduced to sample at decreasing frequencies, thereby capturing fast and slow dynamics, with a decrease of required computational resources. Please refer to section 4.4.2 of the book 'Understanding Molecular Simulation' by Frenkel and Smith [46] for more information about the order-n algorithm. In this study, the OCTP plugin for LAMMPS is used to calculate the MSDs [18], which uses the order-n algorithm as modified by Dubbeldam et al. [64]. The plugin is capable of computing the self- and the Maxwell-Stefan-diffusivity, the shear and bulk viscosity, and the thermal conductivity. Furthermore, it can provide radial distribution functions (RDFs). It was found by Celebi et al. [66] that for aqueous mixtures of reline and ethaline, the thermal conductivity computed through EMD, was almost an order of magnitude lower compared to more accurate values found by NEMD. In this study, the scope is limited to density, viscosity, self-diffusivity and RDF.

3.3.2. Viscosity

The dynamic viscosity, or shear viscosity (η), can intuitively be seen as a measure of resistance of a fluid to flow. In EMD, it can be computed from the integral over the autocorrelation function of the off-diagonal pressure tensor components [51, 65]:

$$\eta_{\alpha\beta} = \lim_{t\to\infty} \frac{1}{2t} \frac{V}{k_{\mathrm{B}}T} \left\langle \left(\int_0^t P_{\alpha\beta}\left(t'\right) \mathrm{d}t' \right)^2 \right\rangle \tag{3.7}$$

where V is the volume of the system, and α and B both denote x, y and z direction, in which $\alpha \neq \beta$. For isotropic systems, by definition the off-diagonal terms of the pressure tensor, and subsequently the

viscosity, are equal for all dimensions ($P_{\alpha\beta} = P_{xy} = P_{xz} = P_{yz}$ and $\eta_{\alpha\beta} = \eta_{xy} = \eta_{xz} = \eta_{yz}$). To make use of this property and maximize the statistical quality for a given simulation, equation 3.7 is averaged over all dimensions [65]:

$$\eta = \lim_{t\to\infty} \frac{V}{2 * 10tk_{\mathrm{B}}T} \sum_{\alpha}\sum_{\beta} \left\langle \int_0^t P_{\alpha\beta}^{os}(t')\, dt' \right\rangle \tag{3.8}$$

with $P_{\alpha\beta}^{os}$ denoting the traceless, symmetric elements of the pressure tensor, given by:

$$P_{\alpha\beta}^{os} = \frac{P_{\alpha\beta} + P_{\beta\alpha}}{2} - \delta_{\alpha\beta}\left(\frac{1}{3}\sum_{k} P_{kk}\right) \tag{3.9}$$

where $\delta_{\alpha\beta}$ is the Kronecker delta, and P_{kk} the diagonal elements of the pressure tensor. Thereby, the term $\delta_{\alpha\beta}\left(\frac{1}{3}\sum_k P_{kk}\right)$ is simply the instantaneous kinetic pressure of the system. It should be noted that the MSD is a function of the properties of the system as a whole, whereas the MSD for the diffusion coefficient is based on the properties of each molecule. To determine the fluid's diffusion coefficient, the average value over all molecules in the system can be calculated. As a consequence, D_{self} is statistically more precise than η. For viscosity, the average value over only the three different shear directions can be used [51].

3.3.3. Self-Diffusivity

The self-diffusion coefficient (D_{self}) of a certain molecule of type i, in an isotropic system is defined as [51]:

$$D_{i,\mathrm{self}} = \lim_{t\to\infty} \frac{1}{2t}\frac{1}{3N_i} \left\langle \sum_{j=1}^{N_i} \left(\mathbf{r}_{j,i}(t) - \mathbf{r}_{j,i}(0)\right)^2 \right\rangle \tag{3.10}$$

where N_i is the total number of molecules of i in the system, and $\mathbf{r}_{j,i}$ is the 3 dimensional position of the j^{th} molecule of type i. The right-hand side of the equation is divided by a factor of 3, to average over the 3 dimensions [46].

In a study by Yeh and Hummer in 2004 [67], it was found that, for systems with periodic boundary conditions, the self-diffusion coefficient calculated through EMD is strongly dependent on the system size. They proposed a correction, later referred to as the Yeh-Hummer correction:

$$D_{\infty} = D_{\mathrm{MD}} + \frac{k_{\mathrm{B}}T\xi}{6\pi\eta L} \tag{3.11}$$

where D_{inf} is the corrected self-diffusion coefficient, D_{MD} is the size-dependent self-diffusion coefficient, k_{B} is the Boltzmann constant, L is the length of the cubic simulation box, T is the temperature, η is the shear viscosity and ξ = 2.837298 is a dimensionless constant. In this study, the viscosity calculated in MD was used.

As described in equation 3.10, the OCTP plugin calculates the MSD based on the position of the molecules. For each molecule, an atom is preassigned which represents the molecule position. The selected atoms are Cl for Cl^-, N for Ch^+, CEG for EG, C_U for urea, O_M for methanol, CP2 for PC, C_C for CO_2, C_F1 for FA and C_O1 for OA (atom labels can be found in appendix 6.3.

3.3.4. Ionic Conductivity

Using the obtained self-diffusion coefficients, the ionic conductivity (κ) can be calculated, according to the Nernst-Einstein relation:

$$\kappa = \frac{e^2}{k_{\mathrm{B}}TV}\sum_i N_i q_i^2 D_i \tag{3.12}$$

where i are the molecule types, e is the elementary charge, k_{B} is the Boltzmann constant, T is the temperature, V is the volume of the system, N_i is the total number of molecules of type i in the system, q_i is the charge of a molecule of type i and D_i is the self-diffusion coefficient of type i.

For non-ionic molecules, the charge is zero, thereby they do not contribute to the ionic conductivity. Integer charges were used for the ions. One might argue this is inconsistent with the scaled charges used in the force field for Coulombic interactions.

The Ionic conductivity could also be derived using the Green–Kubo or Einstein relations, which take into account the cross correlation of charge fluxes/displacements [68]. For this method, atomic trajectories would be required at a sufficient sampling frequency, and extensive subsequent post-processing must be performed. Therefore, for simplicity, the Nernst–Einstein relation was used in this work.

The Nernst-Einstein equation overpredicts the ionic conductivity by nature [69]. Several studies ascribe this difference to ion association [69, 70]. The ion association (ξ_{ion}), or more directly the ion dissociation (1-ξ_{ion}), is quantified by comparing the molar conductivity acquired by electrochemical impedance spectroscopy (EIS) with the molar conductivity calculated from ion diffusivities, measured by pulse field gradient nuclear magnetic resonance spectroscopy (PFG-NMR). The former measures the movement of the dissociated ions, while the latter measures the movement of all ions. This ion dissociation term is added as a factor to the right-hand side of equation 3.12. To the best of my knowledge, no method has been reported in the literature to calculate the ion dissociation using MD. A study by Celebi et al. used the scaled ion charges discussed in Section 3.1 in the Nernst-Einstein equation, resulting in a reduced calculated ionic conductivity [19]. Even though this might result in computed ionic conductivities closer to experimental data, it is not certain whether the assumption that charge transfer is the cause for reduced ionic conductivity is valid. Philippi et al. discussed this approach in two papers [71, 72]. Charge scaling is done independent of the DES concentration, whereas an ion dissociation factor would be dependent on DES concentration. This might lead to different trends of the ionic conductivity as a function of the mole fraction of DES for the two methods. The study by Nordness et al. [69] shows that the sensitivity of ion dissociation to mole concentration of ILs in organic solvents is dependent on the IL. In this study, the Nernst-Einstein equation is used without scaling, complemented with the side note that the scientific debate has not yet settled and different methods are applied in literature.

3.4. Radial Distribution Functions

Another useful property that can be obtained through MD is the radial distribution function (RDF) $g(r)$. It can be used to match MD simulations with experiments, since neutron, X-ray and light scattering experiments can yield information about $g(r)$. Besides, the measured values of the radial distribution function can be compared with theoretical predictions for pure liquids and mixtures, allowing to test a particular theory [46]. The RDF describes how the number density changes as a function of distance from a certain centre reference particle. It is calculated as the ratio between the number density $\rho(r)$ at a distance r from the reference particle and the number density at a distance r from a particle in an ideal gas at the same overall number density. From $\rho_{\mathrm{ave}} = N/V$ and $g(r) = \rho(r)/\rho_{\mathrm{ave}}$, equation 3.13 is derived:

$$g(r) = \frac{N_r}{\rho_{\mathrm{ave}} 4\pi r^2 dr} \tag{3.13}$$

where N is the total number of particles in volume V and N_r is the number of particles in a spherical shell of thickness dr at distance r. The OCTP plugin allows for the calculation of the RDF beyond the cutoff radius, which is not possible in the standard edition of LAMMPS. Furthermore, the plugin corrects for system-size effects, based on the work by Van der Vegt and co-workers [73–75]. The OCTP plugin calculates the distance r between atoms that are assigned by the user. The selected atoms are Cl for Cl^-, N for Ch^+, CEG for EG, C_U for urea, O_M for methanol, CP2 for PC, C_C for CO_2, C_F1 for FA and C_O1 for OA (atom labels can be found in Appendix 6.3). The selection was made to the atoms closest to the centre of mass. For OA and EG, the same atom labels are used for both central carbon atoms. As a result, the RDF for both atoms is calculated. An RDF peak between the two bonded atoms is generated during the simulation and removed afterwards.

In this study, the RDFs are sampled every 1000 time steps in the NVT-ensemble. Next, the average value over all equivalent runs is calculated. Since most mixtures are simulated with 5 equivalent simulations of 10 ns, a total of 50,000 samples are used. Many samples over time are required because the number of solutes is limited.

3.5. Hydrogen Bonds

The number of hydrogen bonds (HBs) between the DES constituents are calculated for varying mole fractions of DES. As criteria, a cut-off distance of 3.5 Å and angle of a cut-off distance of 3.5 Å between the donor-acceptor atoms and an angle of 30° between the donor−hydrogen−acceptor are used. Visual Molecular Dynamics (VMD) [76] and its HBonds plugin version 1.2 are used to count the number of HBs. Samples of equivalent simulations plus simulations containing solutes are combined to calculate the average number of HBs. To account for varying numbers of DES molecules, the values are normalized according to:

$$N_{\mathrm{HBs}} = \frac{100}{N_{\mathrm{HBD\ molecules}}} N_{\mathrm{HBs\ counted}} \tag{3.14}$$

where N_{HBs} is the corrected number of HBs, $N_{\mathrm{HBD\ molecules}}$ is the number of HBD molecules in the system and $N_{\mathrm{HBs\ counted}}$ is the average number of counted HBs before normalization. The number of HBs presented correspond to systems of 50 Cl^- anions, 50 Ch^+ cations, 100 HBD molecules and a number of organic solvent molecules dependent on the mole fraction of DES. Table 3.1 shows the number of DES and organic solvent molecules used in each simulation.

4

Results and Discussion

This chapter comprises all results, obtained as described in the previous chapter. First, the density of the mixtures is discussed in Section 4.1. Next, the viscosities are discussed in Section 4.2. The self-diffusivities of the mixtures and the solutes are discussed in Section 4.3. Based on these self-diffusivities, the ionic conductivities are calculated and presented in Section 4.4. A structural analysis, using radial distribution functions and a hydrogen bond analysis are performed in Sections 4.5 and 4.6, respectively. Lastly, several limitations of the applied methods are mentioned in Section 6.1.

4.1. Density

Figure 4.1 shows the computed densities of the mixtures ethaline-methanol, ethaline-PC and reline-methanol, as a function of mole fraction of DES. The data is in good agreement with the available experimental data by Wang et al. [77], Zafarani-Moattar et al. [78] and Haghbakhsh et al. [79]. The maximum absolute deviations are 1.2, 1.1, and 1.0% for reline-methanol, ethaline-methanol, and ethaline-PC, respectively. Interestingly, the over predictions are smaller for more equal DES-organic solvent ratio's, for all three types of mixtures. All density values can be found in appendix C. The accuracy was found to be too low to provide reliable excess molar volumes. However, from preliminary calculations, a similar trend for the relation of excess molar volume and mole fraction of DES was observed as acquired experimentally [80] for ethaline-methanol. Haghbakhsh [80] suggests the negative excess molar volume is due to the filling of free volumes with small methanol molecules and/or stronger hydrogen bonds between ethaline-methanol than between ethaline-ethaline and methanol-methanol.

4.2. Viscosity

In figure 4.2 the computed viscosities of reline-methanol, ethaline-methanol, and ethaline-PC mixtures as a function of mole fraction of DES are shown. The average viscosity values, standard deviations and number of converged simulations are presented in Appendix C. The obtained results for ethaline-methanol are compared with experimental results by Wang et al. [77] over the entire range of mole fractions. To the best of my knowledge, no literature viscosity data of reline-methanol is available at 298 K, therefore only experimental viscosity of pure reline is plotted [81]. In the case of ethaline-PC, literature data was only available in the range from x_{DES} = 0 to 0.21 [77]. All computed viscosities are listed in Appendix C. The maximum deviations between experimental viscosity and the values found in this study are for pure DESs. For pure ethaline and reline, these deviation are significant, at 31 and 39%. As shown in figure 4.2, the viscosities of all types of mixtures increase monotonically with increasing DES content. Reline is more viscous than ethaline, and propylene carbonate is more viscous than methanol. Especially for reline, the viscosity is drastically reduced by the addition of a mole fraction of 0.2 of methanol: from 455 to 72 MPa · s, whereas ethaline is reduced from 62 to 21 MPa · s for the same addition of methanol. By addition of a mole fraction of 0.2 of PC to pure ethaline, the viscosity is only reduced to 33 MPa · s. This difference in sensitivity might be explained by the difference in molecule size. Molecular size-asymmetry is know to cause complex viscosity behaviour [82]. Celebi et al. reported similar decreases in viscosity by small additions of water for reline and ethaline [19]. By

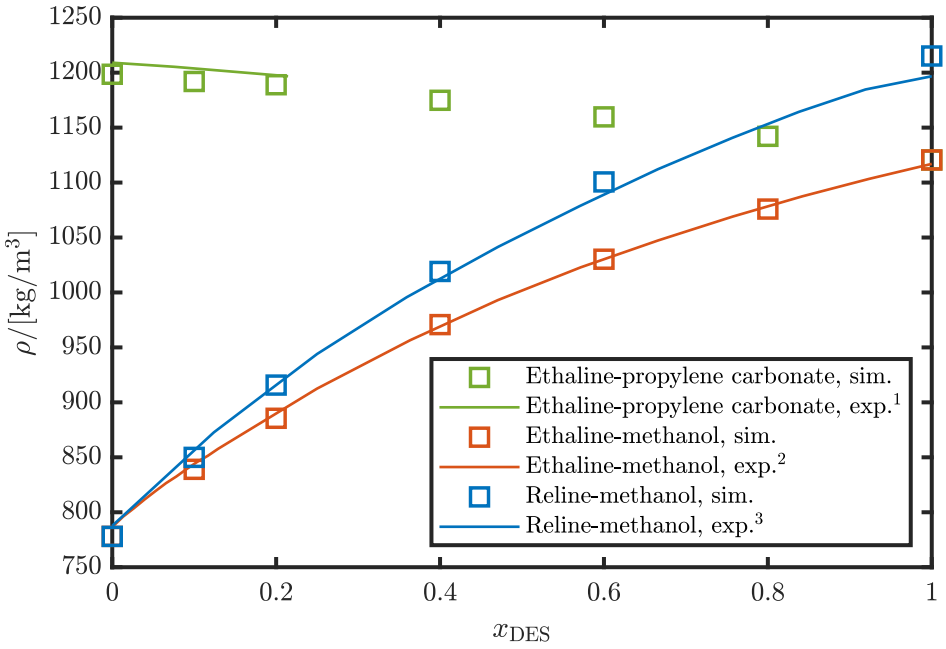

Figure 4.1: Densities of the mixtures ethaline-propylene carbonate, ethaline-methanol and reline-methanol, as a function of mole fraction of Deep Eutectic Solvent, at 298 K and 1 atm. [1]Experiments by Zafarani-Moattar et al. [78]. [2]Experiments by Wang et al. [77]. [3]Experiments by Haghbakhsh et al. [79].

addition of 5% mass fraction of water, the viscosities reduced approximately 83 and 30% for reline and ethaline at 303.15 K, respectively.

4.3. Self-Diffusivity

A comparison is made between the obtained results and experimental and computational literature data for the limit cases of pure DESs and pure organic solvents in Figures 4.3 and 4.3, respectively. Deviations to the experimental data [81] are similar to the simulation data for ethaline [53]. The maximum deviations, calculated over all reported constituents and all available experimental data, are 38, 14, 32 and 58% for PC, methanol, reline and ethaline, respectively. The self-diffusivities are considered in poor agreement with experimental data but fine agreement with other simulation studies. To the best of my knowledge, no experimental or simulation data is available of the self-diffusivities of the relevant mixtures, and no simulation data is available of the self-diffusivities of neat reline at 298 K. There is a paper by Kumar et al. [88] reporting the self-diffusivity of methanol in methanol-ethaline mixtures at different concentrations at 303 K, however, it has not been peer-reviewed and does not apply system-size corrections. Nevertheless, qualitatively, the trend of the self-diffusivity of methanol as a function of mole fraction of DES does look similar to this study.

Self-diffusivities are reported for the constituents of the DES-organic solvent mixtures over the entire concentration range in Figure 4.5. The self-diffusivities of all constituents decrease monotonically for increasing DES concentration. The self-diffusivities of the organic solvents are higher than the self-diffusivities of the HBDs and ions, except for ethaline-PC at a mole fraction of ethaline of 0.8 and higher. Ch^+ is the least mobile constituent. The fact that HBDs are more mobile than Ch^+ over the entire concentration range, can be related to their difference in size and mass (62.07 g/mol for EG, 60.066 g/mol for urea and 104.17 g/mol for Ch^+). The self-diffusivity of EG is higher than that of Cl^-, even though it is heavier. Perkins et al. [53] suggest that this is due to strong hydrogen bonds between EG-EG and EG-anion. Interestingly, in reline-methanol, the self-diffusivity of urea is only higher than Cl^- up to a mole fraction of methanol of 0.2. Celebi et al. found similar behaviour for reline-water mixtures, up to 20% mass fraction of water, and attribute this to the depletion of hydrogen bonds in diluted DES.

By the addition of a mole fraction of methanol of 0.9 to reline, the self-diffusivities increase by a

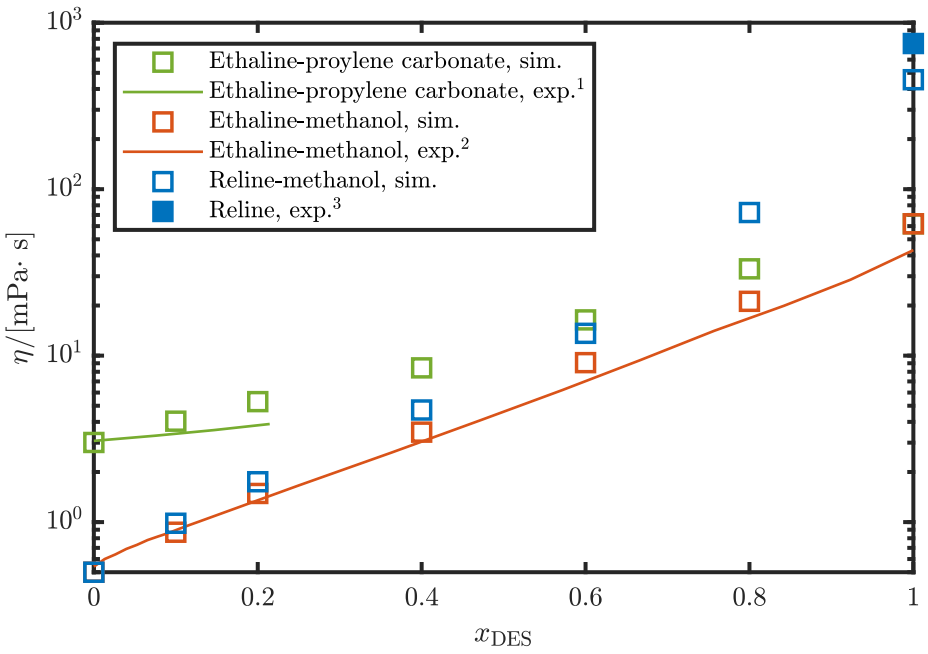

Figure 4.2: Viscosities of the mixtures ethaline-propylene carbonate, ethaline-methanol and reline-methanol, as a function of mole fraction of Deep Eutectic Solvent, at 298 K and 1 atm. [1]Experiments by Zafarani-Moattar et al.[78]. [2]Experiments by Wang et al. [77]. [3]Experiments by D'Agostino et al. [81]. Error bars are excluded for clarity. Standard deviations are presented in appendix C.

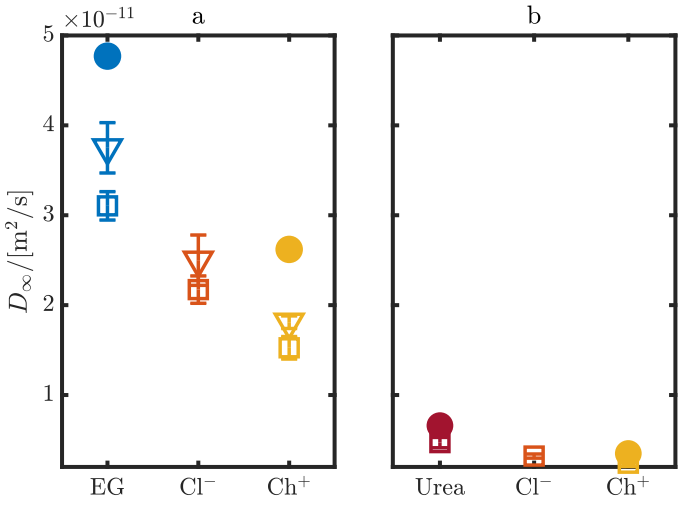

Figure 4.3: Self-diffusivities of the pure DES constituents ethylene glycol (EG), chloride (Cl^-), choline (Ch^+) and urea in ethaline (a) and reline (b), at 298 K and 1 atm. Open squares denote simulation data from this study, solid circles denote experimental data [81] and downward triangles denote simulation data [53]. Colours are constituent-specific, as labelled on the horizontal axis.

factor of 206 for urea, 305 for Cl^- and 346 for Ch^+. Likewise, by diluting ethaline with a mole fraction of methanol of 0.9, the self-diffusivities increase by a factor of 39 for EG, 39 for Cl^- and 52 for Ch^+. Finally, by adding a mole fraction of PC of 0.9 to pure ethaline, the self-diffusivities increase by a factor of 9 for EG, 9 for Cl^- and 11 for Ch^+. Celebi et al. reported similar factors for reline and ethaline mixed with water [19]. For an increase of mass fraction of water of 0 to 80% in a reline-water mixture at 303.15 K, the self-diffusivities increased 439, 319 and 243 times for Cl^-, Ch^+ and urea, respectively.

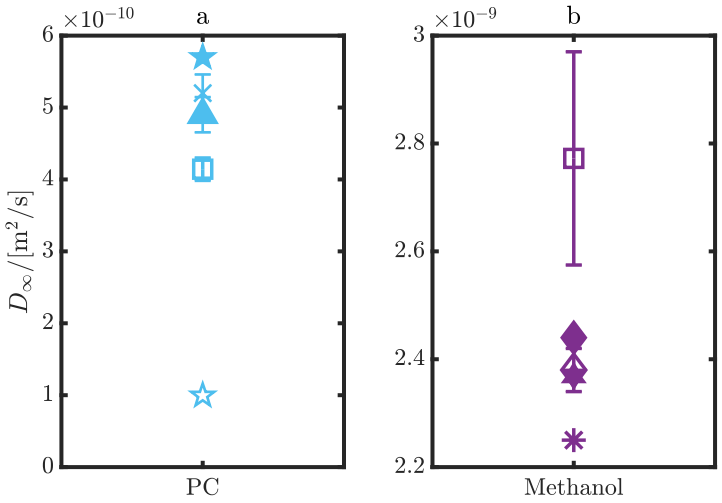

Figure 4.4: Self-diffusivities of the pure organic solvents propylene carbonate (PC) and methanol, at 298 K and 1 atm. Open squares denote simulation data from this study, solid and open pentagrams denote experimental and simulation data, respectively [83], solid upwards triangle denotes experimental data [84], the cross denotes experimental data [85], solid and open diamonds denote experimental and simulation data, respectively [86] and asterisk denotes simulation data [87]. Colours are constituent-specific, as labelled on the horizontal axis.

For the same addition of water to ethaline, the self-diffusivity of Cl^- increased 43 times. These large reductions, especially for reline-water, are attributed to the disappearance of hydrogen bonds.

Figure 4.6 shows the self-diffusivities of the solutes OA, FA and CO_2 in the DES-organic solvent mixtures over the entire concentration range. All self-diffusivities decrease monotonically for increasing mole fraction of DES. For all mixtures and concentrations, self-diffusivities follow. Note that, as discussed in Section 3.2, the mole fractions are defined as the fraction of DES in the mixture of DES and organic solvent without the solutes, since the solute fraction is considered negligible. Subsequently, self-diffusivities of solutes can be reported for x_{DES} = 0, 1. To the best of my knowledge, no experimental data is available for self-diffusivities of these components in methanol, PC, reline and ethaline at atmospheric conditions.

Addition of a mole fraction of reline of 0.8 to methanol, yields a decrease of self-diffusivities of 52, 48 and 111 times for CO_2, FA and OA, respectively. By the addition of a mole fraction of ethaline of 0.8 to methanol, a decrease of self-diffusivities of 29, 23 and 24 times for CO_2, FA and OA, are found respectively. Lastly, the self-diffusivities of PC decrease a factor of 6, 9 and 10 after addition of a mole fraction of ethaline of 0.8 for CO_2, FA and OA, respectively. Interestingly, the self-diffusivity of OA relative to the other constituents behaves differently for the three DES-organic solvent combinations. First in ethaline-PC mixtures, for ethaline mole fractions greater than 0.6, the self-diffusivity of OA is lower than that of EG. For pure ethaline, the self-diffusivity of OA is even lower than the self-diffusivity of Cl^-. Self-diffusivities of EG are within the standard deviation of self-diffusivities of OA for ethaline mole fractions below 0.6. This is remarkable, considering the difference in mass (62 g/mol for EG vs 90 g/mol for OA). At higher ethaline concentrations, the hydrogen bonds play a more significant role, slowing down oxalic acid more severely than EG and Cl^-. Second, in ethaline-methanol mixtures, for mole fractions of DES of 0.8 and lower, the self-diffusivity of OA is much higher than the self-diffusivities of the DES constituents, exhibiting similar mobility to methanol. At high ethaline concentrations, hydrogen bonds seem to decrease the self-diffusivity of oxalic acid more strongly than the other constituents. Lastly, in reline-methanol mixtures, OA self-diffusivity is similar to those of urea and Cl^-. At high reline concentrations, it seems that OA self-diffusivity is even lower than that of all other constituents, although it should be noted that standard deviations are large for these simulations, due to the sparse dynamics. FA is more mobile than OA in the same mixtures, however, at low concentrations of DES this difference is small (within standard deviations).

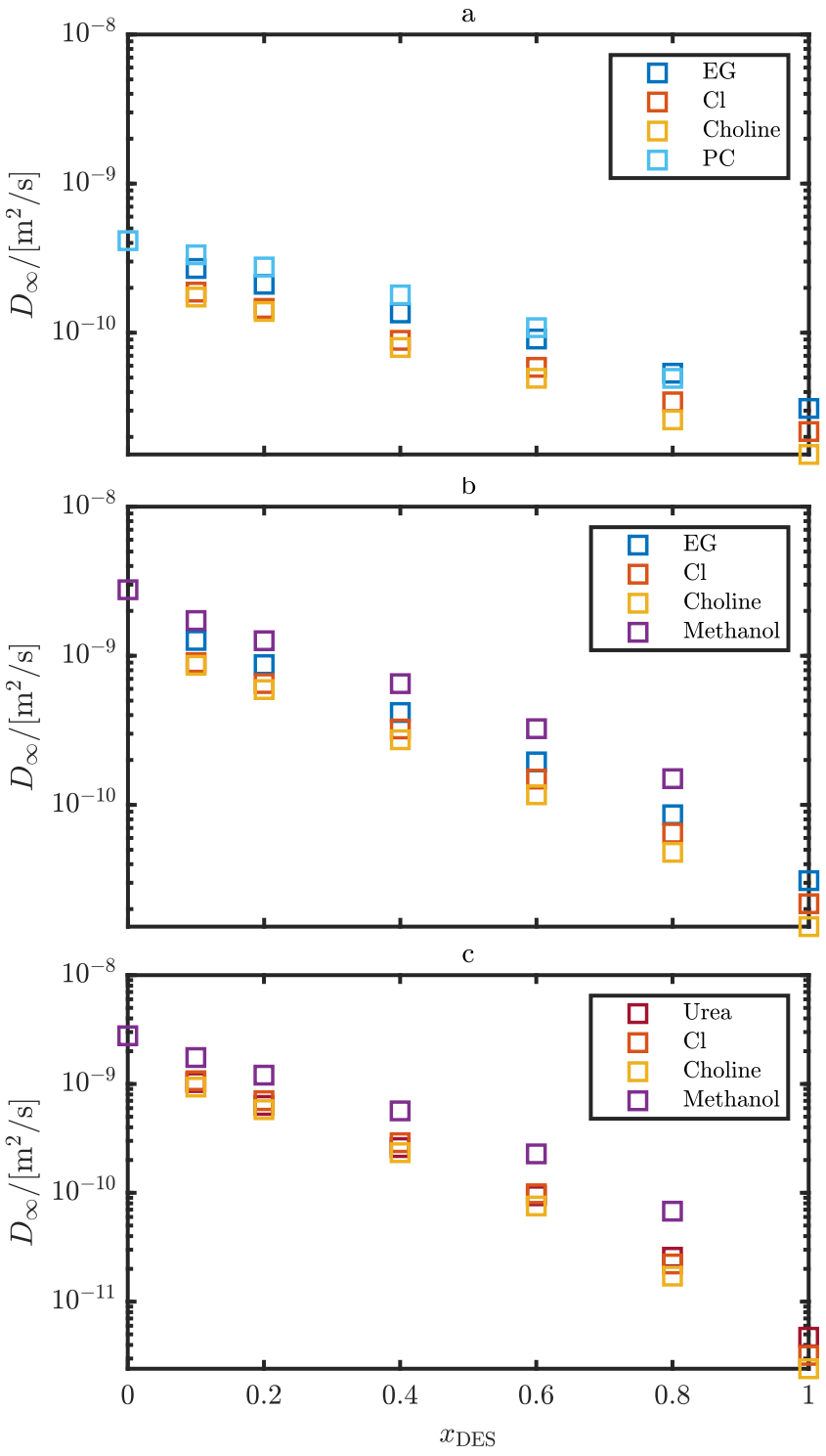

Figure 4.5: Self-diffusivities of the constituents of the mixtures ethaline-propylene carbonate (a), ethaline-methanol (b) and reline-methanol (c) as a function of mole fraction of deep eutectic solvent (DES), at 298 K and 1 atm. Error bars are excluded for clarity. Standard deviations are presented in appendix C.

4.4. Ionic Conductivity

As discussed in Section 3.3, ionic conductivities are calculated based on the Nernst-Einstein equation. To the best of my knowledge, there is no experimental or simulation data available of ionic conductivities of these mixtures. As the Nernst-Einstein equation is known to generally over-predict the ionic

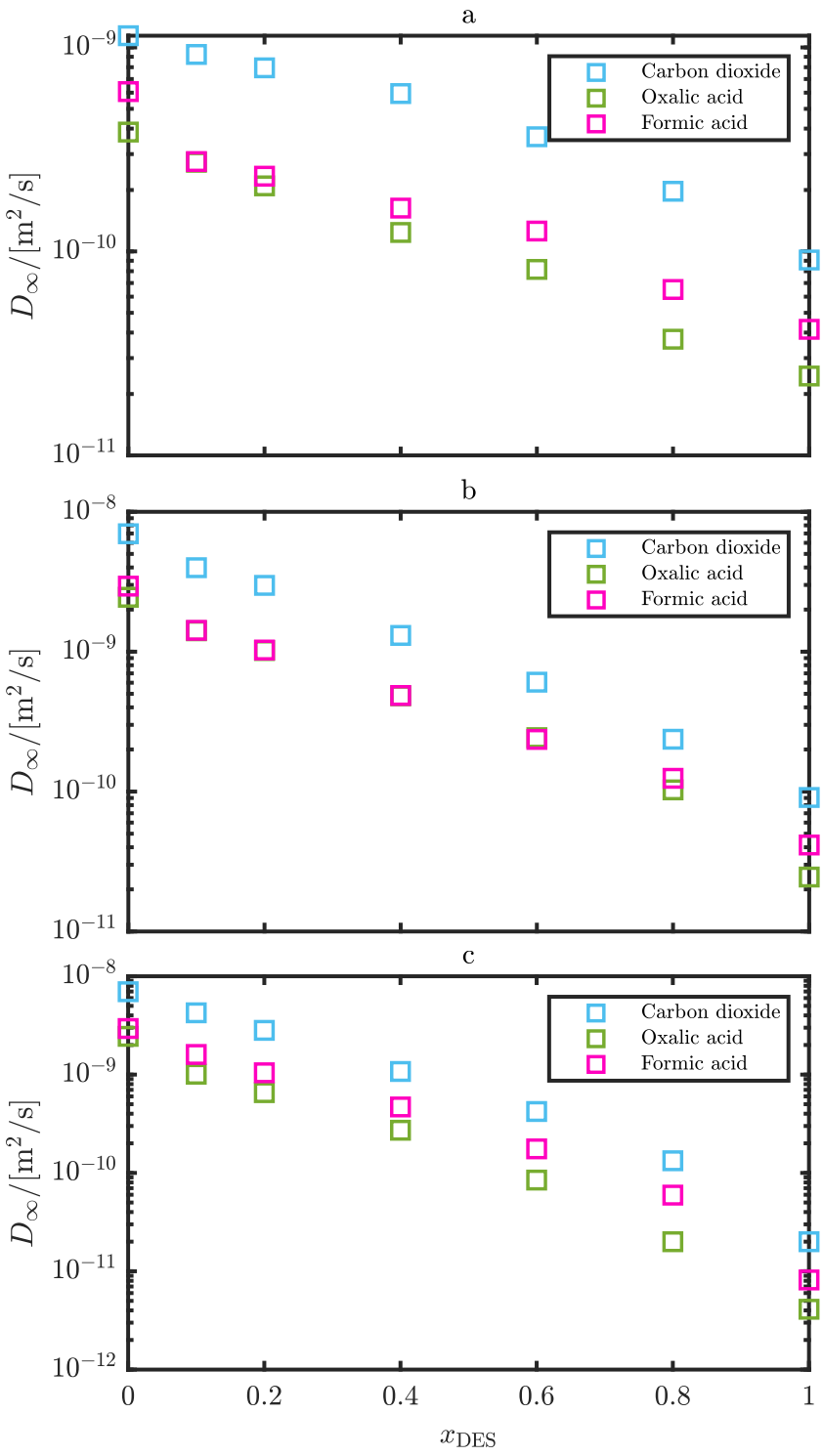

Figure 4.6: Self-diffusivities of solutes carbon dioxide, oxalic acid and formic acid in the mixtures ethaline-propylene carbonate (a), ethaline-methanol (b) and reline-methanol (c) as a function of the mole fraction of deep eutectic solvent (DES), at 298 K and 1 atm. Error bars are excluded for clarity. Standard deviations are presented in appendix C.

conductivity [69], and the self-diffusivities used in the calculation have shown to deviate up to 58% for known cases (Section 4.3, the results should be interpreted mostly qualitatively. Ionic conductivity of pure reline has been measured experimentally at 303 K to be 0.23 S/m [89], whereas in this study a value of 0.11 S/m at a temperature of 298 K has been obtained. Simulation data is available at 303 K for

pure reline, at 0.09 S/m. The simulation setups are similar, however, it should be noted that their calculations were based on the Nernst-Einstein equation using scaled charges, instead of integer charges, responsible for a 0.64 times smaller calculated ionic conductivity (please refer to Section 3.3.4 for details). For ethaline, ionic conductivity data was reported to be 0.763 S/m at 298 K, whereas the value calculated in this study is 0.63 S/m. Figure 4.7 shows the calculated ionic conductivities of the mixtures reline-methanol, ethaline-methanol and ethaline-PC. As defined by the Nernst-Einstein equation, the ionic conductivity is 0 in absence of ions, which is valid for x_{DES} = 0 (the markers overlap in the figure). For all mixtures, the ionic conductivity as a function of mole fraction is non-monotonic. For increasing x_{DES}, the ionic conductivity initially increases, peaks at a mole fraction dependent on the mixture, and decreases. Mixtures containing methanol exhibit higher ionic conductivity than the mixture with PC. Considering the Nernst-Einstein equation, all input parameters are equal for ethaline-methanol and ethaline-PC, except for the self-diffusivities and the number densities of the ions. At the mole fraction corresponding with the peak of ionic conductivity of ethaline-methanol, x_{DES} = 0.2, the number density difference is responsible for a factor of 1.8. The differences in self-diffusivities of the ions are a factor of 1.9 and 2.2 for the anion and cation, respectively. The ionic conductivity behaves non-monotonically because there are two competing attributions; For increasing x_{DES}, the self-diffusivity decreases, while the concentration of ions decreases. Since the increase in mobility by diluting ethaline with an organic solvent is smaller for PC than for methanol, the peak of ionic conductivity of ethaline-PC is shifted towards higher x_{DES} compared to ethaline-methanol.

Remarkably, the ionic conductivity of both methanol mixtures peak at approximately x_{DES} = 0.2, yet the most conductive solution is different at both sides of the peak. Reline-methanol is more conductive at a low mole fraction of DES, while ethaline-methanol is more conductive for higher mole fractions of DES. The sum of the diffusivities of the ions is higher for ethaline, while the density is slightly lower. It should be noted that when scaled charges are used in the Nernst-Einstein equation, as discussed in Section 3.3.4, the ion conductivity of reline is scaled by a factor of 0.64, while ethaline is scaled by a factor of 0.81.

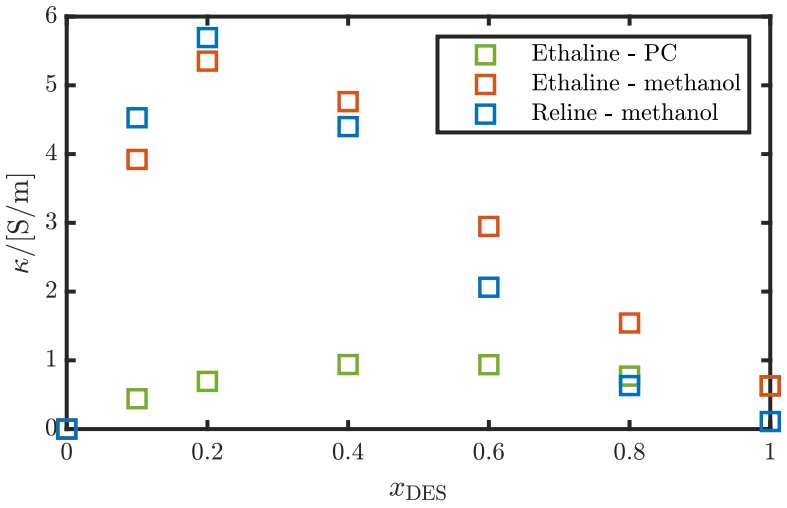

Figure 4.7: Ionic conductivity of reline-methanol, ethaline-methanol and ethaline-propylene carbonate (PC) mixtures as a function of mole fraction of deep eutectic solvent (DES), at 298 K and 1 atm. For all mixtures at x_{DES} = 0, κ = 0 due to absence of ions (not visible since the markers overlap). Error bars are excluded for clarity. Standard deviations are presented in appendix C.

4.5. Radial Distribution Functions

For each of the mixtures reline-methanol, ethaline-methanol and ethaline-PC, 22 RDFs can be plotted, at varying concentrations. A selection is made to be discussed in this chapter. Section 4.5.1 compares the cation-anion and anion-HBD interaction in the three mixtures and the mixtures with water earlier reported by our group because a different effect of addition of organic solvent is observed. The interaction of CO_2 with the solvent components are considered of most interest for the capture and

conversion of CO_2. RDFs of CO_2 with solvent components are discussed in Section 4.5.2. The RDFs of the solutes FA and OA in ethaline-PC mixtures are discussed in Section 4.5.3 because they show remarkable behaviour. The RDFs of the remaining constituent combinations are included in Appendix D.

4.5.1. Anion-Cation and Anion-Hydrogen Bond Donor

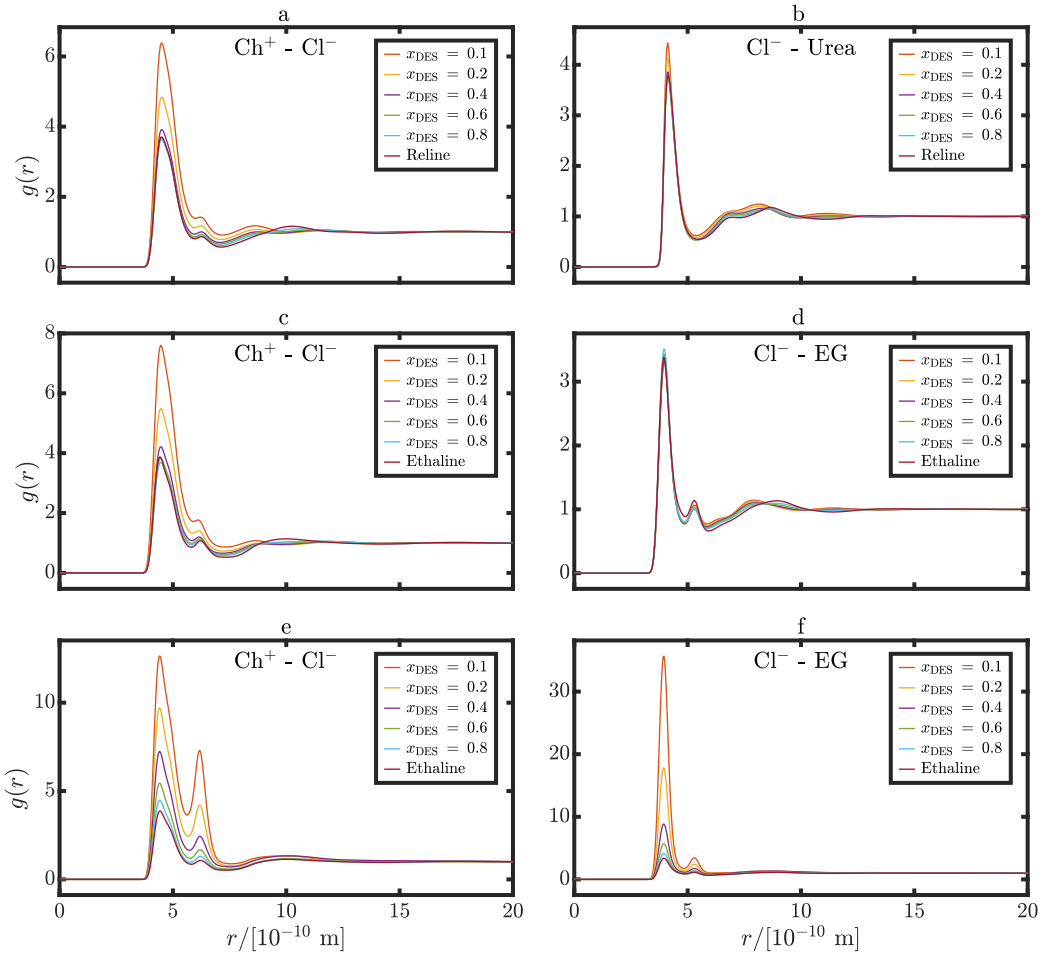

Figure 4.8: Radial distribution functions between choline-chloride (left) and the hydrogen bond donors (urea and ethylene glycol)-chloride (right) in the mixtures reline-methanol (top), ethaline-methanol (middle) and ethaline-propylene carbonate (bottom) at different mole fractions of deep eutectic solvent (DES), at 298 K and 1 atm. Line colours are consistent for all subfigures, both DESs use the same colours.

The RDFs between Ch^+-Cl^- and Cl^--HBD in the mixtures reline-methanol, ethaline-methanol and ethaline-PC are shown in Figure 4.8. Remarkably, the RDF peak intensity of Cl^--HBD barely changes as a function of the mole fraction of methanol (Figures 4.8b,d). In contrast, the corresponding peak intensity in ethaline-PC (Figure 4.8f) increases significantly for the addition of PC. The RDF peak intensities of Ch^+-Cl^- increases for the addition of organic solvent in all three mixtures (Figure 4.8a,c,e), indicating increased intermolecular interactions. For ethaline-PC, the change is the most significant. A second peak is present in all three mixtures and is also most pronounced in the mixture ethaline-PC for high concentrations of PC.

In an earlier study by our group [19], the RDFs of reline-water and ethaline-water are investigated. Remarkable differences comparing the addition of water to methanol and PC, are found in the RDFs between Ch^+-Cl^- and Cl^--HBD, for both reline and methanol. With the addition of water, the RDF peak intensities between Ch^+-Cl^- and Cl^--HBD decrease, quite significantly in the case of Cl^--HBD, indicating weaker intermolecular interactions for increasing water concentrations. For electrochemical

applications, anion-cation interaction might indicate ion association. As discussed in Section 3.3.4, ion association has a negative effect on conductivity. Experimental studies measuring the ionic conductivity of the mixtures could be conducted to test this effect.

The first and second RDF peaks between Ch^+-Cl^- are located at a distance of 4.5 and 6.2 Å for reline-methanol, 4.5 and 6.1 Å for ethaline-methanol and 4.4 and 6.2 Å for ethaline-PC, respectively. The first RDF peaks between Cl^--EG are located at a distance of 4.1 Å for reline-methanol, 4.0 Å for ethaline-methanol and 3.9 Å for ethaline-PC. The second RDF peaks of ethaline-methanol and ethaline-PC are both located at a distance of 5.3 Å. No peak shift is observed for varying mole fractions.

4.5.2. CO_2

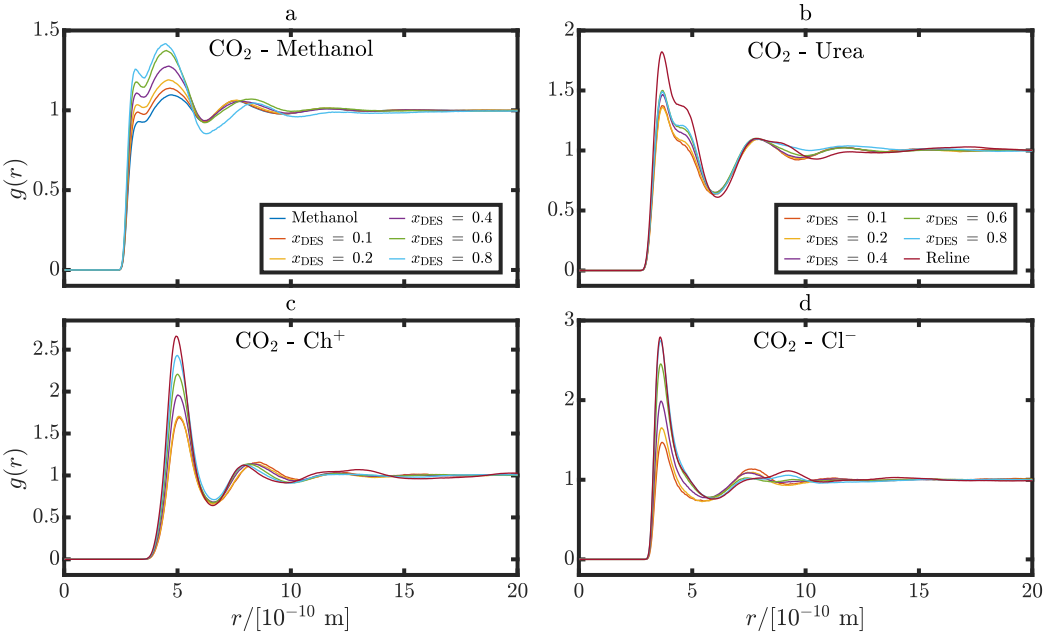

Figure 4.9: Radial distribution functions of (a) carbon dioxide-methanol, (b) carbon dioxide-urea, (c) carbon dioxide-choline, (d) carbon dioxide-chloride in reline-methanol mixtures at different mole fractions of reline, at 298 K and 1 atm. Line colours are consistent for all subfigures.

Figure 4.9 shows the RDFs of CO_2 with the solvent components methanol (a), urea (b), Ch^+ (c) and Cl^- (d). For all RDFs, the intensity of the first peak decreases with the addition of methanol. This is an indication that the interactions between these molecules become weaker as the mole fraction of reline decreases. The RDF of CO_2-Methanol (Figure 4.9a) shows a maximum at its second peak. Both the first and second peak intensity decreases by the addition of methanol, while the first peak almost vanishes for pure methanol. It should be noted that the RDF peaks of CO_2-Ch^+ and CO_2-Cl^- are the highest for high concentrations of ethaline and are therefore the most effective on the characteristics of CO_2 dissolved in reline. However, by diluting with methanol, those peaks show the greatest decline and become less effective. The RDF between CO_2-EG is mildly affected by the addition of methanol. It is characterized by a sharp peak, which continues as a bulge that is less pronounced and almost vanishes for increasing methanol mole fraction. The first peaks of RDFs between CO_2-urea, CO_2-Ch^+ and CO_2-Cl^- are placed at approximately 3.6, 4.9 and 3.5 Å, respectively. The first two RDF peaks of CO_2-methanol are located at a distance of 3.1 and 4.6 Å. No peak shift for the addition of methanol is found.

Figure 4.10 shows the RDFs of CO_2 with the solvent constituents of ethaline-methanol. The intensity of the first RDF peaks between CO_2-EG, CO_2-Ch^+ and CO_2-Cl^- decrease with the addition of methanol, as shown in Figures 4.10b,c,d. This indicates that the interactions between these molecules become weaker as the mole fraction of ethaline decreases. The RDF of CO_2-Methanol (Figure 4.10a) shows a maximum at its second peak, similar to reline-methanol. The peaks of CO_2 with the ions are the highest for high mole fractions of ethaline. The addition of methanol has a strong effect on those

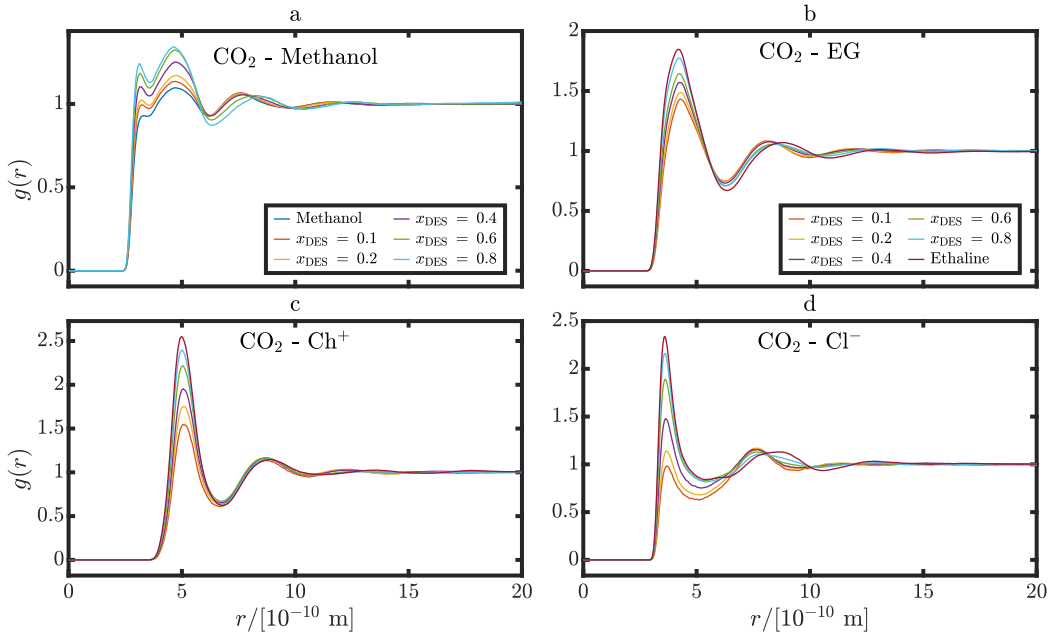

Figure 4.10: Radial distribution functions of (a) carbon dioxide-methanol, (b) carbon dioxide-ethylene glycol, (c) carbon dioxide-choline, (d) carbon dioxide-chloride in ethaline-methanol mixtures at different mole fractions of ethaline, at 298 K and 1 atm. Line colours are consistent for all subfigures.

peaks. The reported bulge in the RDF of CO_2-urea is not found in the RDF of (CO2)-EG. The positions of all aforementioned peaks do not change significantly with the addition of methanol. The first peaks of RDFs between CO_2-EG, CO_2-Ch^+ and CO_2-Cl^- are placed at approximately 4.2, 5.0 and 3.6 Å, respectively. The first two RDF peaks of CO_2-methanol are located at a distance of 3.1 and 4.6 Å.

Figure 4.10 shows the RDFs of CO_2 with the solvent constituents of ethaline-PC. the first peaks of the RDFs of CO_2-PC, CO_2-Ch^+ and CO_2-Cl^- become weaker for the addition of PC. The peak intensity of the RDF between CO_2-EG decreases by the addition of PC, reaches a minimum around a mole fraction of ethaline of 0.4, and increases for further addition of PC. It should be noted that the precision of the RDFs including solutes are relatively low due to the limited number of solute molecules. The peaks of the RDFs of CO_2 with the ions are the highest for high mole fractions of ethaline. The addition of PC has a strong effect on those peaks, similar to the other mixtures. The positions of all aforementioned peaks do not change significantly with the addition of methanol. The first peaks of RDFs between CO_2-EG, CO_2-Ch^+ and CO_2-Cl^- are placed at approximately 4.2, 5.0 and 3.6 Å, respectively, which are the same distances as for ethaline-methanol. The first peak of the RDF between CO_2-PC is found at 4.8 Å. The convergence towards 1 is found to be at large r for the RDFs of the ions. After evaluating plots of the 5 equivalent simulations separately, it was concluded to be an effect of the aforementioned low precision (plots not reported).

4.5.3. Formic Acid and Oxalic Acid in Ethaline-Propylene Carbonate

The RDFs related to formic acid in the mixture ethaline-PC are shown in Figure 4.12. The intensities of the RDF peaks between FA-EG, FA-Ch^+ and FA-Cl^- increase for an increase of PC mole fraction, indicating that the intermolecular interactions become stronger for the addition of PC. The RDF between FA-PC shows a decrease of intensity for the addition of PC, reaching a minimum around x_{PC} = 0.8, to rise again for further addition of PC. The first peak is blunt, most probably due to a combination of two peaks that overlap. A second, weak peak is formed for pure PC, which is not observed at x_{PC} = 0.9 or lower. Most probably, this interaction is too weak to survive in an environment with highly electrostatic DESs. The RDF between FA-EG shows a distinctive relation between the PC content and intensity for ethaline mole fractions in the range of 1 to 0.4. By further decreasing the ethaline concentration, the RDF peak intensity strongly increases. A second peak forms. A similar increase in sensitivity for mole fraction is observed in the RDFs between FA-Ch^+ and FA-Cl^-. These RDFs peak intensities increase slightly for ethaline mole fractions in the range of 1 to 0.4. For a mole fraction of x_{DES} = 0.1, the peak

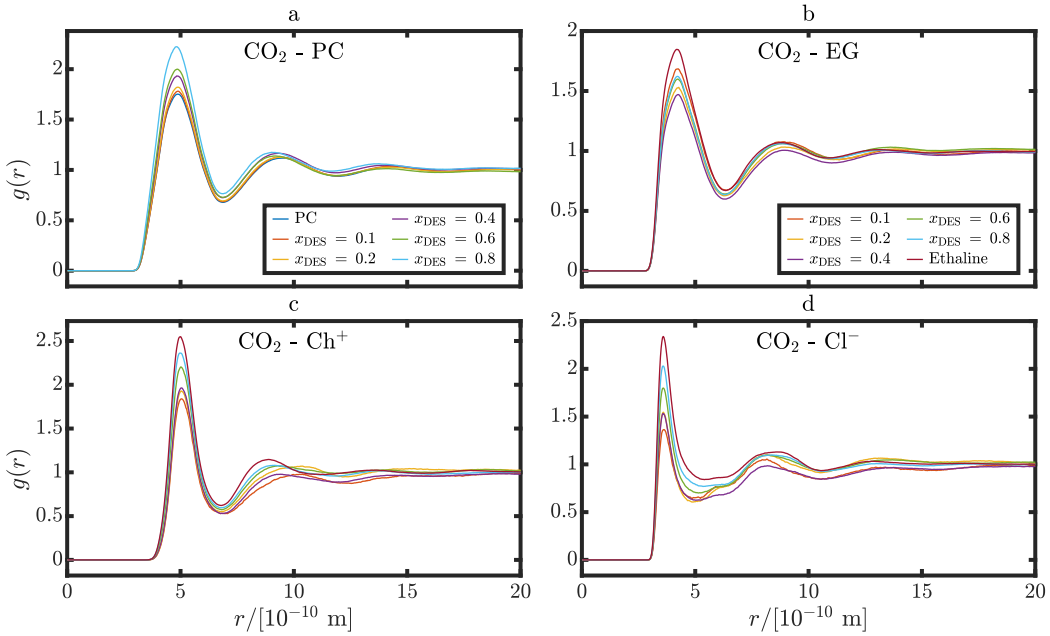

Figure 4.11: Radial distribution functions of (a) carbon dioxide-propylene carbonate, (b) carbon dioxide-ethylene glycol, (c) carbon dioxide-choline, (d) carbon dioxide-chloride in ethaline-propylene carbonate mixtures at different mole fractions of ethaline, at 298 K and 1 atm. Line colours are consistent for all subfigures.

height rises to approximately 60 for FA-Cl^-. A high, sharp peak is formed for FA-Cl^- as the FA and Cl^- are relatively small molecules. This indicates a strong attraction between FA and Cl^-. A sign of a second peak is formed for FA-Ch^+ at low mole fractions of ethaline. The secondary RDF peaks that form at low ethaline mole fractions between FA-Ch^+ and FA-EG indicate that Cl^- anions permeate between these molecules. The blunt RDF peak between FA-PC consists of two overlapping peaks located at a distance of approximately 4.3 and 4.9 Å. The first two RDF peaks between FA-EG are located at a distance of approximately 4.2 and 7.3 Å. The first distance slightly increases for an increase of the mole fraction of PC. The first two peaks between FA-Ch^+ are located at a distance of approximately 4.7 and 8.0 Å. The sharp RDF peak between FA-Cl^- is located at a distance of approximately 3.7 Å. All peaks remain at a constant distance for varying mole fractions, except for FA-EG.

The RDFs related to oxalic acid in the mixture ethaline-PC are shown in Figure 4.13. The intensities of the RDF peaks between OA-EG, OA-Ch^+ and OA-Cl^- increase for an increase of PC mole fraction, indicating that the intermolecular interactions become stronger for the addition of PC. The RDF between OA-PC shows a decrease of intensity for the addition of PC over the entire range of mole fractions, which is in contrast with the RDF between FA-PC. The first peak is blunt due to a combination of two peaks that overlap. Most probably, there are two stable orientations in which the molecules co-exist. The RDF between OA-EG is characterized by 3 peaks. For pure ethaline, the second peak is weak. By the addition of PC, the intensity of the first peak initially decreases, while the second peak intensity increases. The first peak intensity stays approximately constant for mole fractions of ethaline of 0.8 to 0.4. By further addition of PC, the intensity of the first and second peaks strongly increases. This indicates that the intermolecular interaction of OA-EG is promoted by a large PC concentration. For a mole fraction of ethaline of 0.1, the RDF is also higher for distances r beyond the first two peaks compared to the other mole fractions. The increase in peak intensity of the RDF between OA-Ch^+ mainly occurs for low ethaline concentrations.

The RDF between OA-Cl^- is characterized by two sharp, distinct peaks at a short distance r. Again, the increase in peak intensity mainly occurs for low mole fractions of ethaline. A small third peak forms for mole fractions of ethaline of 0.1 to 0.2. Most probably, the second RDF peak is an artefact of the off-centre RDF measurement of OA. As described in Section 3.4, the distance is measured between selected atoms of the molecules. Since OA consists of two equal, but mirrored acid groups, in which a carbon atom is used to compute the RDF. The secondary peak could be formed due to Cl^- interacting with the acid group furthest of the relevant carbon atom. Note that the second and third peaks are not

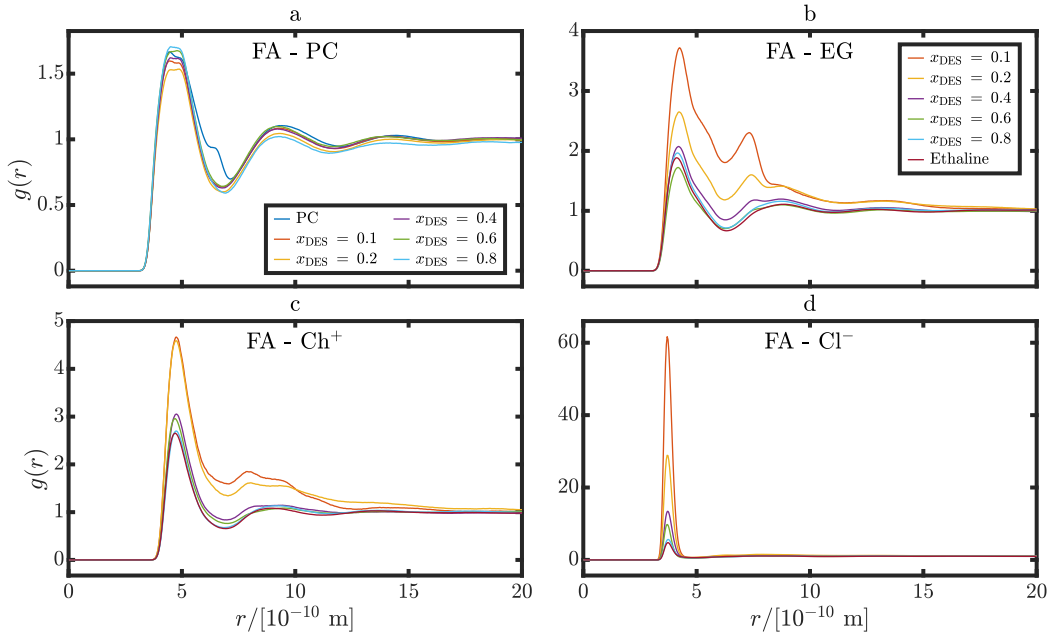

Figure 4.12: Radial distribution functions of (a) formic acid-propylene carbonate, (b) formic acid-ethylene glycol, (c) formic acid-choline, (d) formic acid-chloride in ethaline-propylene carbonate mixtures at different mole fractions of ethaline, at 298 K and 1 atm. Line colours are consistent for all subfigures.

found for FA-Cl^-, as there is only one oxalic group. The same phenomenon might explain the second peak the secondary peak in the RDF between OA-EG. A discrepancy for this theory is the lack of a second RDF peak between OA-EG for pure ethaline. Simulations using the centre of mass of OA would be required to verify this assumption. The blunt RDF peak between OA-PC consists of two overlapping peaks located at a distance of approximately 4.6 and 5.1 Å. The first three RDF peaks between OA-EG are located at a distance of approximately 4.3, 5.5 and 9.0 Å. The first two peaks between OA-Ch^+ are located at a distance of approximately 5.0 and 9.7 Å, except for pure ethaline, for which the second peak lies at approximately 9.2 Å. The sharp RDF peaks between OA-Cl^- are located at a distance of approximately 4.1 and 5.5 Å. All peaks remain at a constant distance for varying mole fractions, except for OA-EG, and OA-Ch^+ in pure ethaline.

4.6. Hydrogen Bonds

Figure 4.14 shows the number of HBs as a function of the mole fraction of DES for the mixtures reline-methanol (a), ethaline-methanol (b) and ethaline-PC (c). The numbers shown have been corrected for varying numbers of HBD molecules per mole fraction, as in equation 3.14. The numbers of HBs between all DES constituents increase monotonically for ethaline-methanol and reline-methanol mixtures. Note that a study by Celebi et al. [19] reported non-monotonic behaviour for the number of HBs of ethaline and reline mixed with water as a function of the mass fraction of water at mass fractions of water below 0.1. Simulations at low concentrations of DES would be required to check whether this behaviour is seen in mixtures with methanol as well. For reline-methanol, the number of HBs between the constituents follows Cl^--EG > EG-EG > Ch^+-Cl^- > Ch^+-EG^- for all mole fractions. For ethaline-methanol, the number of HBs between the constituents follows urea-urea > Cl^--urea > Ch^+-urea > Ch^+-Cl^- for all mole fractions. In reline, choline slightly prefers to form HBs with the HBD, while in ethaline, Ch^+ prefers to form HBs with Cl^-. The abbreviation HBD refers to urea and EG in this entire document, regardless of its role in the formation of HBs. Please note the ratio of the number of molecules in the systems of Cl^-:HBD = 1:2, indicating that Ch^+ would prefer to form hydrogen bonds with Cl^- in an equiproportional Cl^-:HBD system. Ethylene glycol prefers to form HBs with chloride, while urea prefers to form HBs with other urea molecules. This difference was also reported by Celebi et al. [19] for aqueous mixtures.

For pure reline and ethaline, the aforementioned study shows the same HB formation preferences

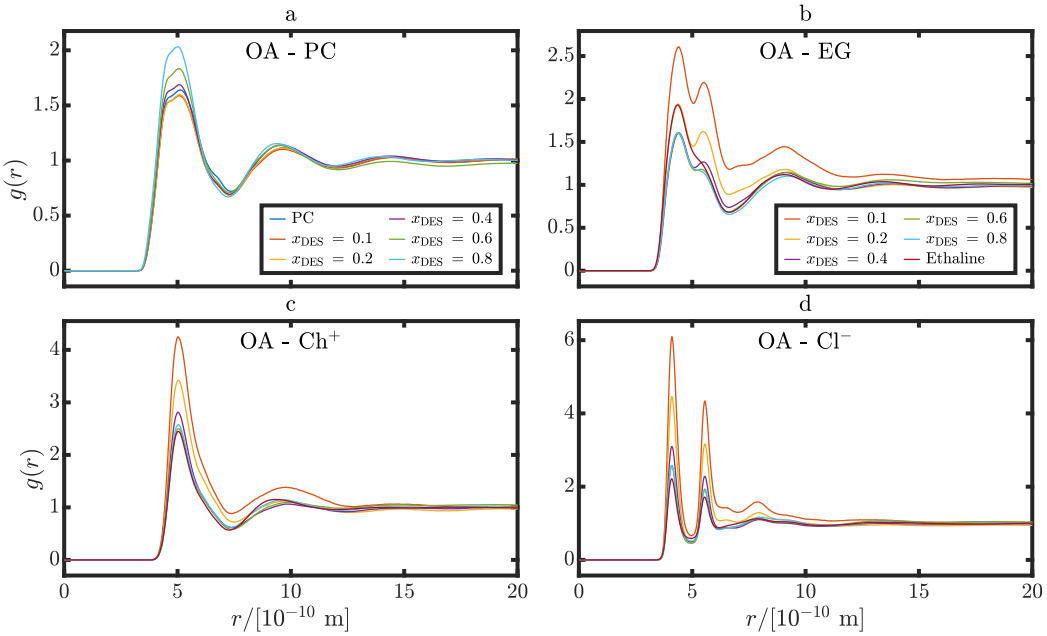

Figure 4.13: Radial distribution functions of (a) oxalic acid-propylene carbonate, (b) oxalic acid-ethylene glycol, (c) oxalic acid-choline, (d) oxalic acid-chloride in ethaline-propylene carbonate mixtures at different mole fractions of ethaline, at 298 K and 1 atm. Line colours are consistent for all subfigures.

as found in this study. The numbers of HBs found in this study are at least slightly higher for all reported molecule combinations. No deviations and sample sizes are reported. The difference might (partly) be explained by the difference in temperature of 5 K. This explanation is weakened by the relation between the number of HBs and temperature, reported by Celebi et al. [19]. A small effect of the temperature is reported for ethaline and reline mixed with a mass fraction of water of 0.4. The number of HBs between EG-EG reported by Celebi et al. is approximately a factor 2 lower than those reported in this study. No solid explanation is found for this difference. A study by Cea-Klapp et al. [90] reports the number of hydrogen bonds for mixtures of ethaline-methanol as a function of mole fraction of ethaline, at 308.15 K. The values found are in good agreement with those obtained in this study, except for the number of HBs between Cl^--EG. Cea-Klapp et al. reported approximately 1.5 times as many HBs between Cl^--EG. A fully quantitative comparison is not made, as the simulated temperatures differ. An explanation for this difference was not found. Note that Cea-Klapp et al. used an OPLS-AA FF, with ion-charge scaling by a factor of 0.8, while in our study the charges of ethaline ions were scaled by a factor of 0.9. The numbers of HBs used in above comparison were not reported in the paper of Cea-Klapp et al. but received on request.

For ethaline-PC, the effect of mixing with organic solvent on the number of HBs is less pronounced than for the previously discussed mixtures. the number of HBs between Ch^+-EG and EG-EG seem to increase monotonically for increasing mole fraction of ethaline, however statistically insignificant. The numbers of HBs between Cl^--EG and Ch^+-Cl^- do not show a distinctive effect of the mole fraction of DES. As a result, at low mole fractions of DES, there are significantly more HBs in ethaline-PC than in ethaline-methanol. At a mole fraction of DES of 0.1, this results in factors of approximately 6.0 for Ch^+-EG, 2.5 for Ch^+-Cl^-, 2.4 for EG-EG and 2.5 for Ch^+-EG. These observations are in agreement with the high RDF peaks for ethaline-PC between CH^+-Cl^- and, in particular Cl^--EG. The numbers of hydrogen bonds between organic solvent molecules and DES molecules are reported in Figure E.1 and Tables E.5, E.4 and E.6.

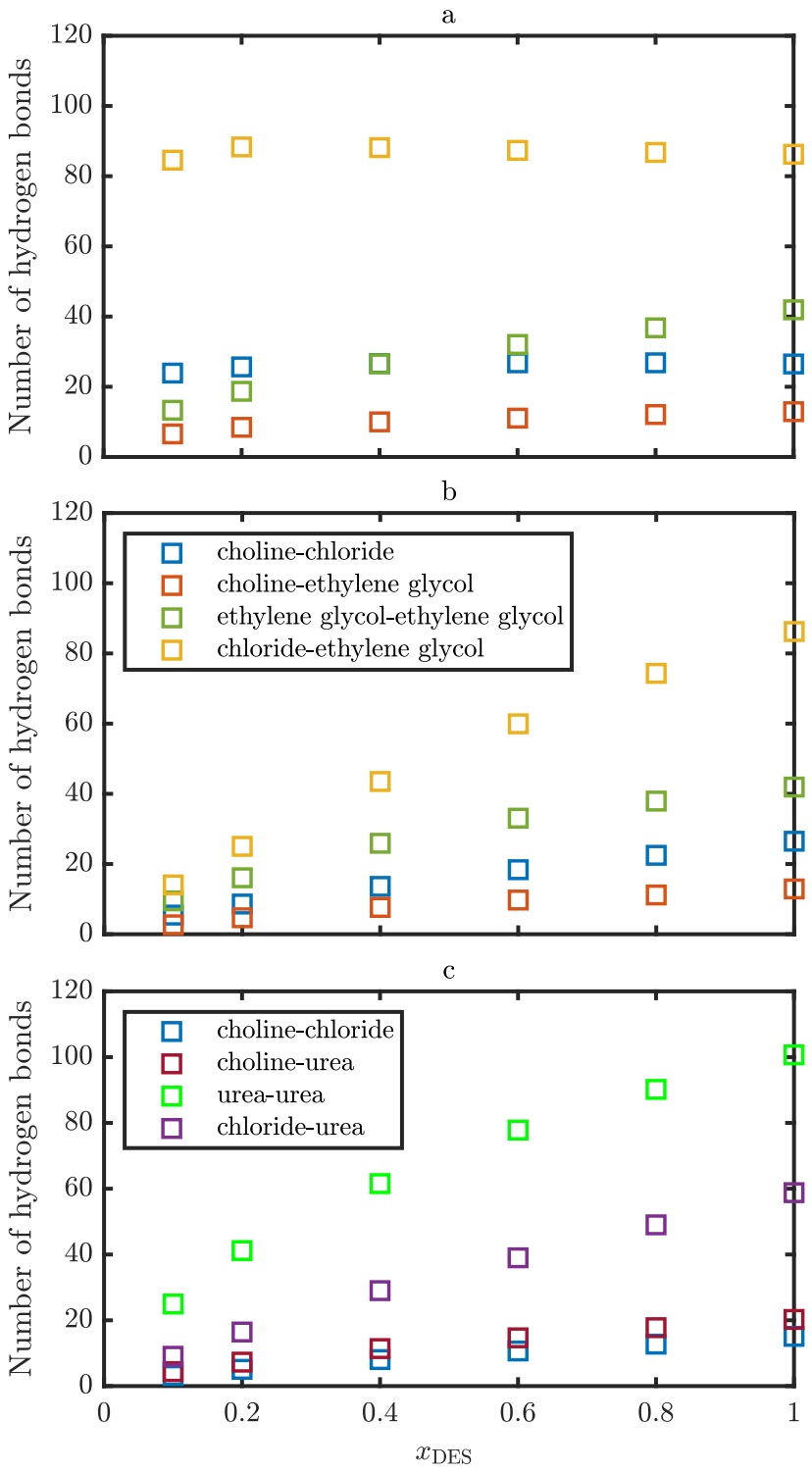

Figure 4.14: The number of hydrogen bonds between deep eutectic solvent (DES) constituents as a function of the mole fraction of DES for the mixtures reline-methanol (a), ethaline-methanol (b) and ethaline-PC (c), at 298 K and 1 atm. The measured number of hydrogen bonds is divided by the number of hydrogen bond donor (HBD) molecules and multiplied by 100 to represent a system of 50 choline, 50 chloride, 100 HBD molecules and a number of organic solvent molecules dependent on the mole fraction of DES. Equation 3.14 and table 3.1 denote the applied calculation and number of molecules per simulation, respectively. Error bars are excluded for clarity. Mean average deviations and sample sizes are presented in appendix E. Colors are consistent for all subfigures.

5

Conclusions

This research aimed to acquire the densities, transport properties and structural insight in deep eutectic solvents mixed with organic solvents, ultimately for the application of CO_2 capture and conversion. Molecular dynamics simulations were performed for reline and ethaline mixed with methanol and propylene carbonate. Other than the viscosity of ethaline-methanol, no transport properties of these mixtures have been reported before in literature. Furthermore, the self-diffusivities and RDFs of the solutes CO_2, oxalic acid and formic acid in all three mixtures were obtained, for the majority of mole fractions.

The results indicate that the viscosities of DESs can be reduced significantly by the addition of organic solvents. In industrial applications, this would reduce the energy required for pumping and allow for the use of standardized equipment. Furthermore, the self-diffusivities of the ions and solutes are enhanced by the addition of organic solvents. For a higher self-diffusivity of CO_2, the absorption requires less time, which is beneficial during the capture step. Due to the increased self-diffusivities of the ions, the calculated ionic conductivity is increased almost an order of magnitude at its optimal methanol concentration, which is beneficial for the electrochemical conversion of CO_2. However, experimental verification is required as the calculation based on the self-diffusivities of the ions is known to overpredict the ionic conductivity.

The structure was studied through radial distribution functions and a hydrogen bond analysis. The RDF between Cl^--EG, shows a sharp, high peak, for all three mixtures. For both methanol mixtures, this peak stays approximately constant for varying mole concentrations. For the mixture ethaline-PC, the peak intensity increases strongly by addition of PC. Interestingly, the peak intensities between Cl^--EG and between Ch^+-Cl^- decreases by the addition of water, as reported earlier by our group. By addition of methanol or PC, these peak intensities increase, or stay constant. The hydrogen bond analysis shows that the number of hydrogen bonds between DES constituents decreases strongly by the addition of methanol, whereas the addition of PC has a small effect. Most hydrogen bonds are formed by the hydrogen bond donors urea and ethylene glycol. The depletion of hydrogen bonds at low mole fractions of deep eutectic solvent is in correspondence with the decrease in viscosity and increase in self-diffusivities.

No studies reporting the viscosity of reline-methanol mixtures or ethaline-propylene carbonate mixtures for mole fractions of ethaline higher than 0.2 have been published before. The self-diffusivities of all the reported mixtures, plus the constituents CO_2, oxalic acid and formic acid in these mixtures, are novel. Radial distribution functions of ethaline-methanol have been reported at a different temperature, for a single mole fraction. Radial distribution functions of ethaline-propylene carbonate, reline-methanol and the constituents CO_2, formic acid and oxalic acid in these mixtures have not been reported before. The numbers of hydrogen bonds are also unique in literature for the mixtures ethaline-propylene carbonate and reline-methanol.

In conclusion, the results indicate that, for the studied properties, deep eutectic solvents mixed with organic solvents are more favourable than pure deep eutectic solvents for the absorption and electrochemical conversion of CO_2. Other important properties, like the solubility of CO_2 and the faradaic efficiency of the conversion reaction, are investigated in complementary studies. Furthermore, a techno-economical assessment will be performed in a complementary study, which is required to compare the

combined capture and conversion to alternative processes. These studies are joined in the Bio-cel project. At the time of writing, these studies have not been published yet.

6

Limitations and Recommendations

First, limitations of the applied methods are listed. Several recommendations for further research are proposed. These are subdivided into recommendations for improving the accuracy of the mixtures studied, in Section 6.2, and recommendations for extending the available data in Section 6.3.

6.1. Limitations

There are factors that impact the accuracy of the acquired results. The most important ones are discussed in this section. The limitations of the Nernst-Einstein equation have been discussed in Section 3.3.4.

6.1.1. Force Fields

DES dynamics are dominated by electrostatic interactions. In this study, non-polarizable FFs were used, with scaled ion charges. The scaling of the charges, independent of the position of the molecule relative to its neighbours, is a simplification. This might lead to an error in the level of movement of the molecules and/or an error in the affinity of molecules to the different types of molecules in the mixture. Potential methods to reduce this error are discussed in Section 6.2.

FA was modelled using parameters obtained by Salas et al. [59]. It should be noted that, in pure PC simulations, the dihedral angle distribution, representing the ratio of trans/cis conformers, does not match that of Salas et al. Salas et al. report an distribution of similar proportions of cis and trans conformers, whereas the fraction of trans is low in the simulations of this study. Further investigation is required to determine whether this yields deviations.

As mentioned in Section 3.1, propylene carbonate was modelled by the (S)-enantiomer only. Simulations to compare enantiopure to racemic PC showed negligible differences in density and transport properties. A study by Jankowski et al. reports a difference of ionic conductivity between enantiopure and racemic propylene carbonate mixed with lithium trifluorometha-nesulfonate up to 15% mass fraction at low temperatures (<233 K). It is stressed that the differences are at the level of the measurement error. Although aforementioned simulations indicate no correlation between enantiomer fractions and transport properties, studying the transport properties of both enantiopure and racemic ethaline-propylene carbonate mixtures could be performed to increase the certainty of the indication.

6.1.2. Negative pressures

In the transition of the NPT-ensemble to the NVT-ensemble, the sampled volume is fixed. During the NVT-simulation, the average pressure is calculated, which is approximately between -200 and +92 atm. Checks for a correlation between the pressure and the transport properties were performed in preliminary simulations. No strong indication of a correlation was found. In tests with manual simulation box scaling, the average pressure was found to be sensitive to the box volume. It is expected that a small deviation of the calculated average volume during the simulation in the NPT-ensemble causes a deviation in pressure. Even though no correlation between the pressure deviations and the transport properties was found, it might cause inaccuracies.

6.1.3. Sample Size

The solutes CO_2, oxalic acid and formic acid comprised of 5 molecules in the respective simulated systems. The precision of the self-diffusivities and radial distribution functions related to these solutes could improve by increasing the sample size. As the goal is to model an infinitely dilute solution, the entire system would have to be scaled up. Alternatively, to improve the precision of the self-diffusivities, more and longer simulations could be performed. To improve the precision of the RDFs related to the solutes, more samples over time could be obtained.

Due to the slow dynamics of the mixtures with high concentrations of deep eutectic solvent, some simulations yielded unconverged mean-squared-displacements. The statistics of the resulting transport properties could be improved by running longer simulations of these mixtures. In this study, a maximum wall time of 5 days was the limiting factor in the calculation of transport properties of mixtures with high deep eutectic solvent concentrations.

6.2. Improving the Accuracy

The force fields that are used to model the interactions have a significant impact on the molecular movement and structure of the modelled mixtures. The force fields used to model the deep eutectic solvents use scaled ion charges to achieve better agreement to pure deep eutectic solvents experimental data. The scaled charges account for charge transfer and/or polarization. These phenomena could change for varying mole fractions. One could model the deep eutectic solvents at other mole fractions using different values for the ion charges to match with experimentally acquired transport properties.

Alternatively, one could apply polarizable force fields. A study on ionic liquids shows promising results for acquiring transport properties using polarized force fields [55]. One step further is the use of ab initio molecular dynamics simulations. However, this comes at a great computational cost, and is therefore limited to small systems. Since large systems and time scales are required for the modelled mixtures to deal with low concentrations of solutes and clustering effects, this is not considered possible in the near future. In an optimistic further future, quantum computers provide the computational power to deal with the quantum-mechanical calculations involved in ab initio molecular dynamics simulations.

To model the solvents methanol and PC and the solutes CO_2, formic acid and oxalic acid in mixtures with deep eutectic solvents, different force fields could be applied and compared. To model CO_2, Aimoli et al. [56] recommend using the Zhang force field. Zhong et al. [91] found the best agreement with experimental transport properties using EPM2-flex for temperatures above 273 K. These studies compare force fields for pure CO_2. In a study by Moultos et al. [92], the best agreement with experimental diffusivity of CO_2 dissolved in water was found using EPM2 for temperatures below 323 K.

As discussed in Section 4.5.3, there are two sharp peaks in the radial distribution functions between oxalic acid-ethylene glycol and oxalic acid-chloride, which might result from off-centred distance calculations. It is recommended to test this artefact with simulations that sample the radial distribution functions calculated from the centre of mass of oxalic acid.

In general, it is recommended to validate all acquired transport properties and structural properties through experiments. Gaining knowledge about the disagreement with experimental data can be useful for future studies that aim to extend the knowledge on deep eutectic solvent-organic solvent mixtures too.

6.3. Extending the Knowledge

For the application of carbon capture utilization and storage, elevated temperatures and pressures are used. It is recommended to simulate the systems at these conditions, especially since the transport properties have been shown to be sensitive to temperature [19]. When the combined process of capture and conversion is applied, the concentrations of CO_2, oxalic acid and formic acid might vary through the reactor. It is recommended to simulate at higher mole fractions of these solutes, to identify the effect on the transport properties and structures of the mixtures.

The family of deep eutectic solvents consists of 10^6 - 10^8 members, of which two were investigated in this study. To find the deep eutectic solvent with the best properties for capture and conversion, more deep eutectic solvents could be screened using molecular dynamics simulations. During this master thesis, the available time limited the number of systems that could be simulated. In the course of this study, manual steps for the pre and post-processing of simulations were automated, providing the basis for systematic screening of more mixtures and/or thermodynamic conditions. Note that the automation

mentioned is not novel, however manual execution was needed to gain experience. Next, a database, similar to ILThermo [93] can be made to facilitate systematic analysis of the data.

In Section 3.3.4, the effect of ion association on the calculated ionic conductivity is discussed. This property can be quantified using the difference in ionic conductivity acquired via two experimental methods. Using molecular dynamics simulations, the relative positions of the ions are estimated. It is recommended to develop a method to calculate the ion association factor based on the radial density function or directly from the coordinates of the ions. If successful, the accuracy of the ionic conductivity calculated using the Nernst-Einstein equation could be improved and insight into the ionic conductivity of deep eutectic solvents and ionic liquids could be extended.

As discussed in Section 2.5, an electrolyte with protic components favours other reaction pathways over the formation of oxalic acid. A combination of an aprotic deep eutectic solvent with an aprotic organic solvent should be chosen to facilitate the production of oxalic acid. One example of such a deep eutectic solvent is 1-butyl-3-methylimidazolium chloroaluminate (BmimCl/$AlCl_3$), which was investigated by Zheng et al. [94]. At a mole fraction of x_{AlCl_3} = 0.6667, and temperature T = 293.15 K, a viscosity and conductivity of η = 22.54 mPa · s and κ = 9.12 mS · cm^{-1}, were measured, respectively. A DES comprised of the same HBA, 1-butyl-3-methylimidazolium chloride monoethanolamine (BmimCl/MEA) was tested to absorb up to 21.7% mass fraction of CO_2 at the eutectic ratio of 1:4 in a study by Cao et al. [95]. MEA is protic, therefore it is unlikely to facilitate the production of oxalic acid, as described in Section 2.5. Deep eutectic solvents based on Bmim could be explored in future research in combination with different hydrogen bond acceptors and organic solvents, to determine which combination yields the most desirable properties.

Bibliography

(1) Ritchie, H.; Roser, M. https://ourworldindata.org/co2-and-other-greenhouse-gas-emissions (accessed 03/04/2021).

(2) NASA Vital Signs Carbon Dioxide https://climate.nasa.gov/vital-signs/carbon-dioxide/#:~:text=Over%20the%20past%20171%20years,185%20ppm%20to%20280%20ppm). (accessed 03/04/2021).

(3) European Union Climate strategies & targets https://ec.europa.eu/clima/policies/strategies (accessed 04/06/2021).

(4) IEA CCUS in Clean Energy Transitions https://www.iea.org/reports/ccus-in-clean-energy-transitions (accessed 04/06/2021).

(5) Zhang, M. High Quality Best Price 99.6% Oxalic Acid from China Largest Manufacturer https://www.alibaba.com/product-detail/Price-Oxalic-Acid-Oxalic-Acid-Price_60855082411.html?spm=a2700.7724857.topad_classic.d_title.737f6796Z67cZy (accessed 04/12/2021).

(6) Marketprimes Oxalic Acid market to showcase an annual growth rate of -1.1% over 2019-2025 https://marketprimes.com/oxalic-acid-market/ (accessed 04/11/2021).

(7) Riemenschneider, W.; Tanifuji, M. Oxalic Acid. *Ullmann's Encyclopedia of Industrial Chemistry* **2012**.

(8) Yu, B. Y.; Chien, I. L. Design and optimization of dimethyl oxalate (DMO) hydrogenation process to produce ethylene glycol (EG). *Chemical Engineering Research and Design* **2017**, *121*, 173–190.

(9) PlasticsInsight Mono-Ethylene Glycol (MEG): Production, Market, Price and its Properties https://www.plasticsinsight.com/resin-intelligence/resin-prices/mono-ethylene-glycol-meg/ (accessed 04/12/2021).

(10) Smith, E. L.; Abbott, A. P.; Ryder, K. S. Deep Eutectic Solvents (DESs) and Their Applications. *Chemical Reviews* **2014**, *114*, 11060–11082.

(11) Wang, J.; Cheng, H.; Song, Z.; Chen, L.; Deng, L.; Qi, Z. Carbon Dioxide Solubility in Phosphonium-Based Deep Eutectic Solvents: An Experimental and Molecular Dynamics Study. *Industrial and Engineering Chemistry Research* **2019**, *58*, 17514–17523.

(12) Yan, H.; Zhao, L.; Bai, Y.; Li, F.; Dong, H.; Wang, H.; Zhang, X.; Zeng, S. Superbase Ionic Liquid-Based Deep Eutectic Solvents for Improving CO2 Absorption. *ACS Sustainable Chemistry and Engineering* **2020**, *8*, 2523–2530.

(13) Zhang, K.; Hou, Y.; Wang, Y.; Wang, K.; Ren, S.; Wu, W. Efficient and Reversible Absorption of CO2 by Functional Deep Eutectic Solvents. *Energy and Fuels* **2018**, *32*, 7727–7733.

(14) Hansen, B. B. et al. Deep Eutectic Solvents: A Review of Fundamentals and Applications. *Chemical Reviews* **2021**.

(15) Lei, Z.; Chen, B.; Koo, Y. M.; Macfarlane, D. R. Introduction: Ionic Liquids. *Chemical Reviews* **2017**, *117*, 6633–6635.

(16) Dong, K.; Liu, X.; Dong, H.; Zhang, X.; Zhang, S. Multiscale Studies on Ionic Liquids. *Chemical Reviews* **2017**, *117*, 6636–6695.

(17) Singh, S. K.; Savoy, A. W. Ionic liquids synthesis and applications: An overview. *Journal of Molecular Liquids* **2020**, *297*, 112038.

(18) Jamali, S. H.; Wolff, L.; Becker, T. M.; De Groen, M.; Ramdin, M.; Hartkamp, R.; Bardow, A.; Vlugt, T. J.; Moultos, O. A. OCTP: A Tool for On-the-Fly Calculation of Transport Properties of Fluids with the Order- n Algorithm in LAMMPS. *Journal of Chemical Information and Modeling* **2019**, *59*, 1290–1294.

(19) Celebi, A. T.; Vlugt, T. J.; Moultos, O. A. Structural, Thermodynamic, and Transport Properties of Aqueous Reline and Ethaline Solutions from Molecular Dynamics Simulations. *Journal of Physical Chemistry B* **2019**, *123*, 11014–11025.

(20) Abbott, A. P.; Capper, G.; Davies, D. L.; Rasheed, R. K.; Tambyrajah, V. Novel solvent properties of choline chloride/urea mixtures. *Chemical Communications* **2003**, 70–71.

(21) Salehi, H. S.; Hens, R.; Moultos, O. A.; Vlugt, T. J. Computation of gas solubilities in choline chloride urea and choline chloride ethylene glycol deep eutectic solvents using Monte Carlo simulations. *Journal of Molecular Liquids* **2020**, *316*, 113729.

(22) Marcus, A. I., *Introduction*, 2016, pp 1–16.

(23) Sas, O. G.; Fidalgo, R.; Domínguez, I.; Macedo, E. A.; González, B. Physical properties of the pure deep eutectic solvent, [ChCl]:[Lev] (1:2) DES, and its binary mixtures with alcohols. *Journal of Chemical and Engineering Data* **2016**, *61*, 4191–4202.

(24) Altamash, T.; Nasser, M. S.; Elhamarnah, Y.; Magzoub, M.; Ullah, R.; Qiblawey, H.; Aparicio, S.; Atilhan, M. Gas solubility and rheological behavior study of betaine and alanine based natural deep eutectic solvents (NADES). *Journal of Molecular Liquids* **2018**, *256*, 286–295.

(25) Yadav, A.; Pandey, S. Densities and viscosities of (choline chloride + urea) deep eutectic solvent and its aqueous mixtures in the temperature range 293.15 K to 363.15 K. *Journal of Chemical and Engineering Data* **2014**, *59*, 2221–2229.

(26) Abbott, A. P.; Capper, G.; Gray, S. Design of improved deep eutectic solvents using hole theory. *ChemPhysChem* **2006**, *7*, 803–806.

(27) Zubeir, L. F.; Van Osch, D. J.; Rocha, M. A.; Banat, F.; Kroon, M. C. Carbon Dioxide Solubilities in Decanoic Acid-Based Hydrophobic Deep Eutectic Solvents. *Journal of Chemical and Engineering Data* **2018**, *63*, 913–919.

(28) Dietz, C. H.; van Osch, D. J.; Kroon, M. C.; Sadowski, G.; van Sint Annaland, M.; Gallucci, F.; Zubeir, L. F.; Held, C. PC-SAFT modeling of CO2 solubilities in hydrophobic deep eutectic solvents. *Fluid Phase Equilibria* **2017**, *448*, 94–98.

(29) Wang, M.; Lawal, A.; Stephenson, P.; Sidders, J.; Ramshaw, C. Post-combustion CO2 capture with chemical absorption: A state-of-the-art review. *Chemical Engineering Research and Design* **2011**, *89*, 1609–1624.

(30) Ramdin, M.; De Loos, T. W.; Vlugt, T. J. State-of-the-art of CO 2 capture with ionic liquids. *Industrial and Engineering Chemistry Research* **2012**, *51*, 8149–8177.

(31) Metz, B.; Davidson, O.; de Coninck, H.; Loos, M.; Meyer, L. *IPCC Special Report on Carbon Dioxide Capture and Storage*; tech. rep.; 2005.

(32) Rackley, S. Carbon capture and storage: How Green Can Black Be? *Science* **2009**, *325*, 1647–1652.

(33) Ramdin, M.; De Loos, T. W.; Vlugt, T. J. State-of-the-art of CO 2 capture with ionic liquids. *Industrial and Engineering Chemistry Research* **2012**, *51*, 8149–8177.

(34) Jouny, M.; Luc, W.; Jiao, F. General Techno-Economic Analysis of CO2 Electrolysis Systems. *Industrial and Engineering Chemistry Research* **2018**, *57*, 2165–2177.

(35) Smith, W. A.; Burdyny, T.; Vermaas, D. A.; Geerlings, H. Pathways to Industrial-Scale Fuel Out of Thin Air from CO2 Electrolysis. *Joule* **2019**, *3*, 1822–1834.

(36) Tomita, Y.; Hori, Y. Electrochemical reduction of carbon dioxide at a platinum electrode in acetonitrile-water mixtures. *Studies in Surface Science and Catalysis* **1998**, *114*, 581–584.

(37) Ikeda, S.; Takagi, T.; Ito, K. Selective formation of formic acid, oxalic acid, and carbon monoxide by electrochemical reduction of carbon dioxide, 1987.

(38) Eneau-Innocent, B.; Pasquier, D.; Ropital, F.; Léger, J. M.; Kokoh, K. B. Electroreduction of carbon dioxide at a lead electrode in propylene carbonate: A spectroscopic study. *Applied Catalysis B: Environmental* **2010**, *98*, 65–71.

(39) Senthil Kumar, R.; Senthil Kumar, S.; Anbu Kulandainathan, M. Highly selective electrochemical reduction of carbon dioxide using Cu based metal organic framework as an electrocatalyst. *Electrochemistry Communications* **2012**, *25*, 70–73.

(40) Boor, V. S. Electrochemical reduction of CO2 to Oxalic Acid. **2020**, 84.

(41) Rosen, B. A.; Salehi-khojin, A.; Thorson, M. R.; Zhu, W.; Whipple, D. T.; Kenis, P. J. A.; Masel, R. I. Ionic Liquid – Mediated Selective Conversion of CO 2 to CO at. *Science* **2011**, 643–644.

(42) Lim, H. K.; Kim, H. The mechanism of room-Temperature ionic-liquid-based electrochemical CO2 reduction: A Review. *Molecules* **2017**, *22*.

(43) Chen, Y.; Mu, T., *Conversion of CO2 to value-added products mediated by ionic liquids*; 10; Royal Society of Chemistry: 2019; Vol. 21, pp 2544–2574.

(44) Yang, Y.; Gao, H.; Feng, J.; Zeng, S.; Liu, L.; Liu, L.; Ren, B.; Li, T.; Zhang, S.; Zhang, X. Aromatic Ester-Functionalized Ionic Liquid for Highly Efficient CO2 Electrochemical Reduction to Oxalic Acid. *ChemSusChem* **2020**, *13*, 4900–4905.

(45) Vasilyev, D. V.; Rudnev, A. V.; Broekmann, P.; Dyson, P. J. A General and Facile Approach for the Electrochemical Reduction of Carbon Dioxide Inspired by Deep Eutectic Solvents. *ChemSusChem* **2019**, *12*, 1635–1639.

(46) Frenkel, D.; Smit, B., *Understanding Molecular Simulation*, 2nd ed., 2002.

(47) Pearlman, D. A.; Case, D. A.; Caldwell, J. W.; Ross, W. S.; Cheatham, T. E.; Debolt, S.; Ferguson, D.; Seibel, G.; Kollman, P. AMBER , a package of computer programs for applying molecular mechanics , normal mode analysis , molecular dynamics and free energy calculations to simulate the structural and energetic properties of molecules. **1995**, *91*, 1–41.

(48) Damm, W.; Frontera, A.; Rives, J. T.; Jorgensen, W. L. for Carbohydrates. *Journal of Computational Chemistry* **1997**, *18*, 1955–1970.

(49) Wang, J.; Wolf, R. M.; Caldwell, J. W.; Kollman, P. A.; Case, D. A. Development and testing of a general Amber force field. *Journal of Computational Chemistry* **2004**, *25*, 1157–1174.

(50) Thompson, A. P.; Aktulga, H. M.; Berger, R.; Bolintineanu, D. S.; Brown, W. M.; Crozier, P. S.; in 't Veld, P. J.; Kohlmeyer, A.; Moore, S. G.; Nguyen, T. D.; Shan, R.; Stevens, M. J.; Tranchida, J.; Trott, C.; Plimpton, S. J. LAMMPS - a flexible simulation tool for particle-based materials modeling at the atomic, meso, and continuum scales. *Computer Physics Communications* **2022**, *271*, 108171.

(51) Scott, R.; Allen, M. P.; Tildesley, D. J., *Computer Simulation of Liquids.* 195, 1991; Vol. 57, p 442.

(52) Celebi, A. T.; Dawass, N.; Moultos, O. A.; Vlugt, T. J. How sensitive are physical properties of choline chloride-urea mixtures to composition changes: Molecular dynamics simulations and Kirkwood-Buff theory. *Journal of Chemical Physics* **2021**, *154*.

(53) Perkins, S. L.; Painter, P.; Colina, C. M. Experimental and computational studies of choline chloride-based deep eutectic solvents. *Journal of Chemical and Engineering Data* **2014**, *59*, 3652–3662.

(54) Rigby, J.; Izgorodina, E. I. Assessment of atomic partial charge schemes for polarisation and charge transfer effects in ionic liquids. *Physical Chemistry Chemical Physics* **2013**, *15*, 1632–1646.

(55) Borodin, O. Polarizable force field development and molecular dynamics simulations of ionic liquids. *Journal of Physical Chemistry B* **2009**, *113*, 11463–11478.

(56) Aimoli, C. G.; Maginn, E. J.; Abreu, C. R. Transport properties of carbon dioxide and methane from molecular dynamics simulations. *Journal of Chemical Physics* **2014**, *141*.

(57) Chen, B.; Potoff, J. J.; Siepmann, J. I. Monte Carlo calculations for alcohols and their mixtures with alkanes. Transferable potentials for phase equilibria. 5. United-atom description of primary, secondary, and tertiary alcohols. *Journal of Physical Chemistry B* **2002**, *105*, 3093–3104.

(58) Doherty, B.; Acevedo, O. OPLS Force Field for Choline Chloride-Based Deep Eutectic Solvents. *Journal of Physical Chemistry B* **2018**, *122*, 9982–9993.

(59) Salas, F. J.; Núñez-Rojas, E.; Alejandre, J. Stability of formic acid/pyridine and isonicotinamide/formamide cocrystals by molecular dynamics simulations. *Theoretical Chemistry Accounts* **2017**, *136*, 1–12.

(60) Sousa Da Silva, A. W.; Vranken, W. F. ACPYPE - AnteChamber PYthon Parser interfacE. *BMC Research Notes* **2012**, *5*, 1–8.

(61) Wang, J.; Wang, W.; Kollman, P. A.; Case, D. A. Automatic atom type and bond type perception in molecular mechanical calculations. *Journal of Molecular Graphics and Modelling* **2006**, *25*, 247–260.

(62) Silva, L. B.; Freitas, L. C. G. Structural and thermodynamic properties of liquid ethylene carbonate and propylene carbonate by Monte Carlo Simulations. *Journal of Molecular Structure: THEOCHEM* **2007**, *806*, 23–34.

(63) Martinez, I.; Andrade, B.; Birgin, E.; Martinez, J. Software News and Updates Gabedit — A Graphical User Interface for Computational Chemistry Softwares. *Journal of computational chemistry* **2009**, *32*, 2157–2164.

(64) Dubbeldam, D.; Ford, D. C.; Ellis, D. E.; Snurr, R. Q. A new perspective on the order-n algorithm for computing correlation functions. *Molecular Simulation* **2009**, *35*, 1084–1097.

(65) Tenney, C. M.; Maginn, E. J. Limitations and recommendations for the calculation of shear viscosity using reverse nonequilibrium molecular dynamics. *Journal of Chemical Physics* **2010**, *132*.

(66) Celebi, A. T.; Vlugt, T. J.; Moultos, O. A. Thermal conductivity of aqueous solutions of reline, ethaline, and glyceline deep eutectic solvents; a molecular dynamics simulation study. *Molecular Physics* **2021**.

(67) Yeh, I. C.; Hummer, G. System-size dependence of diffusion coefficients and viscosities from molecular dynamics simulations with periodic boundary conditions. *Journal of Physical Chemistry B* **2004**, *108*, 15873–15879.

(68) Humbert, M. T.; Zhang, Y.; Maginn, E. J. PyLAT: Python LAMMPS Analysis Tools. *Journal of Chemical Information and Modeling* **2019**, *59*, 1301–1305.

(69) Nordness, O.; Brennecke, J. F. Ion Dissociation in Ionic Liquids and Ionic Liquid Solutions. *Chemical Reviews* **2020**, *120*, 12873–12902.

(70) Hayamizu, K. Temperature dependence of self-diffusion coefficients of ions and solvents in ethylene carbonate, propylene carbonate, and diethyl carbonate single solutions and ethylene carbonate + diethyl carbonate binary solutions of LiPF 6 studied by NMR. *Journal of Chemical and Engineering Data* **2012**, *57*, 2012–2017.

(71) Philippi, F.; Rauber, D.; Springborg, M.; Hempelmann, R. Density Functional Theory Descriptors for Ionic Liquids and the Charge-Transfer Interpretation of the Haven Ratio. *Journal of Physical Chemistry A* **2019**, *123*, 851–861.

(72) Philippi, F.; Quinten, A.; Rauber, D.; Springborg, M.; Hempelmann, R. Density Functional Theory Descriptors for Ionic Liquids and the Introduction of a Coulomb Correction. *Journal of Physical Chemistry A* **2019**, *123*, 4188–4200.

(73) Ganguly, P.; Van Der Vegt, N. F. Convergence of sampling Kirkwood-Buff integrals of aqueous solutions with molecular dynamics simulations. *Journal of Chemical Theory and Computation* **2013**, *9*, 1347–1355.

(74) Milzetti, J.; Nayar, D.; Van Der Vegt, N. F. Convergence of Kirkwood-Buff Integrals of Ideal and Nonideal Aqueous Solutions Using Molecular Dynamics Simulations. *Journal of Physical Chemistry B* **2018**, *122*, 5515–5526.

(75) Dawass, N.; Krüger, P.; Schnell, S. K.; Simon, J. M.; Vlugt, T. J. Kirkwood-Buff integrals from molecular simulation. *Fluid Phase Equilibria* **2019**, *486*, 21–36.

(76) Humphrey, W.; Dalke, A.; Schulten, K. Sartorius products. *Journal of molecular graphics* **1996**, *14*, 33–38.

(77) Wang, Y.; Ma, C.; Liu, C.; Lu, X.; Feng, X.; Ji, X. Thermodynamic Study of Choline Chloride-Based Deep Eutectic Solvents with Water and Methanol. *Journal of Chemical and Engineering Data* **2020**, *65*, 2446–2457.

(78) Zafarani-Moattar, M. T.; Shekaari, H.; Sadrmousavi Dizaj, A. Investigation of solute-solvent interactions in binary and quaternary solutions containing lithium perchlorate, propylene carbonate, and the deep eutectic solvent (choline chloride/ethylene glycol) at T=(288.15 to 318.15) K. *Journal of Molecular Liquids* **2020**, *319*, 114090.

(79) Haghbakhsh, R.; Raeissi, S. Investigation of solutions of ethyl alcohol and the deep eutectic solvent of Reline for their volumetric properties. *Fluid Phase Equilibria* **2018**, *472*, 39–47.

(80) Haghbakhsh, R.; Raeissi, S. Experimental investigation on the volumetric properties of mixtures of the deep eutectic solvent of Ethaline and methanol in the temperature range of 283.15 to 323.15 K. *Journal of Chemical Thermodynamics* **2020**, *147*, 106124.

(81) D'Agostino, C.; Harris, R. C.; Abbott, A. P.; Gladden, L. F.; Mantle, M. D. Molecular motion and ion diffusion in choline chloride based deep eutectic solvents studied by 1H pulsed field gradient NMR spectroscopy. *Physical Chemistry Chemical Physics* **2011**, *13*, 21383–21391.

(82) Fang, S.; He, C.-H. A New One Parameter Viscosity Model for Binary Mixtures. *AIChE Journal* **2011**, *57*, 517–524.

(83) Takeuchi, M.; Kameda, Y.; Umebayashi, Y.; Ogawa, S.; Sonoda, T.; Ishiguro, S. i.; Fujita, M.; Sano, M. Ion-ion interactions of LiPF6 and LiBF4 in propylene carbonate solutions. *Journal of Molecular Liquids* **2009**, *148*, 99–108.

(84) Kondo, K.; Sano, M.; Hiwara, A.; Omi, T.; Fujita, M.; Kuwae, A.; Iida, M.; Mogi, K.; Yokoyama, H. Conductivity and Solvation of Li+ Ions of LiPF6 in Propylene Carbonate Solutions. *Journal of Physical Chemistry B* **2000**, *104*, 5040–5044.

(85) Tsunekawa, H.; Narumi, A.; Sano, M.; Hiwara, A.; Fujita, M.; Yokoyama, H. Solvation and ion association studies of LiBF4-propylenecarbonate and LiBF4-propylenecarbonate-trimethyl phosphate solutions. *Journal of Physical Chemistry B* **2003**, *107*, 10962–10966.

(86) Hawlicka, E.; Swiatla-wojcik, D. Dynamic properties of the NaCl – methanol – water systemsÈMD simulation studies. **2000**, 3175–3180.

(87) Cruz Sanchez, M.; Dominguez, H.; Pizio, O. Molecular dynamics simulations of the properties of water-methanol mixtures. Effects of force fields. *Condensed Matter Physics* **2019**, *22*, 1–14.

(88) Kumar, K.; Sinha, A.; Bharti, A. Structural and Transport Properties of Binary Mixtures of Deep Eutectic Solvent (Ethaline) with Primary Alcohols : A Molecular Dynamics Study. 1–32.

(89) Shah, D.; Mjalli, F. S. Effect of water on the thermo-physical properties of Reline: An experimental and molecular simulation based approach. *Physical Chemistry Chemical Physics* **2014**, *16*, 23900–23907.

(90) Cea-Klapp, E.; Garrido, J. M.; Quinteros-Lama, H. Insights into the orientation and hydrogen bond influence on thermophysical and transport properties in choline-based deep eutectic solvents and methanol. *Journal of Molecular Liquids* **2021**, 117019.

(91) Zhong, H.; Lai, S.; Wang, J.; Qiu, W.; Lüdemann, H. D.; Chen, L. Molecular Dynamics Simulation of Transport and Structural Properties of CO2 Using Different Molecular Models. *Journal of Chemical and Engineering Data* **2015**, *60*, 2188–2196.

(92) Moultos, O. A.; Tsimpanogiannis, I. N.; Panagiotopoulos, A. Z.; Economou, I. G. Atomistic molecular dynamics simulations of CO2 diffusivity in H2O for a wide range of temperatures and pressures. *Journal of Physical Chemistry B* **2014**, *118*, 5532–5541.

(93) Dong, Q.; Muzny, C. D.; Kazakov, A.; Diky, V.; Magee, J. W.; Widegren, J. A.; Chirico, R. D.; Marsh, K. N.; Frenkel, M. ILThermo: A free-access web database for thermodynamic properties of ionic liquids. *Journal of Chemical and Engineering Data* **2007**, *52*, 1151–1159.

(94) Zheng, Y.; Dong, K.; Wang, Q.; Zhang, J.; Lu, X. Density, viscosity, and conductivity of lewis acidic 1-butyl- and 1-hydrogen-3-methylimidazolium chloroaluminate ionic liquids. *Journal of Chemical and Engineering Data* **2013**, *58*, 32–42.

(95) Cao, L.; Huang, J.; Zhang, X.; Zhang, S.; Gao, J.; Zeng, S. Imidazole tailored deep eutectic solvents for CO2 capture enhanced by hydrogen bonds. *Physical Chemistry Chemical Physics* **2015**, *17*, 27306–27316.

Appendices

A

Molecular Structures and Nomenclature

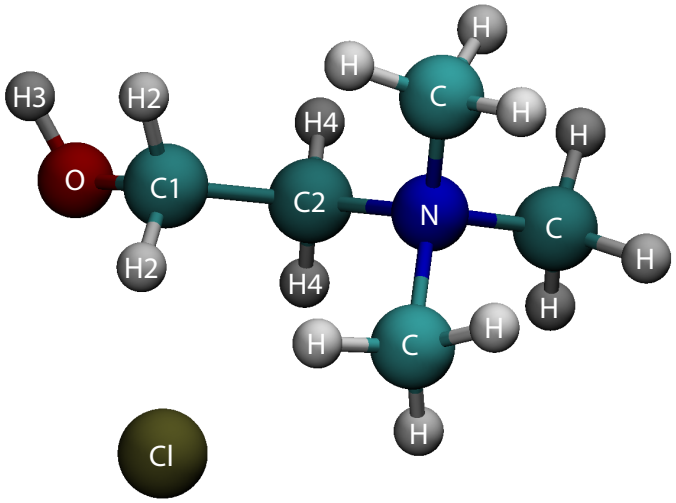

(a) Choline chloride.

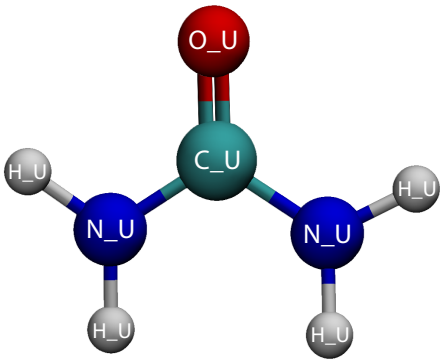

(b) Urea.

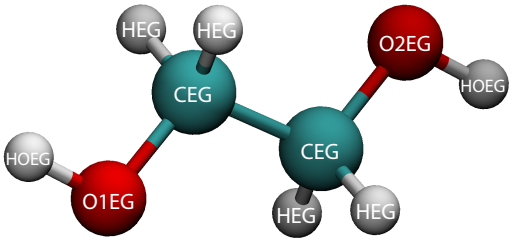

(c) Ethylene glycol.

Figure A.1: Molecular structures and atom labels of the deep eutectic solvent constituents choline chloride, urea and ethylene glycol.

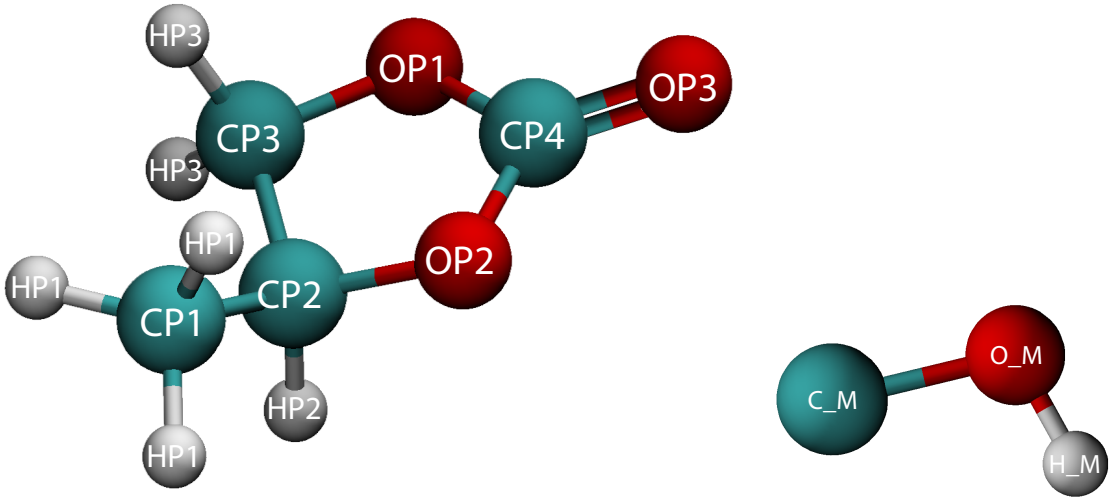

(a) Propylene carbonate.

(b) Methanol.

Figure A.2: Molecular structures and atom labels of the organic solvents propylene carbonate and methanol.

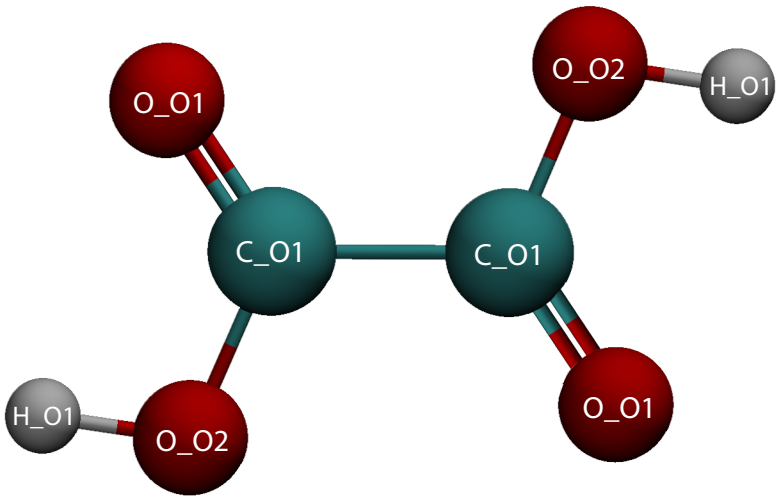

(a) Oxalic acid.

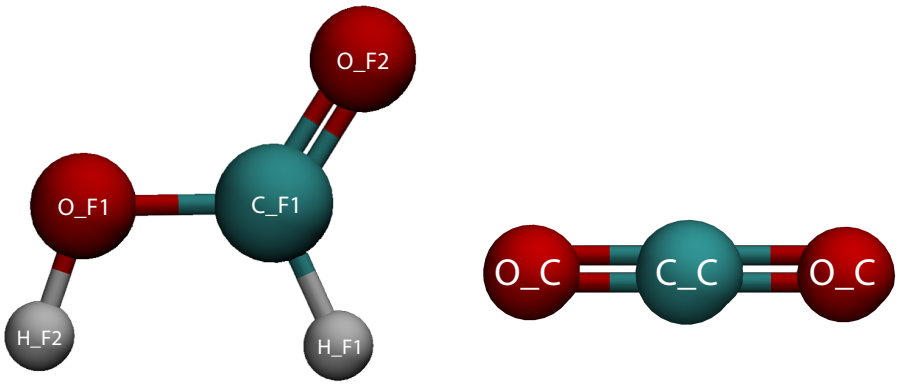

(b) Formic acid.

(c) Carbon dioxide.

Figure A.3: Molecular structures and atom labels of the solutes oxalic acid, formic acid (methanoic acid) and carbon dioxide.

B

Force Field Parameters

$$U_{\mathrm{LJ}} = 4\epsilon[(\frac{\sigma}{r})^{12} - (\frac{\sigma}{r})^{6}] \tag{B.1}$$

$$U_{\mathrm{Coulomb}} = \frac{q_i q_j}{4\pi\varepsilon_0 r} \tag{B.2}$$

$$U_{\text{bond stretching}} = K_r(r - r_0)^2 \tag{B.3}$$

$$U_{\text{angle bending}} = K_\theta(\theta - \theta_0)^2 \tag{B.4}$$

$$U_{\text{dihedral torsion, charmm}} = K[1 + \cos(n\phi - d)] \tag{B.5}$$

$$U_{\text{dihedral torsion, multi/harmonic}} = \sum_{n=1}^{4} K_n \cos^{n-1}(\phi) \tag{B.6}$$

$$U_{\text{dihedral torsion, opls}} = \frac{1}{2}K_1[1 + \cos(\phi)] + \frac{1}{2}K_2[1 + \cos(2\phi)] + \frac{1}{2}K_3[1 + \cos(3\phi)] \tag{B.7}$$

$$U_{\text{Improper torsion}} = K[1 + d\cos(n\phi)] \tag{B.8}$$

Table B.1: Partial charges and Lennard-Jones parameters for all modelled atom types. See appendix 6.3 for the atom labels. See equations B.1 and B.2 for the corresponding calculations. Charges of choline and chloride are shown scaled down by factors of 0.9 and 0.8 for ethaline and reline, respectively. Abbreviations: Ch^+ is choline, Cl^- is chloride, EG is ethylene glycol, FA is formic acid, OA is oxalic acid, and PC is propylene carbonate.

Molecule	Atom	ϵ [kcal/mol]	σ [Å]	q [e]	Force field
Ch^+	C	0.1094	3.3996	-0.12078 / -0.10736	GAFF
	C1	0.1094	3.3996	0.13509 / 0.12008	GAFF
	C2	0.1094	3.3996	-0.02898 / -0.02576	GAFF
	H	0.0157	1.9599	0.10737 / 0.09544	GAFF
	H2	0.0157	2.4713	0.0459 / 0.0408	GAFF
	H3	0.001	0.1	0.40905 / 0.3636	GAFF
	H4	0.0157	1.9599	0.10044 / 0.08928	GAFF
	N	0.17	3.2499	0.04518 / 0.04016	GAFF
	O	0.2104	3.0664	-0.55701 / -0.49512	GAFF
Cl^-	Cl	0.1	4.401	-0.9 / -0.8	GAFF
CO_2	C_C	0.05365	2.8	0.7	TraPPE-flex
	O_C	0.15698	3.028	-0.35	TraPPE-flex
EG	CEG	0.1094	3.3996	0.1615	GAFF
	HEG	0.0157	2.4713	0.0328	GAFF
	HOEG	0.001	0.1	0.4069	GAFF
	O1EG	0.2104	3.0664	-0.634	GAFF
	O2EG	0.2104	3.0664	-0.634	GAFF
FA	C_F1	0.0987	3.67	0.52	by Salas et al. [59]
	H_F1	0.0141	2.37	0	by Salas et al. [59]
	H_F2	0.002	1	0.45	by Salas et al. [59]
	O_F1	0.1599	2.94	-0.53	by Salas et al. [59]
	O_F2	0.1974	2.9	-0.44	by Salas et al. [59]
Methanol	C_M	0.19475	3.75	0.265	TraPPE
	H_M	0	0	0.435	TraPPE
	O_M	0.18481	3.02	-0.7	TraPPE
OA	C_O1	0.1575	3.75	0.416	OPLS
	H_O1	0.001	0.1	0.33	OPLS
	O_O1	0.315	2.96	-0.352	OPLS
	O_O2	0.255	2.92	-0.394	OPLS
PC	CP1	0.066	3.5	-0.365	GAFF
	CP2	0.066	3.5	0.349	GAFF
	CP3	0.066	3.5	0.194	GAFF
	CP4	0.105	3.75	0.878	GAFF
	HP1	0.015	2.42	0.113	GAFF
	HP2	0.015	2.42	0.032	GAFF
	HP3	0.015	2.42	0.008	GAFF
	OP1	0.17	3	-0.46	GAFF
	OP2	0.17	3	-0.507	GAFF
	OP3	0.21	2.96	-0.476	GAFF
Urea	C_U	0.086	3.3996	1.0401	GAFF
	H_U	0.0157	1.069	0.4167	GAFF
	N_U	0.17	3.25	-1.0246	GAFF
	O_U	0.21	2.96	-0.6577	GAFF

Table B.2: Bond stretching parameters. See appendix 6.3 for the atom labels. See equation B.3 for the corresponding calculations. Abreviations: Ch^+ is choline, EG is ethylene glycol, FA is formic acid, OA is oxalic acid, and PC is propylene carbonate.

molecule	Bond	K_r [kcal/(mol*Å^2)]	r_0 [Å]	Force field
Choline	C-H	338.7	1.091	GAFF
	C-N	293.6	1.499	GAFF
	C1-C2	303.1	1.535	GAFF
	C1-H2	335.9	1.093	GAFF
	C1-O	314.1	1.426	GAFF
	C2-H4	338.7	1.091	GAFF
	C2-N	293.6	1.499	GAFF
	H3-O	369.6	0.974	GAFF
CO2	C_C-O_C	2058	1.16	TraPPE-flex
EG	CEG-CEG	303.1	1.535	GAFF
	CEG-HEG	335.9	1.093	GAFF
	CEG-O1EG	314.1	1.426	GAFF
	CEG-O2EG	314.1	1.426	GAFF
	HOEG-O1EG	369.6	0.974	GAFF
	HOEG-O2EG	369.6	0.974	GAFF
FA	C_F1-H_F1	361.8	1.105	GAFF
	C_F1-O_F1	383.1	1.351	GAFF
	C_F1-O_F2	652.6	1.218	GAFF
	H_F2-O_F1	563.5	0.973	GAFF
Methanol	C_M-O_M	1000	1.43	TraPPE
	H_M-O_M	1000	0.945	TraPPE
OA	C_O1-C_O1	350	1.51	OPLS
	C_O1-O_O1	570	1.229	OPLS
	C_O1-O_O2	450	1.364	OPLS
	H_O1-O_O2	553	0.945	OPLS
PC	CP1-CP2	232.5	1.538	GAFF
	CP1-HP1	375.9	1.097	GAFF
	CP2-CP3	232.5	1.538	GAFF
	CP2-HP2	375.9	1.097	GAFF
	CP2-OP2	284.8	1.432	GAFF
	CP3-HP3	375.9	1.097	GAFF
	CP3-OP1	284.8	1.432	GAFF
	CP4-OP1	372.9	1.358	GAFF
	CP4-OP2	372.9	1.358	GAFF
	CP4-OP3	652.6	1.218	GAFF
Urea	C_U-N_U	478.2	1.35	GAFF
	C_U-O_U	648	1.21	GAFF
	H_U-N_U	410.2	1.01	GAFF

Table B.3: Angle parameters. See appendix 6.3 for the atom labels. See equation B.4 for the corresponding calculations. Abbreviations: Ch^+ is choline, EG is ethylene glycol, FA is formic acid, OA is oxalic acid, and PC is propylene carbonate.

Molecule	Angle	k_θ [kcal/(mol*rad^2)]	θ_0 [°]	Force field
Choline	C-N-C	62.8	110.64	GAFF
	C-N-C2	62.8	110.64	GAFF
	C1-C2-H4	46	111.74	GAFF
	C1-C2-N	66	108.93	GAFF
	C1-O-H3	47.1	108.16	GAFF
	C2-C1-H2	46.4	110.07	GAFF
	C2-C1-O	67.7	109.43	GAFF
	H-C-H	39	110.74	GAFF
	H-C-N	49	107.91	GAFF
	H2-C1-H2	39.2	109.55	GAFF
	H2-C1-O	51	109.88	GAFF
	H4-C2-H4	39	110.74	GAFF
	H4-C2-N	49	107.91	GAFF
CO2	O_C-C_C-O_C	112	180	TraPPE-flex
EG	CEG-CEG-HEG	46.4	110.07	GAFF
	CEG-CEG-O1EG	67.7	109.43	GAFF
	CEG-CEG-O2EG	67.7	109.43	GAFF
	CEG-O1EG-HOEG	47.1	108.16	GAFF
	CEG-O2EG-HOEG	47.1	108.16	GAFF
	HEG-CEG-HEG	39.2	109.55	GAFF
	HEG-CEG-O1EG	51	109.88	GAFF
	HEG-CEG-O2EG	51	109.88	GAFF
FA	C_F1-O_F1-H_F2	51.6	106.55	GAFF
	H_F1-C_F1-O_F1	65.3	109.49	GAFF
	H_F1-C_F1-O_F2	65.9	123.65	GAFF
	O_F1-C_F1-O_F2	115.7	122.1	GAFF
Methanol	C_M-O_M-H_M	55	108.5	TraPPE
OA	C_O1-C_O1-O_O1	80	121.4	OPLS
	C_O1-C_O1-O_O2	70.96	118.03	OPLS
	C_O1-O_O2-H_O1	35	113	OPLS
	O_O1-C_O1-O_O2	80	121	OPLS
PC	CP1-CP2-CP3	64.9	111.51	GAFF
	CP1-CP2-HP2	46.8	109.8	GAFF
	CP1-CP2-OP2	85.3	107.97	GAFF
	CP2-CP1-HP1	46.8	109.8	GAFF
	CP2-CP3-HP3	46.8	109.8	GAFF
	CP2-CP3-OP1	85.3	107.97	GAFF
	CP2-OP2-CP4	66.9	115.98	GAFF
	CP3-CP2-HP2	46.8	109.8	GAFF
	CP3-CP2-OP2	85.3	107.97	GAFF
	CP3-OP1-CP4	66.9	115.98	GAFF
	HP1-CP1-HP1	39	107.58	GAFF
	HP2-CP2-OP2	62.7	108.7	GAFF
	HP3-CP3-HP3	39	107.58	GAFF
	HP3-CP3-OP1	62.7	108.7	GAFF
	OP1-CP4-OP2	115.3	111.29	GAFF
	OP1-CP4-OP3	114.8	123.25	GAFF
	OP2-CP4-OP3	114.8	123.25	GAFF
Urea	C_U-N_U-H_U	49.21	118.5	GAFF
	H_U-N_U-H_U	39.73	117.9	GAFF
	N_U-C_U-N_U	74.8	113.4	GAFF
	N_U-C_U-O_U	75.83	122	GAFF

Table B.4: Dihedral torsion parameters. See appendix 6.3 for the atom labels. See equations B.5, B.6 and B.7 for the corresponding calculations. Abbreviations: Ch^+ is choline, Cl^- is chloride, EG is ethylene glycol, FA is formic acid, OA is oxalic acid, and PC is propylene carbonate.

Molecule	Dihedral	K [kcal/mol]	n	d [°]	Style	Force field
Choline	C1-C2-N-C	0.156	3	0	Charmm	GAFF
	H-C-N-C	0.156	3	0	Charmm	GAFF
	H-C-N-C2	0.156	3	0	Charmm	GAFF
	H2-C1-C2-H4	0.156	3	0	Charmm	GAFF
	H2-C1-C2-N	0.156	3	0	Charmm	GAFF
	H2-C1-O-H3	0.167	3	0	Charmm	GAFF
	H4-C2-N-C	0.156	3	0	Charmm	GAFF
	O-C1-C2-H4	0.156	3	0	Charmm	GAFF
	O-C1-C2-N	0.156	3	0	Charmm	GAFF
EG	HEG-CEG-CEG-HEG	0.156	3	0	Charmm	GAFF
	HEG-CEG-CEG-O1EG	0.25	1	0	Charmm	GAFF
	HEG-CEG-CEG-O2EG	0.25	1	0	Charmm	GAFF
	HEG-CEG-O1EG-HOEG	0.167	3	0	Charmm	GAFF
	HEG-CEG-O2EG-HOEG	0.167	3	0	Charmm	GAFF
PC	CP1-CP2-CP3-HP3	0.16	3	0	Charmm	GAFF
	CP1-CP2-CP3-OP1	0.156	3	0	Charmm	GAFF
	CP1-CP2-OP2-CP4	0.383	3	0	Charmm	GAFF
	CP2-CP3-OP1-CP4	0.383	3	0	Charmm	GAFF
	CP3-CP2-OP2-CP4	0.383	3	0	Charmm	GAFF
	HP1-CP1-CP2-CP3	0.16	3	0	Charmm	GAFF
	HP1-CP1-CP2-HP2	0.156	3	0	Charmm	GAFF
	HP1-CP1-CP2-OP2	0	3	0	Charmm	GAFF
	HP2-CP2-CP3-HP3	0.156	3	0	Charmm	GAFF
	HP2-CP2-CP3-OP1	0	3	0	Charmm	GAFF
	HP2-CP2-OP2-CP4	0.383	3	0	Charmm	GAFF
	HP3-CP3-OP1-CP4	0.383	3	0	Charmm	GAFF
	OP1-CP4-OP2-CP2	2.7	2	180	Charmm	GAFF
	OP2-CP2-CP3-HP3	0	3	0	Charmm	GAFF
	OP2-CP2-CP3-OP1	0.144	3	0	Charmm	GAFF
	OP2-CP4-OP1-CP3	2.7	2	180	Charmm	GAFF
	OP3-CP4-OP1-CP3	2.7	2	180	Charmm	GAFF
	OP3-CP4-OP2-CP2	2.7	2	180	Charmm	GAFF
Urea	N_U-C_U-N_U-H_U	2.5	2	180	Charmm	GAFF

Molecule	Dihedral	K_1 [kcal/mol]	K_2 [kcal/mol]	K_3 [kcal/mol]	K_4 [kcal/mol]	Style	Force field
EG	O1EG-CEG-CEG-O2EG	0.144	-0.432	2.35	0.576	multi/harmonic	GAFF
FA	H_F1-C_F1-O_F1-H_F2	5.1864	-0.62141	-4.565	0	multi/harmonic	by Salas et al. [59]
	O_F2-C_F1-O_F1-H_F2	4.565	0	-4.565	0	multi/harmonic	by Salas et al. [59]

Molecule	Dihedral	K_1 [kcal/mol]	K_2 [kcal/mol]	K_3 [kcal/mol]	Style	Force field
Choline	C2-C1-O-H3	0.5	0	0.32	OPLS	OPLS
EG	CEG-CEG-O1EG-HOEG	0.5	0	0.32	OPLS	OPLS
	CEG-CEG-O2EG-HOEG	0.5	0	0.32	OPLS	OPLS
OA	C_O1-C_O1-O_O2-H_O1	3	5.5	0	OPLS	OPLS
	O_O1-C_O1-C_O1-O_O1	1.6	3.2	0	OPLS	OPLS
	O_O1-C_O1-C_O1-O_O2	1.6	3.2	0	OPLS	OPLS
	O_O1-C_O1-O_O2-H_O1	0	5.5	0	OPLS	OPLS
	O_O2-C_O1-C_O1-O_O2	1.6	3.2	0	OPLS	OPLS
Urea	O_U-C_U-N_U-H_U	4	5	0	OPLS	OPLS

Table B.5: Improper torsion parameters. See appendix 6.3 for atom labels. See equation B.8 for the corresponding calculations. Abbreviations: FA is formic acid, OA is oxalic acid, and PC is propylene carbonate.

Molecule	Improper	K [kcal/mol]	d	n	Style	Force field
FA	H_F1-O_F1-C_F1-O_F2	1.1	-1	2	cvff	by Salas et al. [59]
OA	C_O1-O_O1-C_O1-O_O2	1.1	-1	2	cvff	OPLS
PC	OP1-OP2-CP4-OP3	1.1	-1	2	cvff	GAFF
Urea	C_U-H_U-N_U-H_U	1.1	-1	2	cvff	GAFF
	N_U-N_U-C_U-O_U	10.5	-1	2	cvff	GAFF

C

Density & Transport Properties

C.1. Density

Table C.1: Densities of mixtures of reline-methanol, ethaline-methanol and ethaline-PC as a function of the mole fraction of deep eutectic solvent (DES).

	Densities/[g/cm^3]		
x_{DES}	Reline-methanol	Ethaline-methanol	Ethaline-PC
0	0.778	0.778	1.2
0.1	0.85	0.839	1.19
0.2	0.916	0.886	1.19
0.4	1.02	0.971	1.17
0.6	1.1	1.03	1.16
0.8	-	1.08	1.14
1	-	1.12	1.12

C.2. Viscosity

Table C.2: Viscosities (upper values), standard deviations (middle values) and numbers of samples (lower values) of mixtures of reline-methanol, ethaline-methanol and ethaline-PC as a function of the mole fraction of deep eutectic solvent (DES).

	Viscosities/[mPa·s]		
x_{DES}	Reline-methanol	Ethaline-methanol	Ethaline-PC
0	0.5 0.067 17	0.5 0.067 17	3.01 0.31 16
0.1	0.984 0.12 18	0.869 0.063 12	4.04 0.46 22
0.2	1.75 0.19 20	1.49 0.16 14	5.29 0.75 19
0.4	4.71 0.47 19	3.47 0.37 14	8.44 1.4 15
0.6	13.6 1.4 12	9.08 1 11	16.4 3.9 10
0.8	72.4 13 10	21.2 2.7 8	33.2 5.2 12
1	455 91 6	61.9 14 15	61.9 14 15

C.3. Self-Diffusivity

Table C.3: Finite-size corrected self-diffusion coefficients (upper values), standard deviations (middle values) and numbers of samples (lower values) of choline (Ch^+), chloride (Cl^-), urea, methanol, CO_2, oxalic acid and formic acid in mixtures of reline-methanol as a function of the mole fraction of reline.

	Size-corrected self-diffusion coefficients/[10^{-11} m^2 s^{-1}]						
x_{DES}	Ch^+	Cl^+-	Urea	Methanol	CO_2	OA	FA
	-	-	-	277	697	245	294
0	-	-	-	20	11	22	24
	-	-	-	20	5	4	5
	93.6	107	103	175	425	101	160
0.1	3.1	3.2	1.8	2.9	13	6.8	5.5
	20	20	20	20	5	5	5
	58	70.3	63.5	121	282	65.6	104
0.2	1.6	1.2	1.7	2	14	3.7	6.2
	20	20	20	20	5	5	5
	23.3	28.9	26	56.6	108	27.2	46.9
0.4	0.86	1.2	0.64	1.2	11	2.1	3.4
	20	20	20	20	5	5	4
	7.56	9.79	9.38	22.8	42.1	8.46	17.6
0.6	0.53	0.51	0.5	1.3	4.2	0.84	1.8
	18	19	20	20	5	3	4
	1.88	2.38	2.71	6.93	13.3	2.2	6.09
0.8	0.16	0.19	0.2	0.52	2.3	0.23	1.3
	26	25	30	28	3	3	3
	0.27	0.351	0.501	-	2.03	0.439	0.847
1	0.033	0.023	0.054	-	0.098	0.09	0.11
	24	31	46	-	4	4	5

Table C.4: Finite-size corrected self-diffusion coefficients (upper values), standard deviations (middle values) and numbers of samples (lower values) of choline (Ch^+), chloride (Cl^-), ethylene glycol (EG), methanol, CO_2, oxalic acid (OA) and formic acid(FA) in mixtures of ethaline-methanol as a function of the mole fraction of ethaline.

Size-corrected self-diffusion coefficients/[10^{-11} m^2 s^{-1}]							
x_{DES}	Ch^+	Cl^+-	EG	Methanol	CO_2	OA	FA
	-	-	-	277	697	245	294
0	-	-	-	20	11	22	24
	-	-	-	20	5	4	5
	86.3	90	127	172	399	146	142
0.1	3.3	4.6	9.8	6.3	17	35	9.9
	15	15	15	15	5	10	4
	59.3	65.1	87.2	126	298	105	103
0.2	2.3	2.7	5.7	5.3	13	30	6.5
	15	15	15	15	5	9	5
	27.3	32.3	41.6	65	131	50.4	48.6
0.4	0.94	1.6	3.2	2.9	2.9	17	1.5
	15	15	15	15	5	10	4
	11.7	14.9	19.4	32.4	60.6	25	23.6
0.6	0.45	0.61	1	1.3	3.4	9.5	1.4
	15	15	15	15	5	8	4
	4.81	6.47	8.58	15	23.7	10.7	12.4
0.8	0.32	0.52	0.36	0.78	1.9	4.1	1.5
	15	15	15	15	4	9	5
	1.65	2.29	3.23	-	9.22	2.58	4.32
1	0.096	0.12	0.15	-	1.4	0.45	0.46
	31	33	36	-	6	5	5

Table C.5: Finite-size corrected self-diffusion coefficients (upper values), standard deviations (middle values) and numbers of samples (lower values) of choline (Ch^+), chloride (Cl^-), EG, propylene carbonate (PC), CO_2, oxalic acid (OA) and formic acid (FA) in mixtures of ethaline-propylene carbonate.

Size-corrected self-diffusion coefficients/[10^{-11} m^2 s^{-1}]							
x_{DES}	Ch^+	Cl^+-	EG	PC	CO_2	OA	FA
	-	-	-	41.4	114	38.5	60.7
0	-	-	-	1.6	9.2	2.2	4.5
	-	-	-	20	5	5	5
	18.4	20	27.8	34.3	92.4	27.3	30.7
0.1	1.7	2	1.9	0.98	12	0.92	1.6
	23	19	22	30	4	4	3
	14.5	15.1	21.8	28.1	79.4	21	24.7
0.2	1.1	0.99	1.1	0.62	6.8	1.4	2.4
	18	16	21	25	5	3	4
	8.8	9.64	14.3	18.7	59.4	13.9	17.5
0.4	0.74	0.72	0.96	0.85	6.7	1.3	0.91
	22	27	32	35	5	10	3
	5.31	6.23	9.48	11.2	36.5	8.65	13.3
0.6	0.27	0.36	0.39	0.74	2.2	1.2	1.7
	27	26	33	34	5	6	4
	2.87	3.69	5.59	5.17	20.1	4	6.82
0.8	0.14	0.22	0.27	0.35	3.3	0.26	0.57
	33	38	48	35	4	4	5
	1.65	2.29	3.23	-	9.22	2.58	4.32
1	0.096	0.12	0.15	-	1.4	0.45	0.46
	31	33	36	-	6	5	5

C.4. Ionic Conductivity

Table C.6: Ionic Conductivities (upper values), standard deviations (middle values) and numbers of samples (lower values) of mixtures of reline-methanol, ethaline-methanol and ethaline-propylene carbonate as a function of the mole fraction of deep eutectic solvent (DES).

	Ionic conductivies/[S/m]		
x_{DES}	Reline-methanol	Ethaline-methanol	Ethaline-PC
0.1	4.53 0.12 20	3.92 0.13 15	0.441 0.035 17
0.2	5.69 0.091 20	5.35 0.18 15	0.693 0.035 11
0.4	4.4 0.13 20	4.76 0.17 15	0.939 0.06 19
0.6	2.06 0.11 17	2.95 0.1 15	0.936 0.036 20
0.8	0.633 0.047 24	1.54 0.11 15	0.77 0.037 28
1	0.11 0.0083 15	0.628 0.03 26	0.628 0.03 26

D

Radial Distribution Functions

D.1. Solvents

D.1.1. Reline-Methanol

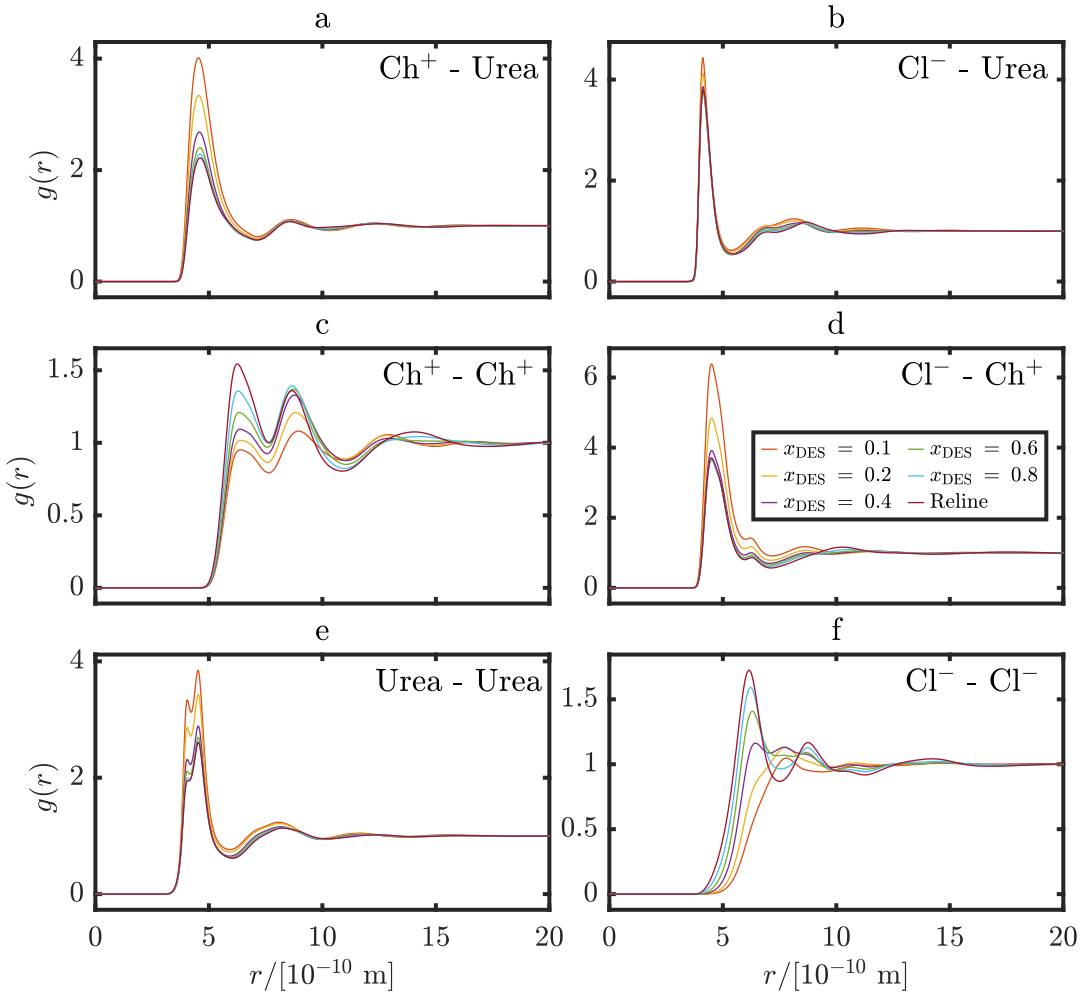

Figure D.1: Radial distribution functions of the deep eutectic solvent constituents in reline-methanol at different mole fractions of deep eutectic solvent, at 298 K and 1 atm. Line colours are consistent for all subfigures.

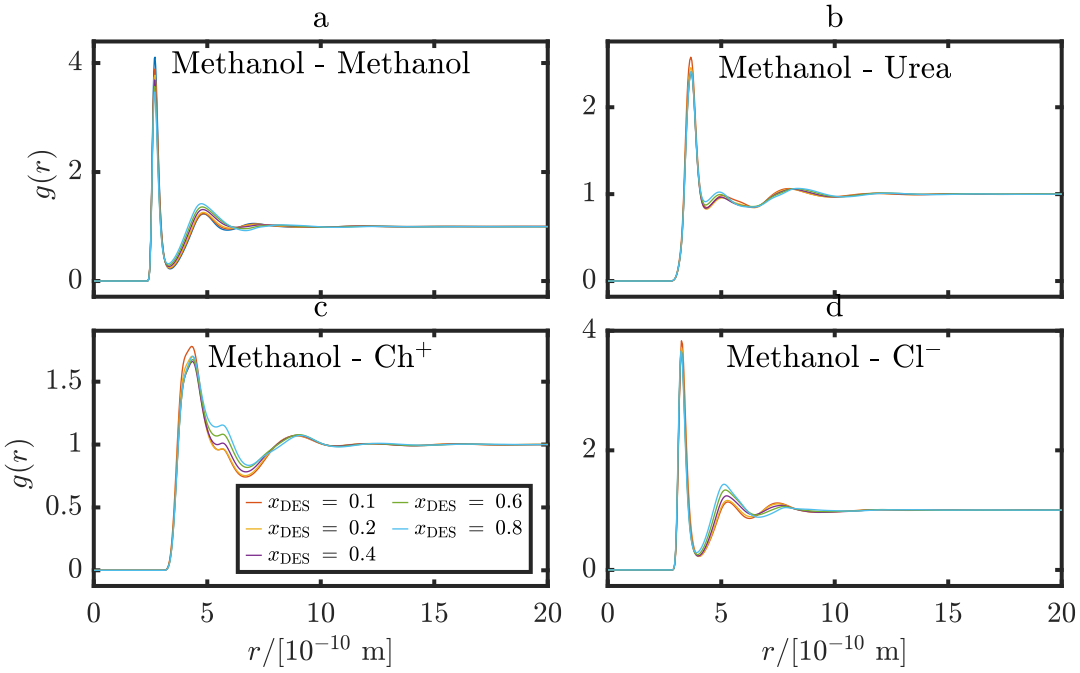

Figure D.2: Radial distribution functions between the organic solvent and the deep eutectic solvent constituents in reline-methanol at different mole fractions of deep eutectic solvent, at 298 K and 1 atm. Line colours are consistent for all subfigures.

D.1.2. Ethaline-Methanol

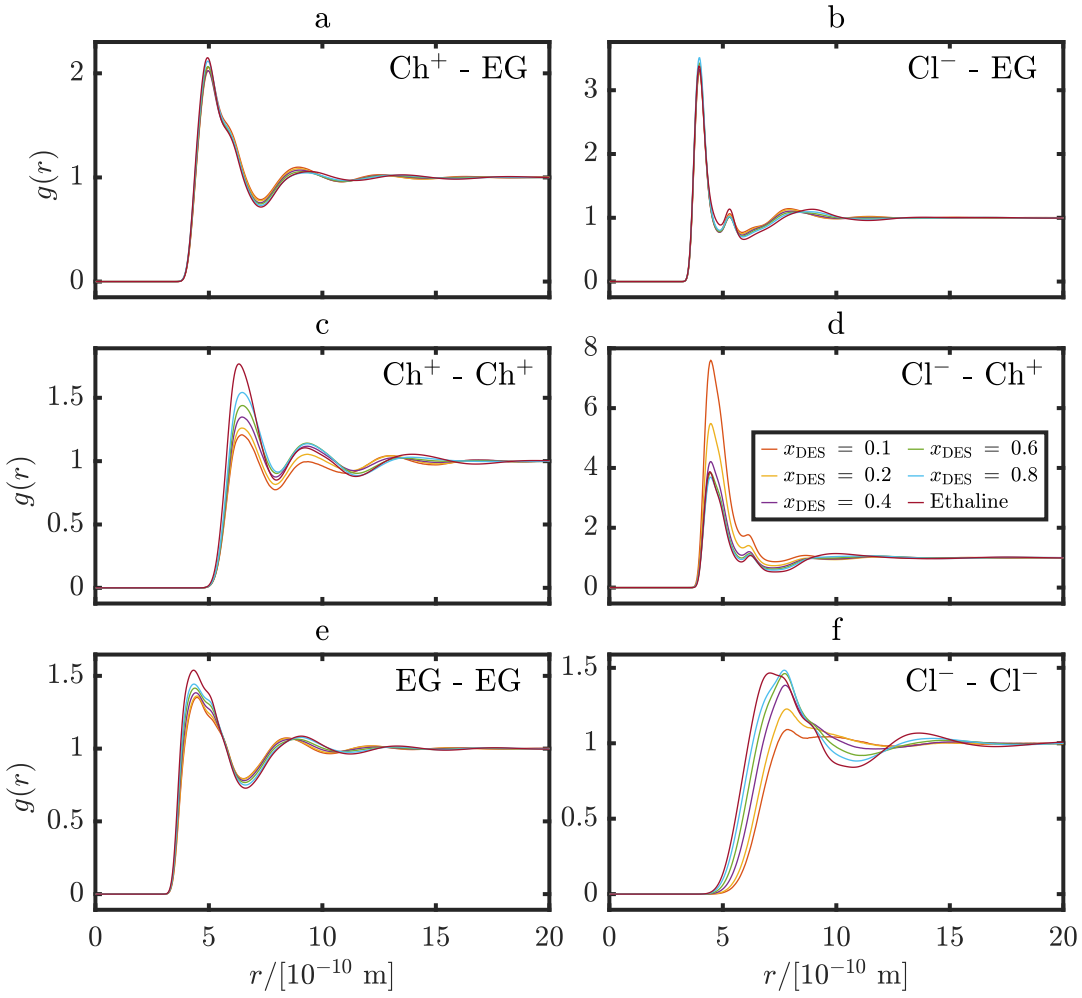

Figure D.3: Radial distribution functions of the deep eutectic solvent constituents in ethaline-methanol at different mole fractions of deep eutectic solvent, at 298 K and 1 atm. Line colours are consistent for all subfigures.

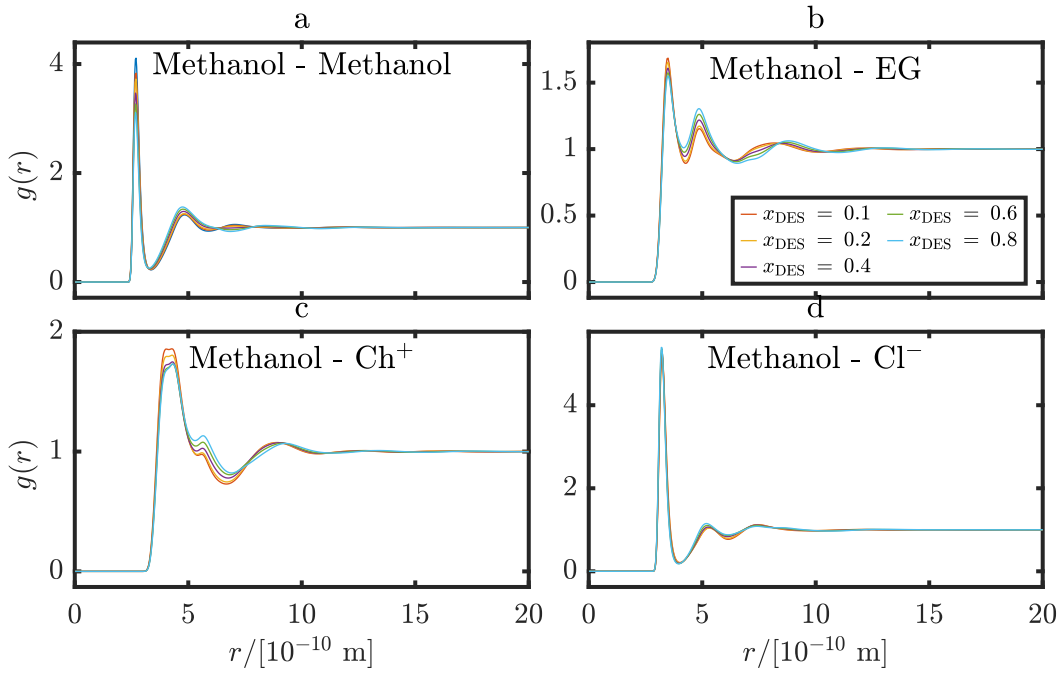

Figure D.4: Radial distribution functions between the organic solvent and the deep eutectic solvent constituents in ethaline-methanol at different mole fractions of deep eutectic solvent, at 298 K and 1 atm. Line colours are consistent for all subfigures.

D.1.3. Ethaline-Propylene Carbonate

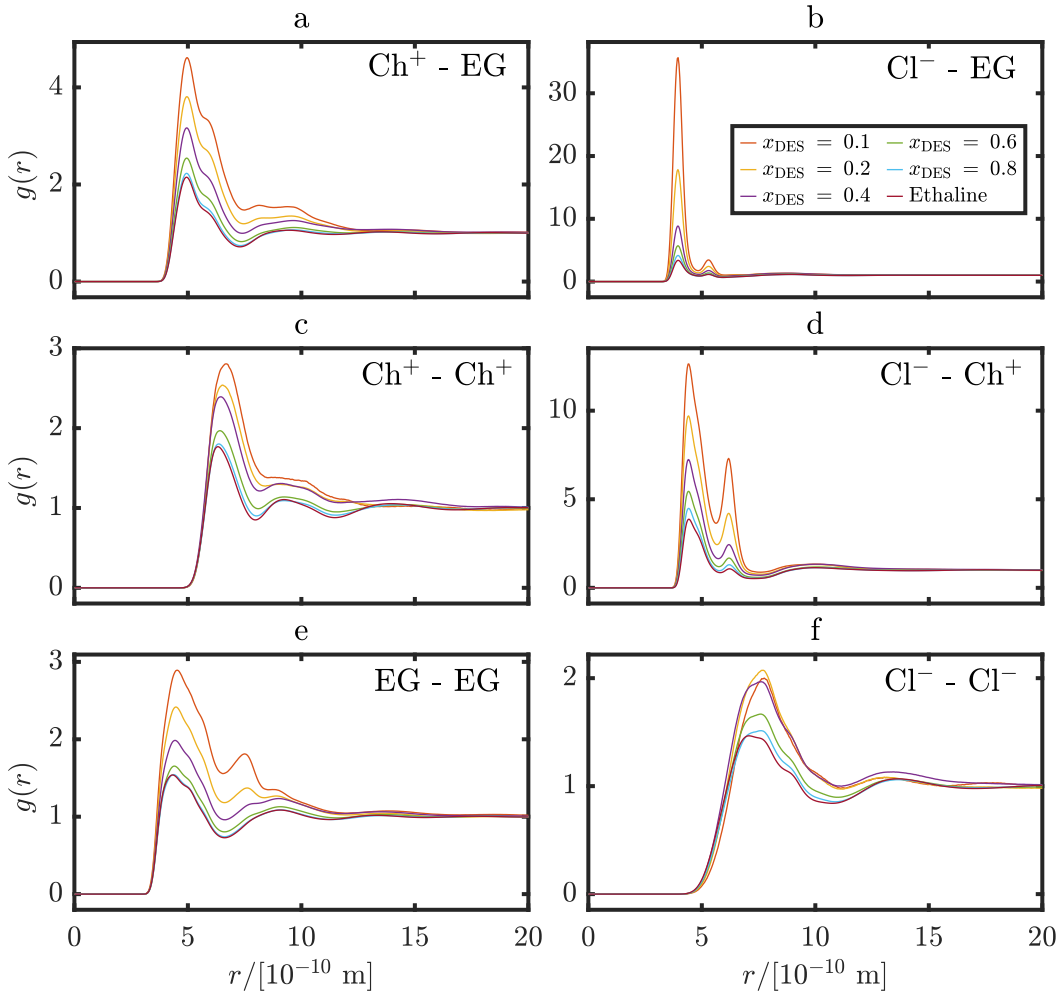

Figure D.5: Radial distribution functions of the deep eutectic solvent constituents in ethaline-propylene carbonate at different mole fractions of deep eutectic solvent, at 298 K and 1 atm. Line colours are consistent for all subfigures.

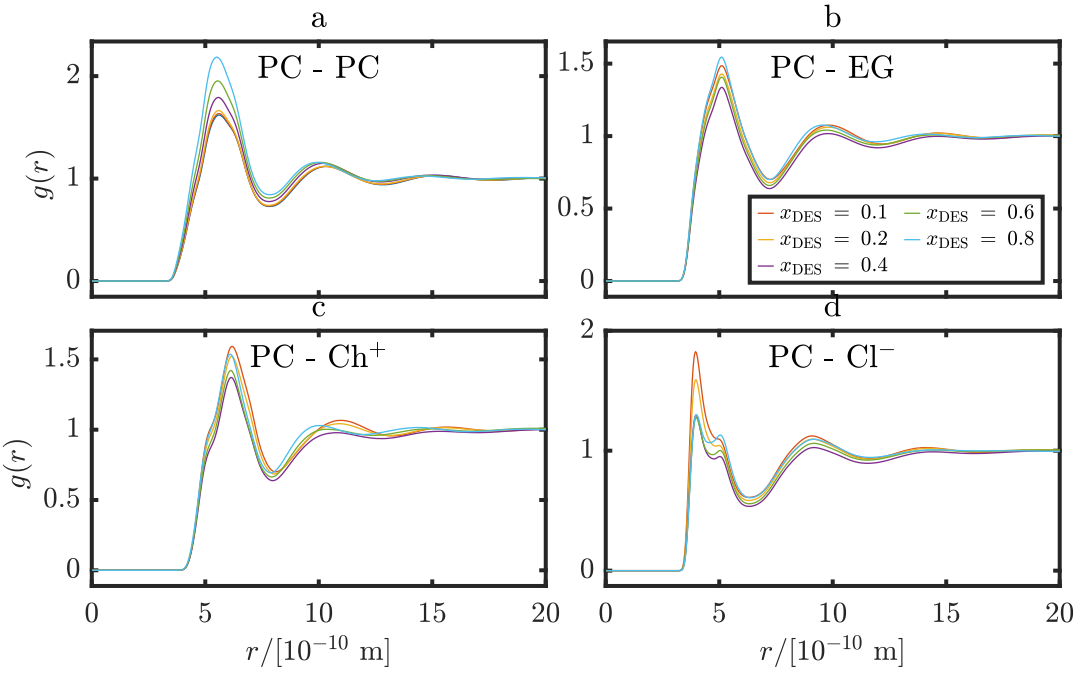

Figure D.6: Radial distribution functions between the organic solvent and the deep eutectic solvent constituents in ethaline-PC at different mole fractions of deep eutectic solvent, at 298 K and 1 atm. Line colours are consistent for all subfigures.

D.2. Solutes

D.2.1. Reline-Methanol

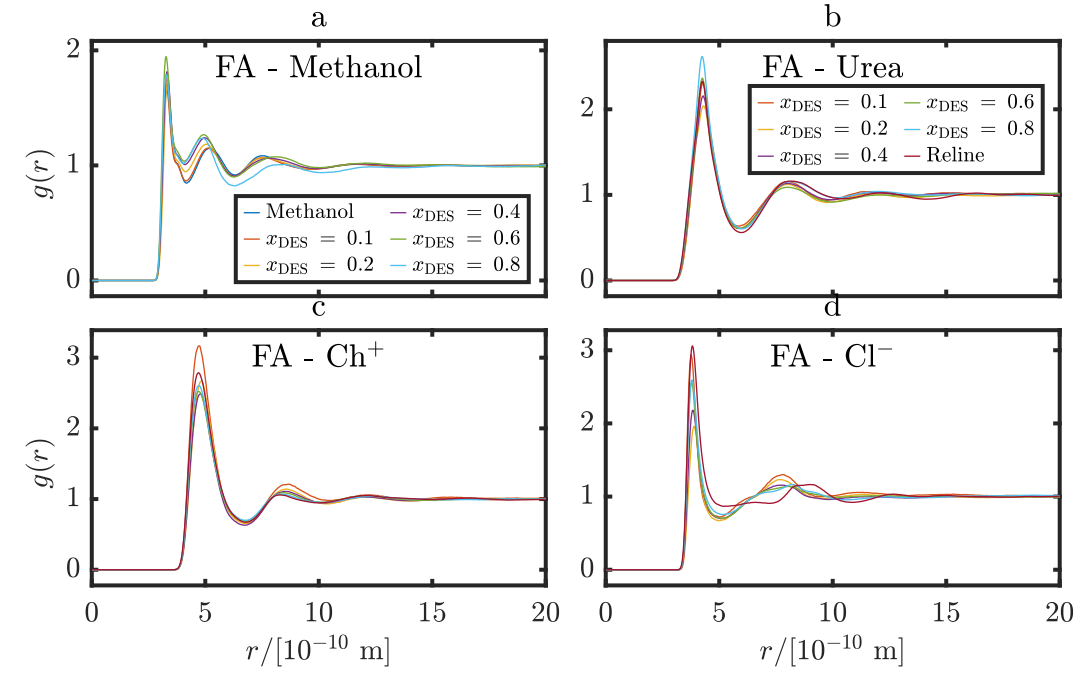

Figure D.7: Radial distribution functions between FA and solvent constituents in reline-methanol at different mole fractions of deep eutectic solvent, at 298 K and 1 atm. Line colours are consistent for all subfigures.

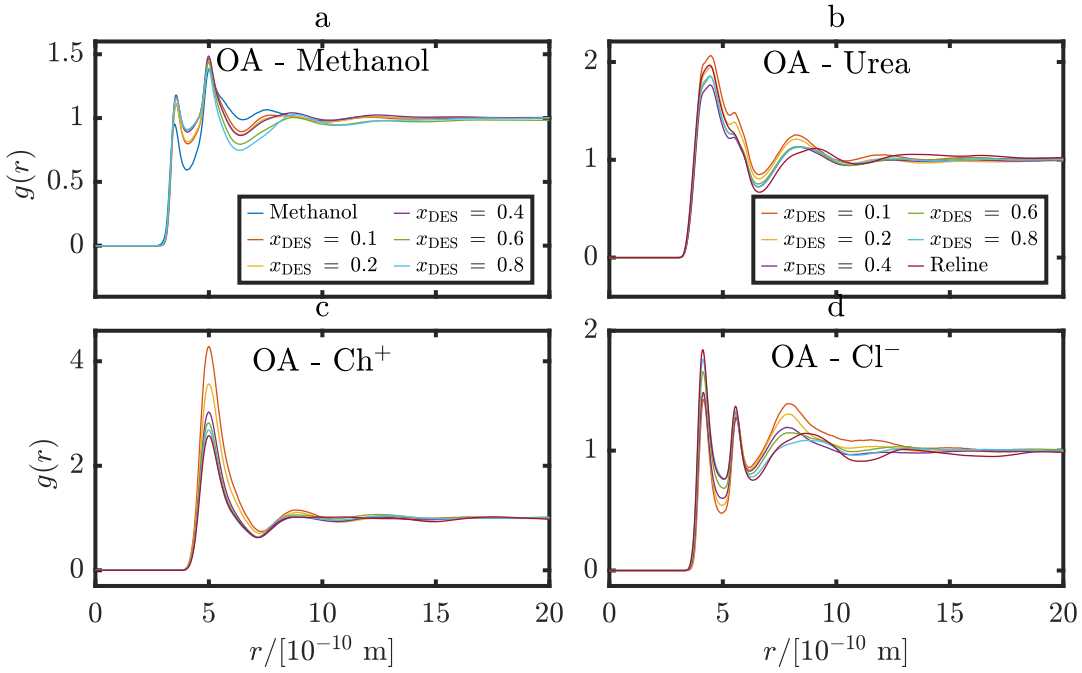

Figure D.8: Radial distribution functions between OA and solvent constituents in reline-methanol at different mole fractions of deep eutectic solvent, at 298 K and 1 atm. Line colours are consistent for all subfigures.

D.2.2. Ethaline-Methanol

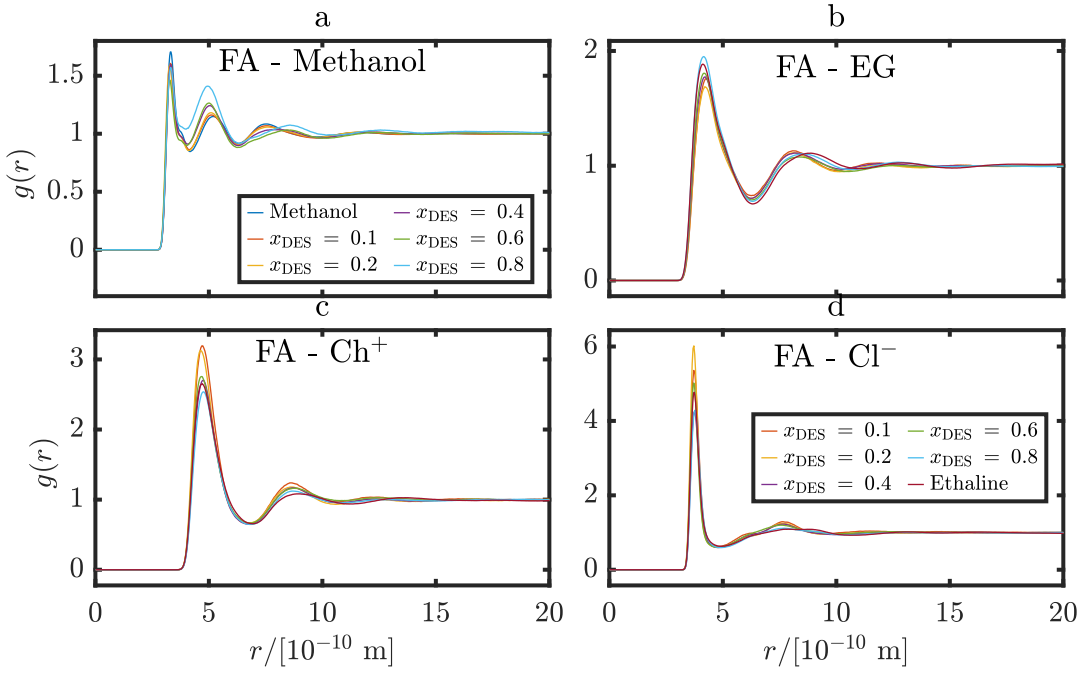

Figure D.9: Radial distribution functions between FA and solvent constituents in ethaline-methanol at different mole fractions of deep eutectic solvent, at 298 K and 1 atm. Line colours are consistent for all subfigures.

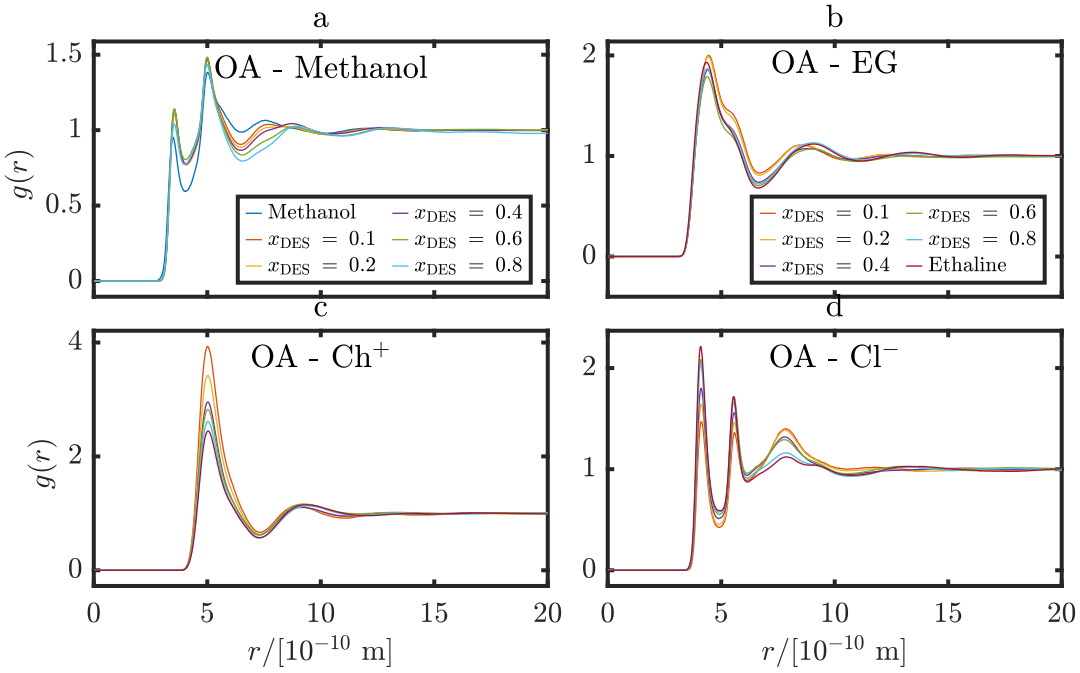

Figure D.10: Radial distribution functions between OA and solvent constituents in ethaline-methanol at different mole fractions of deep eutectic solvent, at 298 K and 1 atm. Line colours are consistent for all subfigures.

E

Hydrogen bonds

The numbers of hydrogen bonds are presented, together with the mean absolute deviation (MAD), calculated as equation E.1

$$MAD = \frac{1}{n}\sum_{i=1}^{n} |N_{\mathrm{HB},\,i} - N_{\mathrm{HB,\,average}}| \tag{E.1}$$

where n is the total number of samples, $N_{\mathrm{HB},\,i}$ is the number of hydrogen bonds of sample i and $N_{\mathrm{HB,\,average}}$ is the average number of hydrogen bonds.

E.1. Deep Eutectic Solvent - Deep Eutectic Solvent

Table E.1: The numbers of hydrogen bonds (upper values), mean absolute deviations (middle values) and numbers of samples (lower values) between all pairs of chloride (Cl^-), choline (Ch^+), urea in mixtures of reline-methanol as a function of the mole fraction of reline. The measured number of hydrogen bonds is divided by the number of hydrogen bond donor (HBD) molecules and multiplied by 100 to represent a system of 50 Cl^-, 50 Ch^+, 100 urea molecules and a number of organic solvent molecules dependent on the mole fraction of reline.

	Number of hydrogen bonds per 200 molecules of reline				
x_{DES}	Cl^--Ch^+	Cl^--urea	Ch^+-Ch^+	Ch^+-urea	urea-urea
	3.22	9.05	0.0519	4.4	24.9
0.1	1.2	2.4	0.22	1.4	5.4
	520	520	520	520	520
	5.09	16.4	0.106	7.28	41.2
0.2	1.5	2.9	0.32	1.7	6.3
	520	520	520	520	520
	8.05	29	0.183	11.4	61.5
0.4	1.7	3.6	0.43	2.1	7.4
	520	520	520	520	520
	10.7	39	0.245	14.7	77.8
0.6	1.8	3.6	0.44	2.2	7.2
	520	520	520	520	520
	12.8	49	0.325	17.8	90.2
0.8	1.7	3.6	0.47	2.2	7.3
	632	632	632	632	632
	15.1	58.8	0.375	20.3	101
1	1.6	3.2	0.42	1.9	6.1
	1307	1307	1307	1307	1307

Table E.2: The numbers of hydrogen bonds (upper values), mean absolute deviations (middle values) and numbers of samples (lower values) between all pairs of chloride (Cl^-), choline (Ch^+), ethylene glycol (EG) in mixtures of ethaline-methanol as a function of the mole fraction of ethaline. The measured number of hydrogen bonds is divided by the number of hydrogen bond donor (HBD) molecules and multiplied by 100 to represent a system of 50 Cl^-, 50 Ch^+, 100 EG molecules and a number of organic solvent molecules dependent on the mole fraction of ethaline.

Number of hydrogen bonds per 200 molecules of ethaline					
x_{DES}	Cl^--Ch^+	Cl^--EG	Ch^+-Ch^+	Ch^+-EG	EG-EG
	5.45	14.1	0.0536	2.68	9.5
0.1	1.5	2.9	0.23	1.2	3
	504	504	504	504	504
	8.6	25	0.107	4.69	16.1
0.2	2	3.4	0.33	1.6	4
	521	521	521	521	521
	13.6	43.5	0.139	7.63	25.9
0.4	2.5	5.6	0.39	2	5.2
	498	498	498	498	498
	18.4	59.9	0.212	9.73	33.1
0.6	2.7	6.6	0.41	2	5.5
	498	498	498	498	498
	22.5	74.3	0.237	11.2	37.9
0.8	2.8	7.8	0.4	2.1	5.8
	478	478	478	478	478
	26.5	86.2	0.268	12.9	41.9
1	1.7	3	0.35	1.5	3.9
	650	650	650	650	650

Table E.3: The numbers of hydrogen bonds (upper values), mean absolute deviations (middle values) and numbers of samples (lower values) between the relevant pairs of chloride (Cl^-), choline (Ch^+), ethylene glycol (EG) in mixtures of ethaline-PC as a function of the mole fraction of ethaline. The measured number of hydrogen bonds is divided by the number of hydrogen bond donor (HBD) molecules and multiplied by 100 to represent a system of 50 Cl^-, 50 Ch^+, 100 EG molecules and a number of organic solvent molecules dependent on the mole fraction of ethaline.

Number of hydrogen bonds per 200 molecules of ethaline					
x_{DES}	Cl^--Ch^+	Cl^--EG	Ch^+-Ch^+	Ch^+-EG	EG-EG
	23.9	84.6	0.115	6.58	13.3
0.1	4.9	11	0.67	3.5	7.5
	627	627	627	627	627
	25.7	88.3	0.177	8.44	18.7
0.2	3.5	6.7	0.57	2.6	5.7
	520	520	520	520	520
	26.6	88.1	0.181	10	26.5
0.4	2.8	5.4	0.5	2.2	6.2
	780	780	780	780	780
	26.8	87.3	0.241	11.1	32
0.6	2.1	4.2	0.44	1.8	4.7
	780	780	780	780	780
	26.8	86.8	0.244	12.1	36.8
0.8	1.9	3.6	0.41	1.7	4.7
	1040	1040	1040	1040	1040
	26.5	86.2	0.268	12.9	41.9
1	1.7	3	0.35	1.5	3.9
	650	650	650	650	650

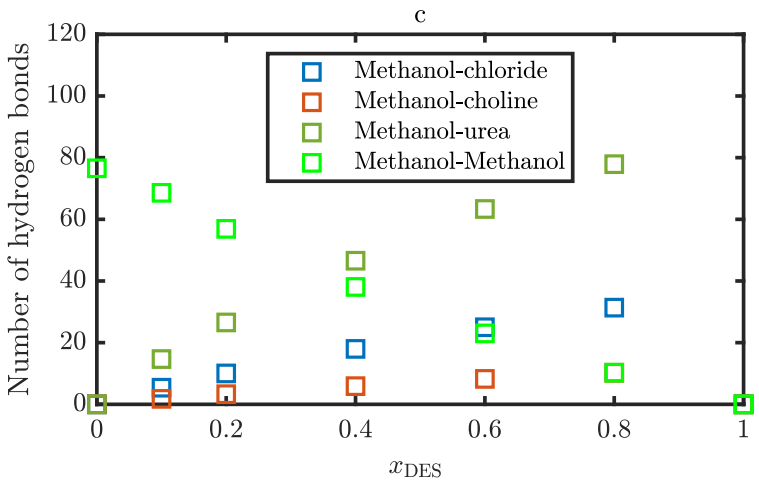

Figure E.1: The number of hydrogen bonds between the organic solvents methanol and propylene carbonate (PC) and the deep eutectic solvent (DES) constituents as a function of the mole fraction of DES for the mixtures reline-methanol (a), ethaline-methanol (b) and ethaline-PC (c), at 298 K and 1 atm. The measured number of hydrogen bonds is divided by the number of organic solvent molecules and multiplied by 100 to represent a system of 100 organic solvent molecules and a number of DES molecules dependent on the mole fraction of DES. Equation 3.14 and table 3.1 denote the applied calculation and number of molecules per simulation, respectively. Error bars are excluded for clarity. Mean average deviations and sample sizes are tabulated in this appendix.

E.2. Organic Solvent - Deep Eutectic Solvent

Table E.4: The numbers of hydrogen bonds (upper values), mean absolute deviations (middle values) and numbers of samples (lower values) between methanol and chloride (Cl^-), choline (Ch^+), and urea in mixtures of reline-methanol as a function of the mole fraction of reline. The measured number of hydrogen bonds is divided by the number of methanol molecules and multiplied by 100 to represent a system of 100 methanol molecules and a number of reline molecules dependent on the mole fraction of reline.

Number of hydrogen bonds per 100 molecules of methanol

x_{DES}	Meth-Cl^-	Meth-Ch^+	Meth-Urea	Meth-Meth
	-	-	-	76.2
0.1	-	-	-	3.6
	-	-	-	130
	5.36	1.77	14.6	68.7
0.2	0.26	0.14	0.55	1.5
	130	130	130	130
	9.98	3.33	26.5	57
0.4	0.58	0.31	1.1	2.1
	130	130	130	130
	17.9	5.85	46.2	38.4
0.6	1.4	0.75	2.8	3.4
	130	130	130	130
	25	8.12	63.2	23.4
0.8	2.3	1.3	4	3.5
	130	130	130	130
	30.5	10.4	78.1	10.6
1	3.5	2.3	6.2	3.8
	66	66	66	66

Table E.5: The numbers of hydrogen bonds (upper values), mean absolute deviations (middle values) and numbers of samples (lower values) between methanol and chloride (Cl^-), choline (Ch^+), and ethylene glycol (EG) in mixtures of ethaline-methanol as a function of the mole fraction of ethaline. The measured number of hydrogen bonds is divided by the number of methanol molecules and multiplied by 100 to represent a system of 100 methanol molecules and a number of ethaline molecules dependent on the mole fraction of ethaline.

Number of hydrogen bonds per 100 molecules of methanol				
x_{DES}	Meth-Cl^-	Meth-Ch^+	Meth-EG	Meth-Meth
	-	-	-	76.2
0.1	-	-	-	3.6
	-	-	-	130
	7.23	2.03	11	67.1
0.2	0.32	0.13	0.4	1.8
	114	114	114	114
	13.6	3.73	19.6	54.4
0.4	1.4	0.49	1.9	5.3
	131	131	131	131
	24.2	6.29	31.9	33.3
0.6	5	1.5	6.6	7.2
	108	108	108	108
	33.4	8.52	41.7	19.5
0.8	6.9	2.2	8.7	4.9
	108	108	108	108
	41	9.83	49.5	8.45
1	9.7	3.1	12	3.6
	88	88	88	88

Table E.6: The numbers of hydrogen bonds (upper values), mean absolute deviations (middle values) and numbers of samples (lower values) between propylene carbonate (PC) and chloride (Cl^-), choline (Ch^+) and ethylene glycol (EG) in mixtures of ethaline-PC as a function of the mole fraction of ethaline. The measured number of hydrogen bonds is divided by the number of PC molecules and multiplied by 100 to represent a system of 100 PC molecules and a number of ethaline molecules dependent on the mole fraction of ethaline.

Number of hydrogen bonds per 100 molecules of PC		
x_{DES}	PC-Ch^+	PC-EG
	6.58	22.2
0.1	3.3	6.4
	627	627
	3.91	15.4
0.2	1.9	4
	520	520
	1.84	9.75
0.4	1.1	2.6
	780	780
	0.94	6.26
0.6	0.58	1.5
	780	780
	0.413	3.25
0.8	0.36	1
	1040	1040

F

Enantiomers of Propylene Carbonate

Table F.1: Comparison of the viscosity, self-diffusivity and density of enantiopure and racemic propylene carbonate.

	Viscosity/[mPa·s]		Self-diffusivity/[10^{-11} m^2 s^{-1}]		Density/[g/cm^3]	
	Racemic	Enantiopure	Racemic	Enantiopure	Racemic	Enantiopure
Average	3.07	3.01	41.4E-10	41.4E-10	1.20	1.20
Standard deviation	0.33	0.31	0.79E-11	1.60E-11	-	-